Summer 8-19-2022

Understanding the Contribution of Gα to the Yeast Pheromone Response

Cory Johnson
University of Maine, cory.p.johnson@maine.edu

UNDERSTANDING THE CONTRIBUTION OF Gα TO THE YEAST PHEROMONE RESPONSE

By

Cory P. Johnson

B.S. in Biology at University of Maine, 2018

A DISSERTATION

Submitted in Partial Fulfillment of the

Requirements for the Degree of

Doctor of Philosophy

(in Biomedical Science)

The Graduate School

The University of Maine

August 2022

Advisory Committee:

Joshua B. Kelley, Assistant Professor of Biochemistry at The University of Maine, Advisor

Melissa Maginnis, Associate Professor of Microbiology at The University of Maine

Samuel T. Hess, Professor of Physics at The University of Maine

Dustin Updike, Associate Professor of Regenerative Biology and Medicine at Mount Desert Island Biological Laboratory

Kristy L. Townsend, Associate Professor of Neurological Surgery at The Ohio State University

UNDERSTANDING THE CONTRIBUTION OF Gα TO THE YEAST PHEROMONE RESPONSE

By Cory P. Johnson

Dissertation Advisor: Dr. Joshua B. Kelley

An Abstract of the Dissertation Presented
in Partial Fulfillment of the Requirements for the
Degree of Doctor of Philosophy
(in Biomedical Science)
August 2022

G-protein coupled receptors (GPCRs) are the target of approximately 35% of all FDA-approved pharmaceuticals. This is because GPCRs regulate different cellular signals including control of cell polarity. The yeast, *Saccharomyces cerevisiae*, use a GPCR for mating which induces chemotropic growth and morphogenesis toward a mate. In mammalian cells, signaling downstream of the receptor is primarily conducted by the Gα subunit of the large G-protein. In the yeast pheromone response little is known about Gα's contribution to signaling and the Gβγ subunit is the primary known contributor. This begs the question, what is the contribution of Gα to the yeast pheromone response? I have found two novel mechanisms in the yeast pheromone response that implicate Gα signaling in yeast mating. First, I have identified a previously unknown role of the regulator of G-protein signaling (RGS), which facilitates hydrolysis of GTP to GDP on Gα to turn off downstream signaling. I found that RGS is phosphorylated early in the pheromone response to facilitate the transition from mitosis to pheromone-induced polarization. Importantly, I also found that the phosphorylation state of the RGS dictates the distribution of the downstream Fus3-MAPK response. The Fus3-MAPK binds directly to Gα-GTP to enhance signal output. In cells with phosphomimetic RGS, the distribution of Fus3-MAPK, is broadly localized across the polar cap while unphosphorylatable RGS mutants were similar to controls. Therefore, the phosphorylation state of RGS controls the distribution of active Gα and drives localization of the Fus3-MAPK signal.

Previous work indicated that cells lacking RGS-activity do not generate mating projections and have aberrant septin distribution. Septins are cytoskeletal filaments that function as diffusion barriers and protein scaffolds during cell division, but their roles in the pheromone response are not well understood. I found that septin distribution is driven by epsin-mediated endocytosis of Gα via its ubiquitination domain. Additionally, the septin chaperone Gic1 and the Cdc42 GTPase activating protein (Cdc42-GAP) Bem3 were differentially involved in pheromone-induced septin deposition when compared to other septin chaperones and Cdc42-GAPs respectively. These results provide new evidence for Gα as a signaling contributor to the yeast pheromone response.

DEDICATION

This dissertation is dedicated to my grandfather who was unable to be here to see me grow as a scientist. Papa, you were always there for me, and I know you're still here for me now. I dedicate this dissertation to you because you always encouraged me to strive for my best, to be present, and to prioritize family and self before everything else. I love you, Papa.

ACKNOWLEDGEMENTS

There are too many people to name here who have supported me through my doctoral journey so I will only name a few. First (and most important) I thank my family. Mom and Dad, you have been the most amazing support system as I have decided to go back to complete my education. Without you both I would not be able to do any of this science and for that I am eternally grateful. Kelly, my partner, my co-pilot, you have been my anchor through all the storms and through all of calm. Maple-Onion, my dog, my little boy. You have brought so much joy to our family and you remind me to be childish every now and again. I thank my advisor, Joshua Kelley. You took me on as a student in your laboratory during an unbelievably difficult time in the world (start of COVID-19 pandemic) and have given me a beautiful opportunity to learn and contribute to the science I present here. I thank Kristy Townsend for giving me a chance in her laboratory. I will never forget the first time I was able to do my first experiment in your laboratory – for reference it was taking images of H&E stained adipose from the lipidomics project. I couldn't forget Magdalena Blaszkiewicz, you taught me so much in Kristy's lab and I'm so grateful for the time and energy you spent on all of us newbies in the lab. I would also like to thank all of my friends, both in science and outside of science, without you I would not have remained sane through these past several years. Finally, I want to thank doxycycline, atovaquone, and azithromycin for ridding me of the tick-borne illnesses I have contracted during the time I am writing this. I wouldn't have been able to make it through without your beautiful bug-killing properties.

TABLE OF CONTENTS

LIST OF FIGURES

LIST OF TABLES

CHAPTER 1

INTRODUCTION AND BACKGROUND

1.1. G-Protein Coupled Receptors and Yeast as a Model System

1.1.1 A Brief History of GPCRs

G-protein coupled receptors (GPCRs) comprise approximately 35% of all FDA-approved therapeutics[1]. Additionally, humans express nearly 1000 known GPCRs that span a wide range of functions including control of cell polarity. GPCRs are seven transmembrane domain proteins that couple to a heterotrimeric, large G-protein, consisting of Gα subunit and Gβγ complex. G-proteins are molecular switches that, when activated by a GPCR, transmit an external signal to an internal signal. Upon activation of the receptor by ligand binding, a conformational shift promotes the receptor's intrinsic guanine nucleotide exchange factor (GEF) activity and catalyzes the exchange of nucleotide bound to Gα, replacing GDP with GTP. Gα-GTP promotes dissociation of the heterotrimeric complex and downstream signaling.

The type of signal output is dependent upon the cognate G-protein. There are 4 major families of Gα: Gαs, Gαi/o, Gaq, and Gα12/13. Each family controls activity of specific signaling pathways in the cell. Generally, the GαS subtype stimulates cAMP production via adenylyl cyclase and leads to transcriptional activity to increase cell growth, proliferation, or any other number of specialized activities. The Gαi/o pathway inhibits the stimulatory effects of GαS by suppressing cAMP production. Gαq activates phospholipase C to ultimately modulate calcium signaling via phosphoinostitol signaling. Finally, Gα12/13 can activate small GTPases, such as the master regulator of cell polarity, Cdc42[2].

The β2 adrenergic receptor (β2AR), was the first human GPCR to be sequenced and structurally solved[3-5]. It is coupled to Gαs and is still the standard model system for many studies probing GPCR signaling.

Although the structural work clarified the activation mechanisms of GPCRs and G-proteins, a large amount of fundamental signal transduction work was conducted in the 1980s, 1990s, and early 2000s. Many contributions to the cell signaling research boom used a new model system, *Saccharomyces cerevisiae* (yeast hereafter)[6].

1.1.2. Yeast as a Model GPCR System

Experiments using the β2AR and other adrenergic receptors were still prevalent, however, yeast became a competitive model system for GPCR research during the late 1980s. This is because yeast had proven to be a powerful model system due to the ease of genetic manipulation that made conducting biochemical and molecular biological experiments relatively easy[7, 8]. Yeast were also the first fully sequenced genome[9] and as the scientific community came to find, there is significant overlap from yeast to humans[10]. Additionally, a large set of tools have been developed for yeast research including comprehensive libraries of yeast deletion mutants[11, 12], over-expression mutants[13], and a collection of green fluorescent protein (GFP)-tagged yeast[14, 15]. The advent of these genetic tools preceded the development of several high-throughput technologies including transcriptomics[16, 17], proteomics[18], and metabolomics[19, 20] – all originally developed in yeast.

As for GPCR signaling, yeast contain DNA encoding only 3 GPCRs, a nutrient-sensing GPCR (Gpr1) and the pheromone, or mating receptors Ste2 (expressed by the haploid mating type-a yeast) and Ste3 (expressed by the haploid mating type-α yeast)[21, 22]. For the purposes of this dissertation, I will only discuss the Ste2 receptor and will use the terms Ste2 and "receptor" interchangeably. Gpr1 signaling mimics the GαS signaling I described earlier – modeled by the β2AR. On the other hand, Ste2 couples to a Gα12/13-like G-protein and is therefore an excellent model to study GPCR-mediated cell polarity. Recently, the crystal structure of Ste2 was solved and showed that the receptor is a homodimer and is coupled to two G-protein complexes[23]. While the direct impacts to physiology of this are unknown, it is a critical finding.

1.2. The Yeast Pheromone Response – Signaling and Regulation

The yeast pheromone response is likely the most well-studied GPCR-mediated signaling pathway. Briefly, when a yeast is in the presence of mating pheromone, the yeast exhibits chemotropic growth toward their potential mate. This type of polarized growth requires precise tracking of the mating pheromone source and tightly regulated signaling to modulate directionality. This pathway has been investigated since the 1970s[24, 25]. However, little is known about Gα's contribution to the pheromone response[26-28] and, as evidenced by mammalian systems, the regulator of G-protein signaling (RGS) is likely to have several roles beyond Gα regulation[29, 30]. But, to understand the regulatory mechanisms of the pheromone response, one must first understand the basic signaling principles of the chemotropic growth in yeast.

1.2.1. An Overview of the Yeast Pheromone Response and Known Contributions of Gα to Signaling

Upon pheromone binding the receptor, a significant conformational shift occurs and the receptor engages the loosely bound Gα subunit to exchange the bound GDP for GTP and promote dissociation of the G-protein complex. Following activation there are three major pathways initiated by Gβγ. First, Gβγ recruits Ste5, the mitogen-activate protein kinase (MAPK) scaffold to the plasma membrane, which functions to recruit and scaffold all signaling components of the MAPK signaling cascade and improve signaling efficiency[31-34] – Ste5 and the MAPK signaling cascade is discussed in detail in section 1.2.2.. Second, Gβγ binds the p21 activated kinase (PAK), Ste20, which promotes MAPK scaffolding and signaling[35]. It is important to note that Ste20 activation requires binding of Cdc42 and the polar cap scaffold Bem1 to alleviate the autoinhibitory effects of the Ste20 CRIB-domain[36, 37]. Finally, Gβγ binds the cyclin dependent kinase inhibitor and Cdc42-GEF scaffold, Far1 to promote activation of

Cdc42[38, 39] (Figure 1.1.). Control of pheromone signaling initiated by Gβγ is clearly well investigated, however, Gα's role in the pheromone response is less well-understood.

The Gα subunit in the yeast pheromone response is canonically responsible for turning off Gβγ signaling. The 'off' signal is achieved when Gα-GTP is hydrolyzed to Gα-GDP, which promotes increased affinity for and reassociation with the Gβγ subunit. In addition to Gα regulation of Gβγ, Gα binds the MAPK, Fus3 and enhances its signaling[26]. However, less is known about Gα's role beyond these canonical functions. In the late 1990s, two studies from David Stone's group revealed a Gα-mediated negative regulation of the pheromone response. The first found that specific Gα mutants were hyper-adaptive to pheromone – turning 'off' the pheromone response faster than WT yeast, however the effect of these mutants were not characterized further[27]. The second paper described that Gα interacts with the phosphatase, Msp5, to partially reduce pheromone signaling[28].

In 2015, Dr. Kelley elucidated a mechanism in which Gα activity influenced cytoskeletal distribution while conducting his postdoctoral research in the Dohlman Lab. In this article, the authors perturbed the activity of the primary negative regulator of Gα, Sst2, and found that cells were unable to form normal mating projections[40]. Coincidentally, mating projection abnormality was to the distribution of specific cytoskeletal proteins called septins, which are discussed in detail in section 1.5..

1.2.2. The MAPK Signaling Cascade

The MAPK family of signaling molecules are involved in several signaling pathways and are characterized by several levels of regulation. First, MAPKs are kinases, meaning they phosphorylate other proteins. Once the MAPK signaling pathway is initiated, a signaling cascade begins. As I will explain in the following paragraph the first activated molecule in the cascade is the MAPKKKK which phosphorylates its substrate MAPKKK, which phosphorylates its substrate MAPKK, and finally MAPKK

phosphorylates MAPK. In yeast the MAPKs are Fus3 and Kss1 and are homologs to the human ERK proteins.

The MAPK scaffold Ste5 binds Gβ near the Ste20-PAK binding site[31-34]. Ste5 is recruited to Gβ complexed with Ste11-MAPKKK[41], which brings Ste11-MAPKKK to Gβ-bound Ste20-PAK, which phosphorylates Ste11-MAPKKK's N-terminal regulatory domain and activates its kinase catalytic domain. Ste50, an adaptor protein, also is bound to Ste11 and links the Cdc42-Ste20 complex to Ste11 to facilitate its activation[42, 43]. Once Ste11 is activated, it phosphorylates the activation loop of Ste7-MAPKK, which in turn phosphorylates Fus3 and Kss1, the two MAPKs. Ste5 binds and scaffolds the gambit of MAPK signaling partners, and by modulating their proximity, enhances signal transmission from the initial MAPKKK to the two MAPKs Fus3 and Kss1[44-51].

Further propagation of the signal is carried by the MAPKs, which are both proline-directed kinases, meaning they phosphorylate serine and threonine residues that are immediately followed by a proline. Once Fus3 and Kss1 are activated, they phosphorylate the transcription factor Ste12, and Ste12 repressors Dig1 and Dig2. Dig 1 and Dig2 repress Ste12 activity by directly binding to Ste12 when unphosphorylated[52, 53]. Although Ste12, Dig1, and Dig2 are substrates for the MAPKs Fus3 and Kss1, the crucial phosphorylation events for Ste12 activation are currently unknown.

Once Ste12 transcription is initiated, nearly 200 pheromone-specific genes are transcribed, many of which are upregulated at least two-fold in transcription[54]. Indeed, the genes upregulated in transcription include positive-feedback components, negative-feedback components, and cell-cell fusion genes essential for zygote formation[55]. In addition to upregulated genes, there are many genes that are transcriptionally repressed in the presence of pheromone, most of which are involved in cell division[54] (Figure 1.1). This makes sense due to the repression of the cell cycle and stall in G1 phase during pheromone-induced polarized growth.

1.3. Negative Regulation of Pheromone-Induced Signaling

Thus far I have discussed primarily positive regulation of the pheromone response via the MAPK signaling cascade. However, it is important to note that for yeast to properly establish a mating projection, they must also incorporate negative-feedback loops to promote signal desensitization. Additionally, negative regulation contributes to selectivity and directionality of polarized growth. In essence, without negative regulation of the pheromone response cells could not select the appropriate direction to begin polarized growth and their mating efforts would be futile. Therefore, I will discuss signal regulation and modulation in detail here.

1.3.1. The Regulator of G-Protein Signaling, Sst2

The regulator of G-protein signaling (RGS), Sst2, is the most important negative feedback mechanism in the yeast pheromone response[56]. Sst2 was the first discovered regulator of G-protein signaling (RGS) and was elucidated by Henrik Dohlman in 1996 in the lab of Jeremy Thorner[56]. I mentioned previously that the primary known role of Gα is inhibition of the Gβγ complex by sequestering it to the receptor; the RGS enhances this activity by accelerating the intrinsic GTPase activity of Gα[57]. This means that RGS helps to hydrolyze Gα-GTP to Gα-GDP, which promotes reassociation with the Gβγ subunit (Figure 1.2.).

The RGS is expressed at low levels during vegetative growth. However, upon pheromone addition it is transcriptionally enhanced by Ste12 and MAPK signaling during the pheromone response[58]. Pheromone-induced transcription of the RGS facilitates signaling modulation in the presence of increased Gα activity, but why expression of RGS in vegetative cells with no active pheromone signal?

There is evidence that basal levels of RGS may be required to turn-off spontaneous activation of the Gα[59], which would facilitate normal progression of the cell cycle in the absence of pheromone.

Modulation of RGS activity also contributes to its role in pheromone response regulation. The RGS is phosphorylated by Fus3-MAPK[58, 60], but little is known about the physiological outputs of these phosphorylation events. I will discuss in Chapter 2 of this dissertation a potential new mechanism for RGS activity during the pheromone response based on its phosphorylation state. Briefly, I found that RGS phosphorylation at Serine 539 is a critical post-translational modification during the early pheromone response and perturbation of this phosphorylation results in cytokinetic defects.

1.3.2. Endocytic Regulation of the Pheromone Response

The RGS is primarily a quick feedback mechanism. Conversely, long-term desensitization of the pheromone response is also necessary. I mentioned previously that without regulation of the pheromone response and directionality of polarized growth, the mating effort would be futile. In addition to that, cells must have a mechanism to turn off the pheromone response that acts more slowly in order to preserve pheromone adaptation over long-term exposure, and re-direct their energy and polarity machinery to asexual reproduction – budding.

In the yeast pheromone response, activation of the receptor drives the pheromone response through MAPK signaling. Therefore, removing receptor from the plasma membrane regulates the response at the highest level of the response. In yeast, clathrin-mediated endocytosis actively removes receptor from the membrane during the pheromone response[61] (Figure 1.2.). Unlike other cellular systems and unlike other GPCR targets, the pheromone receptor, Ste2, does not get recycled[62]. This means that upon internalization the receptor is destined for vacuolar degradation.

Once the receptor is activated by pheromone ligand, the receptor recruits two sister casein kinases, Yck1 and Yck2, that phosphorylate the C-terminus of the receptor[63]. This phosphorylation event

is crucial to endocytosis of the receptor. The newly phosphorylated C-terminus then recruits α-arrestins to facilitate Ste2 internalization and desensitization[63]. Following α-arrestin (Rod1, Rog3, and Ldb19) recruitment, the α-arrestins recruit the E3-ubiquitin ligase, Rsp5, to the receptor C-terminus promoting its ubiquitination. The ubiquitinated receptor then drives endocytosis through the endocytic adaptor proteins called epsins (Ent1 and Ent2)[64]. Epsins are a critical group of endocytic proteins because they not only attach to ubiquitinated receptor, but they also stabilize curvature of the endocytic pit via its interaction with actin and clathrin molecules[65]. Additionally, epsins are known to interact with the negative regulators of Cdc42, aptly named Cdc42 GTPase activating proteins (Cdc42-GAPs) – in yeast these are Bem3, Rga1, and Rga2[66]. The interaction of epsins with Cdc42-GAPs suggests that endocytosis has a significant role in establishing cell polarity.

In the C-terminus of the receptor there is a SINNDAKSS motif, which represents one of the most important sequences for post-translational modifications in the C-terminus[67] . Without this sequence the receptor does not internalize well[67]. Additionally, several studies have either truncated the receptor C-terminus, or generated point mutants along the C-terminus that result in reduced endocytosis, namely the T326 – a C-terminal truncation at the 326th codon just before the SINNDAKSS motif, and the 7KR – a point mutant rendering the 7 lysine residues of the C-terminus un-ubiquitinatable[68, 69]. These endocytic perturbations of the receptor result in hypersensitivity to pheromone and abnormal morphogenesis.

In addition to receptor internalization, the Gα component of the large G-protein is also internalized. Unlike the mammalian Gα subunits, the yeast pheromone response Ga (Gpa1), contains a ubiquitin-domain, which drives its internalization and vacuolar degradation like the receptor[70]. This phenomenon will become important in Chapter 3 of this dissertation where I discuss endocytosis as a driver of septin distribution.

1.3.3. Other Negative Regulators of the Pheromone Response

I have covered the primary negative feedback mechanisms in the previous sections, but I briefly want to mention the remaining negative regulators and signal "tuners". First, in the wild, yeast secrete mating pheromone into the environment to signal to other mating yeast. In order to fine-tune pheromone sensing, yeast secrete the protease Bar1 to degrade pheromone. This limits incoming signal to a confined space by removing signal from areas where the pheromone has become diffuse and not concentrated[71, 72]. Second, Fus3-MAPK promotes a signaling pathway that limits its own phosphorylation, though the mechanism is not yet known[73]. Third, several phosphatases – Ptp2, Ptp3, and Msg5 – dephosphorylate Fus3-MAPK and Kss1-MAPK to downregulate their signaling output[74, 75]. Fourth, protein degradation and turnover helps to reset the pathway. Both Ste11-MAPKKK and Ste7-MAPKK protein turnover is enhanced by pheromone[76-78]. Lastly, the Cdk-inhibitor Far1 regulates initiation of polarized growth. Specifically, Far1 activity stalls the cell in G1-phase to allow for pheromone-induced signaling to occur[79]. Without Far1 and its signaling partner, the Cdc42-GEF – Cdc24 – the pheromone response would not initiate[39]. The Far1-Cdc24 complex is one of the most essential feedback mechanisms for the pheromone response because it regulates the transition from normal cell division to pheromone response – which requires arrest in G1. The following section will describe the yeast cell cycle – with a focus on mitosis and the molecular basis of G1-arrest for the pheromone response.

1.4. The Yeast Cell Cycle

The yeast cell cycle is similar to that of mammalian cells with a slight difference. In yeast, the initial emergence of the daughter bud occurs almost simultaneously as the cell enters S-phase. Of course, in mammalian cells the cell divides evenly so it grows larger as a single cell and once components of the

cell have been distributed appropriately to each half, the cell begins to divide – making mitosis the timing of "bud emergence" in this case.

Put simply, the cell cycle is comprised of four main phases: 1) G1-phase, or the first growth cycle where yeast expand, initiate DNA synthesis, and the daughter cell bud emerges. 2) S-phase, or synthesis, is the phase in which DNA is duplicated. 3) G2-phase, or the second growth phase. Here the daughter cell also expands and recruits the nucleus to the bud neck (where the mother and daughter cell are connected) and initiates nuclear division and elongation of the mitotic spindle. Finally, 4) mitosis, where the cell segregates the nucleus and DNA contained within is distributed between the mother and daughter cells (Figure 1.3.).

1.4.1. Mitosis and Pheromone-Induced G1-Arrest

A critical component of the cell cycle is cytokinesis, the last step in mitosis where a dividing cell partitions cellular components into the mother and daughter cell. Additionally, this step in the cell cycle ensures appropriate inheritance of genetic material and cellular machinery to the daughter cell. The core machinery for this process is conserved from yeast to humans. During G1-phase, the bud-site for yeast is determined by the GTPase, Rsr1 and its polarization of Cdc42[80-84]. Cdc42 recruits several proteins including septins, actin and actin nucleators (e.g. formins), and myosin to the bud-site[85]. Septins are essential cytoskeletal filaments – described in the next section – that assemble as a ring during G1 at the bud-site, which promotes the recruitment of myosin to the septin collar during S-phase[86]. Once the cell has moved through G2 to the last step of mitosis, cytokinesis, the septin collar splits. At the center of the bud neck is the actomyosin ring, which constricts the bud neck during cell separation. The two septin rings are split between the mother and daughter cells[87]. The septins in this case provide stability to membrane curvature and act as diffusion barriers to prevent leakage of cellular components from one cell to the other. Once stabilized, the actomyosin ring constricts, the cells separate, and continue to G1.

In the presence of pheromone, cells that have not yet completed the cell cycle must first finish cell division prior to polarized growth. This is essential to reduce the prevalence of aneuploidy, or the unbalanced division of chromosomes during cell division. Once the cell has divided and entered G1 it may begin the pheromone response. One mechanism that drives completion of cytokinesis prior to initiating pheromone-induced polarization is discussed in Chapter 2 of this dissertation. However, I will not discuss that here.

Once in G1, a cell may respond to pheromone and initiate polarized growth. This is completely dependent on the cyclin-dependent kinase inhibitor, Far1[39, 79]. I have already described the role of Far1 in the pheromone response, but here I will provide a brief reminder. Upon pheromone stimulation, Far1 is recruited to free Gby and recruits the Cdc42-GEF, Cdc24. Additionally, Far1 promotes activity of the Ste20-PAK to initiate the MAPK signaling cascade. In order for this to occur, Cdk1 activity must be downregulated. After G2-phase, cyclins are destroyed and therefore Cdk1 activity is abolished[88, 89]. During this time there is increased transcription of the FAR1 gene – which is only further enhanced in the presence of pheromone[90-92]. Once the cell is in G1, the cyclin pool begins to re-establish and can then re-initiate Cdk1-driven cell division[89] . In the absence of Cdk1-activity, the pheromone response is initiated and Fus3-MAPK phosphorylates Far1, which recently was upregulated in expression. This phosphorylation event promotes an association with the cyclin, Cln2, the cyclin responsible for Cdc28 kinase activity – the regulator of Cdk1. While this phenomenon is known it is not well characterized. The most recent report suggests that Far1 interacts with at least one of the cyclins – in this case Cln2, but the nature of the interaction is unknown (i.e. phosphorylation or binding-based inhibition)[79]. It is likely that only a portion of the Far1 pool is used for this activity, especially once the cell's transcriptional machinery has re-focused to pheromone-induced gene expression and suppression patterns.

1.5. Septins and Their Contribution to Cell Division and The Pheromone Response

Septins are important for cell division. Moreover, septins are so important to yeast cell division that they are capable of dividing without the actomyosin ring as long as they have functional septins[93-95]. Additionally, the assembly of the actomyosin ring requires septins to recruit the necessary proteins to the cytokinetic furrow.

So, what are septins and what do they do in the pheromone response? And, how are septins deposited at the plasma membrane? I'll begin describing septins and their known roles in the pheromone response.

Septins are cytoskeletal filaments discovered in yeast and conserved across opisthokonts – a broad taxanomic term that encompasses the animal and fungi kingdoms[96-98]. They are comprised of two tetrameric protein assemblies to form an octamer. Each tetramer is the same sequence of proteins and are comprised of the septins Cdc3, Cdc10, Cdc11, and Cdc12; and in some cases the septin-like protein, Shs1, takes place of Cdc11. Septins are GTP-binding proteins, some of which also maintain GTPase activity and are nearly the same in structure to each other – except for their N-termini which are considered intrinsically unstructured domains. Each septin is comprised of a C-terminal extension, a Switch II loop, a guanine nucleotide binding pocket, a beta7/8 hairpin motif, and an α0-helix – or N-terminal extension. Septins can either bind at the NC-interface – where the N-termini and C-termini meet – or they can bind at the G-interface – where the guanine nucleotide binding pockets meet[99-102]. Septin tetramers are, in order, Cdc11-Cdc12-Cdc3-Cdc10; where Cdc11-Cdc12 are bound at the G-interface, Cdc12-Cdc3 are bound at the NC-interface, and Cdc3-Cdc10 are bound at the G-interface. Octameric sequences consist of two tetramers, connected at the NC-interface of the two Cdc10 septin monomers. Again, Shs1 can replace the outer Cdc11 monomers and these septin filaments can then organize and assemble into palindromic hetero-octamers called protofilaments[86, 103, 104].

Functionally, septins act as plasma membrane diffusion barriers and scaffolds for the recruitment of proteins including actin, myosin, and formins[86, 103, 104] during the cell cycle. Additionally in yeast, septins can also function in contractility during cytokinesis in the absence of the actomyosin ring[93-95]. However, septin roles during the yeast pheromone response are not well understood. Septins are known for their role in barrier function during cell division and it is thought that septins provide the same plasma membrane barrier function to restrict polarity proteins, such as the receptor, to the leading edge of the cell during polarized growth[105]. The last documented role for septin filaments in pheromone-induced polarization to date, was published by Kelley *et al.* in 2015. The authors found that RGS-activity in WT cells facilitated normal distribution of septins during the pheromone response. Therefore, in cells lacking RGS-activity – on Gα specifically – the cells were unable to shmoo, nor were they able to track a gradient of pheromone. Additionally, the authors note that septins are found on the inside edge of turns during gradient tracking, which suggests that septins drive directionality of pheromone-induced polarized growth[40].

I have expanded our knowledge about the control of septin distribution based on the results of Kelley *et al*. and have provided those results here in Chapter 3. Briefly, I found that it is the endocytic regulation of Gα during the pheromone response that drives septin deposition during the pheromone response. I also found that a specific signaling axis controlled by endocytic proteins controls the distribution of septins.

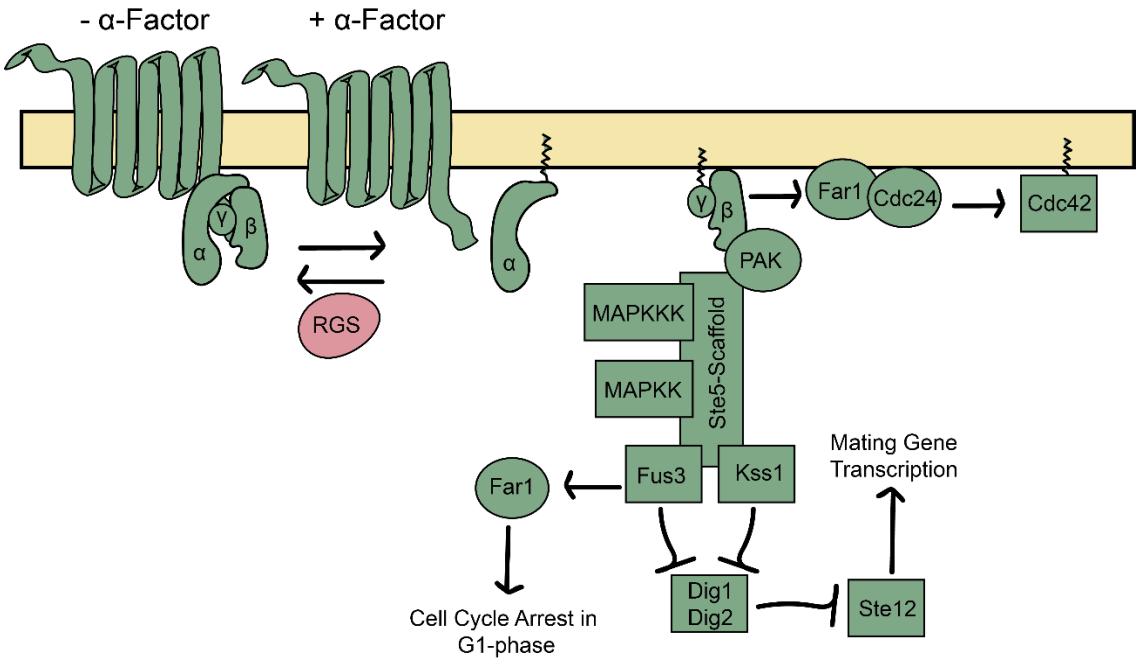

Figure 1.1. Schematic of Yeast Pheromone Response.

Schematic representation of the primary Gβγ signaling during the pheromone response. At left, the receptor is activated by the presence of α-Factor pheromone and promotes separation of the Gα and Gβγ subunits of the G-protein – the process is reversed by RGS activity on Gα. At right, the Gβγ subunit initiates 3 signals: 1) Recruitment of Ste20-PAK, 2) Recruitment of Ste5-MAPK Scaffold, and 3) Recruitment of Far1-Cdc24 complex. These signals enhance MAPK signaling, activate Far1-mediated cell cycle arrest in G1-phase, Ste12-mediated transcription of mating genes, and activation/polarization of Cdc42.

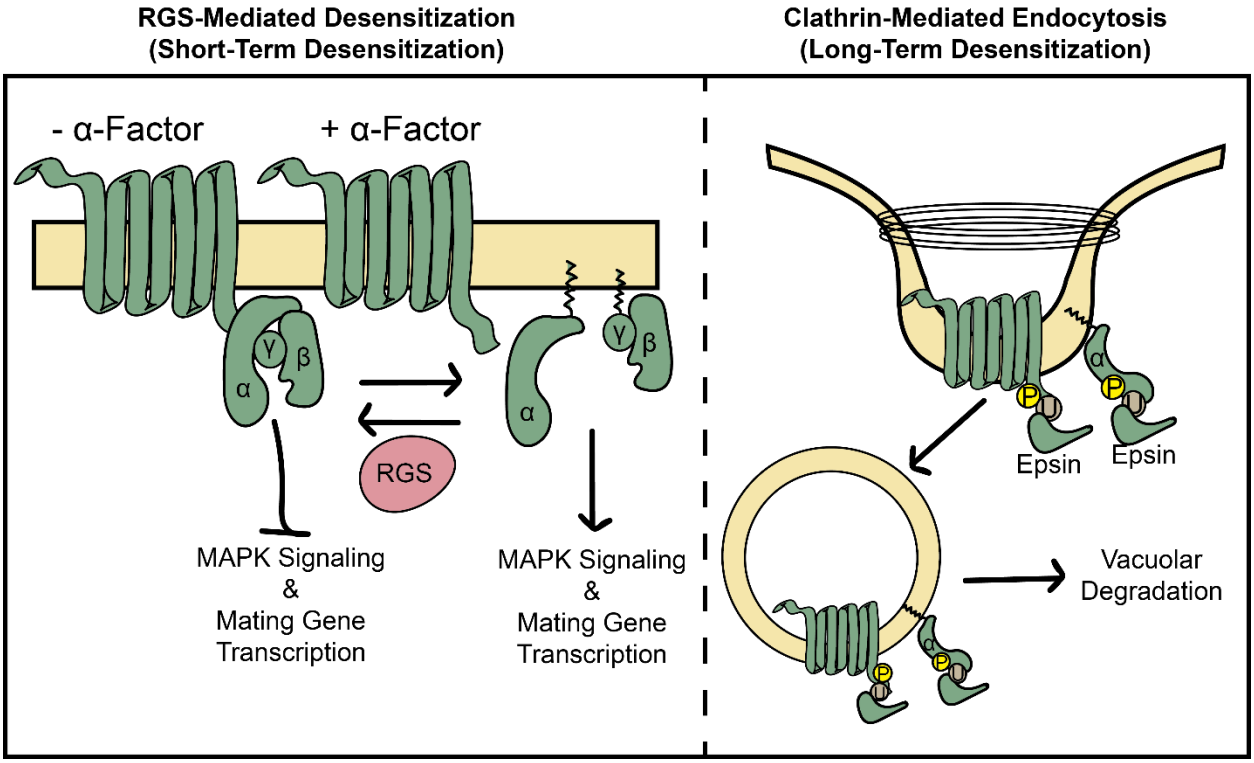

Figure 1.2. RGS promotes short-term desensitization and clathrin-mediated endocytosis promotes long-term desensitization of the yeast pheromone response.

At left, short-term and quick regulation of the pheromone response is accomplished through the RGS's enhancement of Gα's GTPase activity. Activation of the receptor induces dissociation of the Gα and Gβγ complex, MAPK signaling, and mating gene transcription. This process is readily reversible in the presence of RGS which enhances hydrolysis of Gα-GTP to GDP and inhibits MAPK signaling and mating gene transcription. At right, long-term signaling components (long-term = components not turned off by RGS) are phosphorylated and ubiquitinated, then recruited to clathrin-coated pits where they are endocytosed and trafficked to the vacuole for vacuolar degradation.

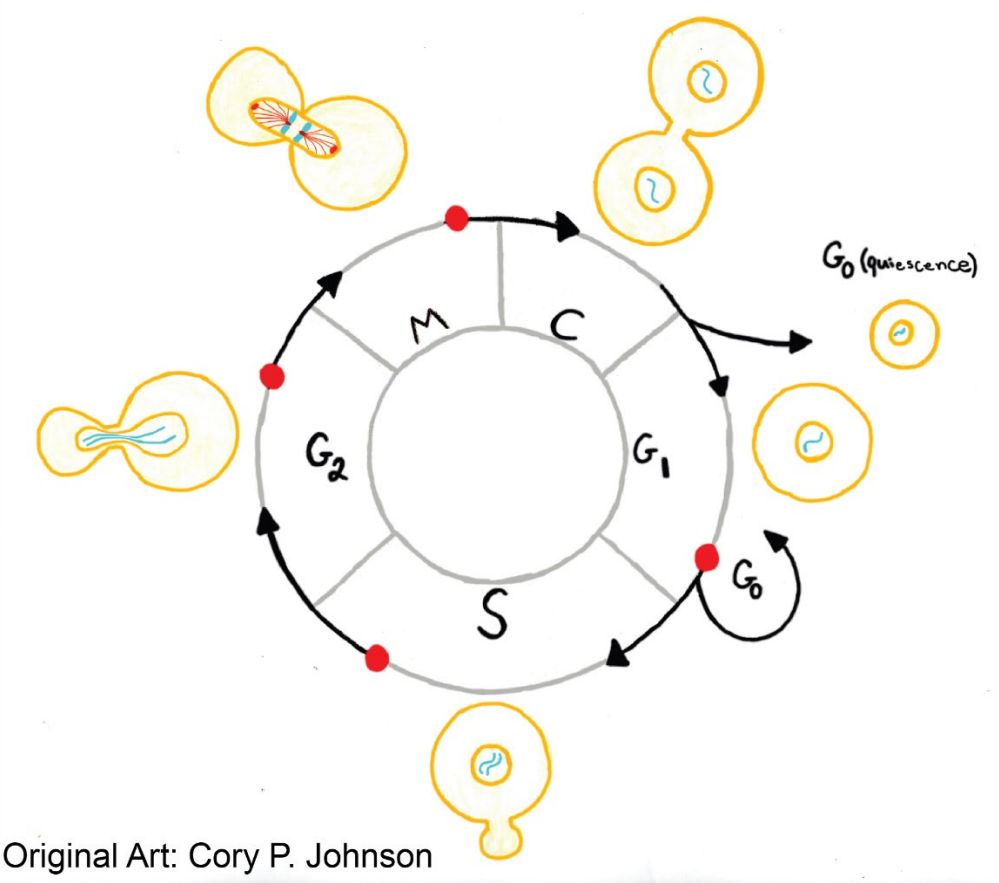

Figure 1.3. The yeast cell cycle.

The yeast cell cycle has four major steps: 1)G1-phase, 2) S-phase, 3) G2-phase, and 4) mitosis (mitosis is split into M-phase and C, or cytokinesis, the last step of the cell cycle). Upon initiation of S-phase the bud of the daughter cell has emerged, and DNA replication is initiated. Once DNA replication has completed and the cell enters G2-phase, the nucleus moves to the bud neck and the daughter cell expands. After G2-phase the cell enters mitosis where DNA (blue lines) and cellular components are distributed between mother and daughter cells by microtubules and other cytoskeletal components (red lines). Lastly, cytokinesis is the final step in mitosis and is when the mother and daughter cells separate. Each step has regulatory checkpoints (red dots) that must be passed to proceed to the next step in the cycle. In G1-phase, the cell can move out from G1 into a quiescent, or non-proliferative state called G0.

CHAPTER 2

DYNAMIC PHOSPHORYLATION OF RGS REGULATES THE SPATIAL DISTRIBUTION OF MAPK AND PROMOTES THE COMPLETION OF CYTOKINESIS DURING THE YEAST PHEROMONE RESPONSE

2.1. Abstract

Yeast use a G-protein coupled receptor (GPCR) signaling pathway to detect mating pheromone, arrest in G1, and direct polarized growth towards the potential mating partner. The primary negative regulator of this pathway is the regulator of G-protein signaling (RGS), Sst2, which induces Gα GTPase activity and subsequent inactivation of downstream signaling, including a MAPK cascade. The MAPK Fus3 phosphorylates the RGS in response to pheromone, but the role of this modification is unknown. We set out to examine the role of RGS phosphorylation during the pheromone response. We found that RGS phosphorylation peaks early in the pheromone response and diminishes RGS localization to the polarity site, while focusing MAPK localization at the polarity site. At later time points, levels of phosphorylated RGS decrease, and we find that unphosphorylatable RGS localizes to the polar cap and broadens the distribution of MAPK complexes relative to the Cdc42 polarity machinery. Surprisingly, we found that phosphorylation of the RGS promotes the completion of cytokinesis prior to pheromone induced growth. The completion of cytokinesis in the presence of pheromone is promoted by the formin Bnr1 and the kelch-repeat protein, Kel1, both proteins previously found to interact with the RGS, while the formin Bni1 promotes cytokinetic failure. We found that the RGS co-immunoprecipitates with Kel1, and that this complex prefers the unphosphorylatable mutant RGS. Overexpression of the unphosphorylatable mutant drives a higher frequency of cytokinetic defect, while overexpression of Kel1 rescues the cytokinetic

defect in the unphosphorylatable RGS mutant strain. Together, these data leads us to a model where unphosphorylated RGS binds to Kel1 and inhibits its function in delaying receptor-mediated polarity until completion of cytokinesis, but this is diminished by the feedback phosphorylation of the RGS.

2.2. Introduction

When cells receive signals to perform competing processes, they must integrate those two signals into a singular outcome. The budding yeast, *Saccharoymyces cerevisiae*, use a G-protein coupled receptor (GPCR) to detect and grow toward potential mating partners[106-108]. However, the cells must complete mitosis and arrest in G1 prior to mating projection morphogenesis (shmoo formation)[109]. This requires that the cell prioritize the signaling that will drive mitosis and cytokinesis to completion, and only after arrest in G1 can the cell allow the pheromone signaling pathway to commandeer the Cdc42 polarity machinery that has shared uses in both mitosis and pheromone-induced morphogenesis[110, 111]. While the mechanism by which G1 arrest occurs is understood, the mechanism responsible for suppression of receptor driven polarization is unknown.

The pheromone response can be thought of as a response of two G-proteins: the receptor-activated large G-protein consisting of the Gα (Gpa1) and Gβγ (Ste4/Ste18), which conveys information about where the pheromone receptor is active, and the small G-protein Cdc42, which controls actin cytoskeleton polarization and MAPK signaling[107]. The GPCR Ste2 activates the large G-protein, causing the Gα and Gβγ subunits to dissociate. Gβγ initiates Cdc42-mediated polarization of the actin cytoskeleton to form a mating projection. Gβγ also promotes the activation of the two yeast ERK homologs, Fus3 and Kss1[108]. Of these two MAP

kinases, Fus3 has pheromone specific roles: it is required for gradient tracking, arrest of the cell cycle in G1, and is scaffolded to the cell periphery by active Gα to regulate actin polymerization [112-116]. For this study we will only be concerned with Fus3 functions, and so all references to MAPK refer to Fus3.

The primary negative regulator of the pheromone pathway is the Regulator of G-protein Signaling (RGS), Sst2, [117] which serves as the GTPase activating protein (GAP) for the Gα subunit [57]. Upon hydrolyzing GTP, the Gα binds to Gβγ, turning off the pathway. RGS function is required for pathway inactivation and for the ability of the cell to track the pheromone gradient [118, 119]. GPCR signaling pathways play a central role in human disease, and so the elucidation of RGS signaling mechanisms by has the potential to inform understanding of human signaling pathways relevant for drug development [120-122].

The RGS Sst2 has characterized interactions with the Gα (Gpa1) subunit, the pheromone receptor (Ste2), and the MAPK (Fus3) [58, 60, 123, 124]. RGS serves as a GTPase activating protein for Gα, a function that is enhanced by its binding to the cytoplasmic tail of the receptor [57, 124, 125]. The MAPK Fus3 phosphorylates the RGS at serine 539 in a pheromone dependent manner, but this does not impact the sensitivity of the pathway or downstream MAPK or transcriptional outputs [58, 60].

In less well-characterized interactions, the RGS has been found in a yeast two-hybrid screen to interact with the formin Bnr1 and the formin regulatory protein Kel1 [126, 127]. Kel1 is a kelch-repeat containing protein which has been shown to act as a negative regulator of Bnr1, is required for efficient mating, and plays a role in the mitotic exit network [128-130]. Recently, Kel1

has been identified as a noise suppressor in the pheromone pathway [131]. We have previously found that the RGS suppresses noise in the pheromone pathway, and so this may indicate a shared function [125]. Bnr1 and Kel1 have clear roles in cytokinesis, but the potential for RGS interactions with Bnr1 and Kel1 during the pheromone response has not been pursued.

Here, we set out to determine the role of MAPK phosphorylation of RGS in response to pheromone. We found that RGS phosphorylation is dynamic, with high phosphorylation early in the response, followed by decreased phosphorylation later. Phosphorylation of the RGS decreases its localization to the polar cap, and reduces the distance between peak active Cdc42 and peak MAP Kinase localization. RGS phosphorylation peaks early in the pheromone response and promotes the completion of cytokinesis prior to the beginning of pheromone-induced polarity. We find that Kel1 also promotes cytokinetic completion in the presence of pheromone. Improper polarization prior to cytokinesis is dependent upon the formin Bni1, and suppressed by the formin Bnr1. We found that the RGS, Sst2, forms a complex with Kel1 during the pheromone response, and that overexpression of Kel1 rescues the cytokinetic defects seen in the unphosphorylatable RGS mutant.

2.3. Materials and Methods

2.3.1. Yeast Strains

Strains used in this study are shown in Table A.1.. Strains were constructed in the MATa haploid Saccharomyces cerevisiae strain, BY4741. Proteins were tagged with EGFP or mRuby2 at the native chromosomal locus through oligonucleotide-directed homologous recombination with using the primers listed in Table A.3.. For tagging Bem1 with Ruby, we created the

integrating plasmid pRSII-Bem1-yomRuby2-Kan (Table A.2.). Bem1 nucleic acids 522-1653 were cloned into pRSII405 [132] followed by link-yomRuby2 from pFA6a-link-yomRuby2 [133] using the primers indicated in Table A.3.. GFP tagging was generated by using pFA6a-link-yoEGFP-spHis5 Kan [133] or by amplifying the GFP cassette from the yeast GFP collection [134]. pFA6a-link-yomRuby2-Kan was a gift from Wendell Lim & Kurt Thorn (Addgene plasmid # 44953 ; http://n2t.net/addgene:44953 ; RRID:Addgene_44953). pRSII405 was a gift from Steven Haase (Addgene plasmid #35440; http://n2t.net/addgene:35440; RRID:Addgene_35440). All other plasmids are listed in Table A.3..

Sst2 phosphomutants were made by integrating the codon of interest with a PCR amplified CORE cassette[135]. Deletions were performed by first amplifying the genomic locus from the MATa haploid deletion collection (Dharmacon) with primers listed in Table 3 and transformed using a standard lithium acetate transformation [136].

Cells were grown in rich medium (YPD) or synthetic medium (SC) at 30°C unless otherwise indicated. PCR products were transformed into yeast strains using standard lithium acetate transformation procedure. Individual colonies were isolated by growth on standard selective media (SC leu-, SC ura-, SC his-,), selective media with 5-fluoroorotic acid (Zymo Research, Tustin, CA), or YPD selective media (YPD G418+). Transformants were verified using fluorescence microscopy, sequencing, and/or PCR.

2.3.2 Sst2-3xFLAG Plasmid Construction

The plasmids used for overexpression of Sst2 or Kel1 by the ADH1 promoter were constructed using the NEB Gibson Assembly Cloning Kit (NEB, E2611S) as advised by the manufacturer's

instructions. All plasmids were built using the pRSII416 vector backbone (Addgene, Plasmid #: 35456 [132]). The vector backbone was linearized with SacI-HF (NEB, R3156S) and ApaI (NEB, R0114S) restriction enzymes prior to Gibson assembly. Primers were constructed using the online NEBuilder assembly tool (v2.6.0, https://nebuilder.neb.com/) and are listed in Table A.3.. The forward and reverse 3XFLAG sequences were obtained from p3xFLAG-CMV-14 and synthesized as oligos for PCR amplification with primers in Table A.3.. The 1 kilobase of DNA upstream of the ADH1 was amplified from genomic DNA to provide the ADH1 promoter. All plasmids are listed in Table A.2..

2.3.3. Hydroxyurea Experiments

Yeast cultures were grown to an OD600 of 0.4-0.6 at 30°C and then pre-treated with 100 mM hydroxyurea (Alfa Aesar, Tewksbury, MA) for 2 hours at 30°C. After 2 hours of pre-treatment with HU, a saturating concentration of α-factor was added and cultures continued to incubate. Cultures were then fixed at 90 minutes and 240 minutes using an overnight ethanol fixation at -20°C. Following ethanol fixation, yeast were resuspended and washed twice in 50 nM sodium citrate buffer (pH 7.2). Next, the cultures were incubated with 20mg/mL RNase A (Thermo Scientific) for a minimum of 1 hour at 37°C. Following RNase incubation, proteinase K (Thermo Scientific) was added to the cultures at a final concentration of 0.4mg/mL and incubated at 55°C for a minimum of 1 hour then placed at 4°C overnight. For imaging, cells were pelleted, then washed and mounted in 1X PBS (pH 7.4). Cells were then imaged on the IX83 epiflourescent microscope (Olympus).

2.3.4. Spontaneous Cytokinesis Experiments

Yeast strains were grown in liquid synthetic complete media with 2 % dextrose (SCD) at 30 °C to an OD600 of 0.6 – 0.8. Cells were treated with 30 µM α-factor for 90 minutes. Cells then were fixed in 4 % paraformaldehyde, 2 % glucose, and 30 µM α-factor for 20 minutes. After fixation and 3 washes with 1 X phosphate buffered saline (PBS), the cells were stained with 7 µM Calcofluor White for 20 minutes and 50 µg/mL of Concanavalin A (both obtained from Biotium, Fremont CA) for 30 minutes. The cells were once again washed 3 times with 1x PBS and then imaged. Randomly chosen fields were imaged and then cells were scored for failed cytokinesis.

2.3.5. Antibody Production

The following peptides corresponding to the Sst2 amino acid sequence surround Serine 539 were synthesized by Genscript (Piscataway NJ), the phospho-Sst2 S539 peptide LHPH**S**PLSEC, where the **S** was phosphorylated, and the unphosphorylated peptide LHPHSPLSEC. The phospho-peptide was injected into rabbits by Cocalico Biologicals (Reamstown PA) according to their standard protocol. Antibody was affinity purified on phospho-peptide covalently bound to a SulfoLink column according to the manufacturer's instructions (Thermo Scientific).

2.3.6. Sst2 Phospho-State Western Blotting

Yeast cultures were grown overnight in 30°C. Cells were lysed with TCA buffer and protein concentrations were determined using DC protein assay kit (BioRad). Protein separation was performed with a 7.5% SDS-PAGE and transferred to nitrocellulose at 100 V for 90 mins. Primary antibody (1:1,000) and non-phosphopepetide (1:10,000) were incubated in 1% PBST blocking solution overnight followed by secondary antibody incubation (1:10,000) in 1% PBST

blocking solution for 1 hr. Band intensity was detected via Odyssey CLx imaging system (LI-COR) and then quantified using ImageJ.

2.3.7. Co-Immunoprecipitation of Kel1-GFP and Sst2-3xFLAG

Cells expressing Kel1-GFP and transformed with pRSII416-based plasmids overexpressing Sst2-3XFLAG, $Sst2^{S539A}$-3XFLAG, or $Sst2^{S539D}$-3XFLAG (Table S2) were grown to an OD600 of 0.2-0.8 in Synthetic Complete -Leucine media at 30°C. Cells were then treated with 10µM pheromone for 1hr shaking at 30°C. Pheromone-treated cells were immediately placed on ice then centrifuged at max speed in an Eppendorf 5420R (Eppendorf) swinging bucket centrifuge for 5 minutes at 4°C and supernatant was subsequently aspirated. Cell pellets were resuspended in 1pellet-volume lysis buffer (10mM Tris pH 7.4, 150mM NaCl, 0.5mM EDTA) containing 1X HALT protease inhibitor (ThermoFisher, 78429) and 1X phosphatase inhibitor (Alfa Aesar, J61022.AA) and transferred to a reinforced screw-cap tube (Fisherbrand, 15-340—162) containing 100µL acid-washed glass beads (Sigma, G8772). Cells were homogenized using a Bead Mill 4 homogenizer (Fisher Scientific) at max speed for 3x40 second rounds with 60 second rest cycles on ice. Homogenization was conducted at 4°C. After homogenization, Triton X-100 was added to the whole-cell lysate to a final concentration of 0.5% and followed by a 30-minute rotating incubation at 4°C. After incubation, whole-cell lysate was transferred to a 1.5mL tube and centrifuged at max speed for 20 minutes at 4°C. The resultant supernatant was transferred to a final tube and kept on ice. Protein concentration was determined using a DC Protein Assay kit (Bio-Rad) and assay was conducted in triplicate using a Biotek Synergy 2 plate reader (Biotek).

Following the protein assay, GFP-Trap Magnetic Particles M-270 (Chromotek) were washed 3-times with IP Lysis Buffer containing protease and phosphatase inhibitors and raised in 100uL IP

Lysis Buffer containing 200µg protein lysate. GFP-Trap particles were incubated for 1hr at 4°C on a rotator. GFP-trap particles were washed 3-times with lysis buffer containing protease and phosphatase inhibitors, then bound proteins were solublized in 2X Laemmli sample buffer. Input samples containing whole-cell lysate were made with 20 µg total protein in 1X sample Laemmli. Samples were boiled for 5 minutes at 95°C, allowed to cool to room temperature, and spun at max speed for 1 minute using an Eppendorf 5424 centrifuge (Eppendorf).

Protein separation was performed using 8% SurePAGE Bis-Tris gels (GenScript) and MOPS buffer followed by transfer to low fluorescence PVDF membranes using Towbin Transfer Buffer containing 0.1% SDS at 100V for 150 minutes on ice. Membranes were incubated in Ponceau S (Fisher BioReagents, BP103-10) on a rocker for 5 minutes at room temperature then washed with a 10% acetic acid solution rocking for 10 minutes prior to imaging. Membranes were blocked with a 5% milk solution in PBS-T (1X PBS+0.1% Tween-20) for 1hr at room temperature. Membranes were then incubated overnight at 4°C in a 1% milk solution in PBS-T containing 1:1,000 Rabbit anti-GFP (Cell Signaling, 2956S) and 1:1,000 Mouse anti-M2-FLAG (Sigma, F1804). Following overnight primary antibody incubation, membranes were washed 3 times with PBS-T for 5 minutes each and incubated with 1% milk in PBS-T containing 1:5,000 Donkey anti-Rabbit 800 CW (LiCor, 926-32213) and 1:5,000 Donkey anti-Mouse 680 RD (LiCor, 926-68072) secondary antibodies for 1hr at room temperature. Finally, membranes were washed 2 times with PBS-T for 5 minutes and once with PBS for 5 minutes prior to imaging using at 42µm resolution and “High” quality settings on a Li-COR Odessey CLx imaging system (Li-COR Biosciences). Quantitation of integrated density was conducted using FIJI’s gel analysis tool. The fraction of GFP-Trap bound Sst2-3XFLAG was normalized to the input fraction. Data from 8

replicate experiments were averaged and error bars were constructed by bootstrapping the 95% confidence interval in MATLAB. Statistical significance was assessed by bootstrapping the 95% confidence of a non-zero difference in means.

2.3.8. Agarose Pad Imaging

Yeast were imaged on an Olympus IX83 with a 60X-TIRF 1.49 NA objective, a Photometrics Prime95b camera, X-Cite LED 120 Boost fluorescence light source (Excelitas), and filters for DAPI and GFP (Semrock). Cells were grown to mid-log phase (OD600 = 0.1 to 0.8) at 30°C in Synthetic Complete Media with 2% dextrose (SCD) and then imaged on pads made of 2% agarose in SCD, as the use of agarose leads to lower autofluorescence than standard agar pads. Imaging was performed with an objective heater (Bioptechs) set to 30°C. Cells were pelleted and then resuspended in SC with 3uM α-factor and placed on an agarose pad as above.

2.3.9. Microfluidic Experiments

Microfluidic devices were made by using a Silicone polymer poured onto a microfluidics device mold [137] fabricated by UMaine FIRST. SYLGARD 184 Silicone Polymer was mixed at a ratio of 10:1, part A to part B, using a glass stirring rod to mix (Dow). Mixed polymer was poured onto the device mold and placed in a vacuum chamber for 1hr. After all air bubbles were removed, the mixture was placed in an oven at 80°C for 1hr. After cooling to room temperature, devices were cut out using a razor and ports were punctured using an 18g Leuer stub. Prepped devices and coverslips were cleaned by spraying with methanol, ethanol, then water, and dried using an air hose. Devices and coverslips were exposed to oxygen plasma for 45 seconds in a Harrick Plasma PDC32G Cleaner followed by fusion of the device to the cover slip.

Cultures were grown in SC to an OD600 between 0.1–0.8 at 30°C. Live-cell microfluidics experiments were performed using an IX83 (Olympus, Waltham MA) microscope with a Prime 95B CMOS Camera (Photometrics) controlled by Cell Sens 1.17 (Olympus). Fluorescence and Differential Interference Contrast (DIC) images were acquired using an Olympus-APON-60X-TIRF objective. Z-stacks of GFP and RFP images were acquired using an X-Cite 120 LEDBoost (Excelitas). Cells were imaged in a microfluidic device based on the Dial-a-wave design that allows for the rapid switching of media while holding the yeast in place (Bennett 2008, Dixit 2014)[137]. Pheromone addition was verified using AlexaFluor 647 dye (Life Technologies) imaged with a single plane image. Cells were imaged at 20 min intervals for 12 hours for 300nM experiments and 5 min intervals for 0-150nM experiments. Confocal microscopy was conducted on a Leica DMi8 (Leica) imaging platform equipped with an automated stage, SP8X white light laser (capped at 70% of total power), an argon laser (Leica Microsystems Buffalo Grove, IL). All imaging was conducted using HyD hybrid detectors. Imaging settings were determined based on experimental needs and were replicated for repeat experiments.

2.3.10. Image Analysis

Images were deconvolved using Huygens Software (Scientific Volume Imaging, Hilversum, Netherlands) Classic Maximum Likelihood Estimation (CMLE) Deconvolution Algorithm. Masks of cells were made using ImageJ [138] and data analysis was performed using MATLAB (MathWorks, Natick, MA). To quantify the fraction of protein localization over time, MATLAB was utilized as described in Figure 2 and previously [139, 140]. The fluorescent intensity of each fluorescent protein was extracted over time using a line width of 5 pixels. Peak Bem1 was used as a reference to normalize the spatial distribution of proteins of interest in relation to the

polar cap. This was done by setting peak Bem1 as the midpoint and shifting the protein of interest in the same manner. For profiles reporting fraction of protein at each position, fluorescence was normalized by subtracting the minimum value from each line-scan, followed by normalization of the subtracted data to sum to one. The normalized fluorescence intensity was plotted at each point along the cell periphery with shaded regions showing 95% confidence intervals derived by bootstrapping with 10000 resamplings. Statistical analysis was performed between profiles using a sliding one-way ANOVA and Tukeys honestly significant difference (HSD) test followed by false discover rate adjustment with the MATLAB *mafdr()* function with p values <0.05 denoted as significant. Where indicated, a pairwise Kolmogorov-Smirnov test was performed using the MATLAB *kstest2()* function. When excluding nuclear fluorescence from Fus3-GFP images, we modified the "granulinator" script [141] to select nuclei for removal. We used cell masks to calculate fluorescence histograms for each cell and adjusted the size (minimum size of 25 pixels) and threshold (1 standard deviation above mean) cutoffs to detect nuclei but not polar caps.

2.4. Results

2.4.1. Cells Track a Gradient of Pheromone Independent of Phosphorylation at Ser 539

The ability to track a gradient of pheromone is dependent upon RGS, specifically its GTPase activating protein (GAP) function [118, 125]. While previous studies found that GAP activity was not affected by S539 phosphorylation, we hypothesized that phosphorylation might change Sst2 function in time or space in a way that affects gradient tracking [58]. We tested this hypothesis by using strains expressing an unphosphorylatable RGS mutant (*sst2*^{S539A}, denoted

~~p~~RGS) and phospho-mimetic RGS mutant (*sst2*^{S539D}, denoted p*RGS) from the endogenous SST2 genomic locus, each fused to GFP. As a marker of the polar cap, we used the Cdc42-GTP binding protein Bem1, a common polar cap marker [139], fused to mRuby2. These strains were examined in a microfluidic gradient chamber by live cell microscopy [137]. We exposed these cells to a 0-150 nM gradient of pheromone and measured their ability to grow toward the source of pheromone (Figure 2.1.). Both phospho-mutant strains were able to track a gradient of pheromone (Figure 2.1B.). Thus, feedback phosphorylation of RGS has no effect on gradient tracking.

2.4.2. RGS Localization is Regulated by Its Phosphorylation State

Since GAP activity is unchanged, we hypothesized that it may be the spatial distribution of the RGS that is controlled by MAPK phosphorylation. To test this, we again used the p*RGS (*sst2*^{S539D}) and ~~p~~RGS (*sst2*^{S539A}) mutants tagged with EGFP, as well as Bem1-mRuby2 for polar cap localization. Cells were exposed to saturating pheromone (300 nM) in the microfluidic chamber as above. To examine the distribution of the RGS along the periphery of the cell, we used our previously reported approach of spatial normalization to the polar cap [139, 140]. Briefly, the signal of RGS along the periphery of the cell is spatially registered to the center of the polar cap as identified by peak Bem1 signal, and then averaged to generate a distribution of the protein during the pheromone response (Figure B.1.) [139]. Fluorescence intensity was normalized to sum to 1, so that the values shown indicate the average fraction of protein found at that position relative to the center of the polar cap.

We found that WT RGS localizes to both the polar cap and to the periphery of projections where septins would be, consistent with our previous findings (Figure 2.2A-B.) [125,

[139]. Quantitation shows that the phospho-mimetic p*RGS mutation diminishes RGS localization to the polar cap (Figure 2.2C-D.). In contrast, the ~~p~~RGS mutation leads to a small but statistically significant increase in association with the polar cap. The similarity between the profiles of WT and unphosphorylatable ~~p~~RGS suggests that much of the RGS measured in WT cells may be in the unphosphorylated form (Figure 2.2C.). When we examined changes in RGS distribution using an averaged 3D-kymograph (Figure 2.2D.) WT and mutant RGS fluorescence increases throughout the time course as expected, which is due to persistent pheromone-induced production of RGS [56].

2.4.3. RGS Phosphorylation Alters the Distance Between the Polar Cap and the Gα-MAPK Complex

We hypothesized that the phospho-dependent changes in RGS localization would lead to corresponding changes in the localization of active Gα. While Gα is localized across the membrane [70], its localization alone does not indicate activation state. However, active Gα is known to recruit active MAPK [112], forming a Gα-MAPK complex that activates the formin Bni1 and promotes gradient tracking [112, 116, 142]. We therefore hypothesized that we could monitor the localization of the Gα-MAPK complex as a proxy for the activation state of Gα.

To test the use of MAPK as a marker for active Gα, we examined a GFP tagged MAPK (Fus3-GFP) in wild type cells, and two mutants with opposing effects: a Gα mutant that does not bind MAPK, *gpa1*$^{E21\,E22}$ [112]; and a Gα mutant that is hyperactive because it no longer interacts with the RGS, *gpa1*^{G302S} (Figure 2.3A.)[123]. In all cells, MAPK localizes to the nucleus and to the polar cap (Figure 2.3B.). In the *gpa1*^{E21E22} mutant that cannot bind MAPK, there was a marked decrease in association with the polar cap, although at later time points, it appeared at the polar cap more often, potentially through an interaction with a different binding partner

(Figure 2.4D.). In the hyperactive *gpa1*^{G302S} mutant, MAPK levels consistently increased and there were often multiple discernable spots of MAPK accumulation (Figure 2.3B.). We assessed MAPK levels along the periphery of the cell in these strains using the same techniques as above, with the exception that the nuclei were masked to exclude nuclear signal from our measurements of the periphery (Figure 2.4C.). We found that If the quantitation was performed with the nuclear signal present, the nuclei were frequently close enough to the periphery of the cell to create spikes in signal ~1-2 μm from the center of the polar cap. To solve this problem, nuclear masks were generated by using single cell histogram analysis of the Fus3-GFP signal and removing large objects that were more than 1 standard deviation above the mean, an adaptation of an algorithm we designed to detect granules [141]. With this approach we were able to use the Fus3-GFP signal to identify 86.7% of nuclear pixels from a control with the nucleus marked by Hoechst stain (Figure B.2.). When examining the shapes of the protein distributions, it is clear that WT cells have the sharpest distribution of MAPK with respect to the location of the polar cap. Both loss of MAPK binding and excess binding of MAPK broadened its distribution (Figure 2.3E.). We believe the distribution of signal in the Gα MAPK-binding mutant (*gpa1*^{E21E22}) likely represents the profile of the remaining MAPK binding partners at the polar cap (Figure 2.3D.). Fus3 binds to the MAPK scaffold Ste5, and the polar cap is populated with many MAPK substrates [115, 143]. We conclude that MAPK localization is measurably affected by binding to active Gα.

Having determined that MAPK localization is affected by its association with active Gα and that RGS localization is altered by phosphorylation, we next examined whether phosphorylation of the RGS affects the distribution of the MAPK, which is predominantly

associated with Gα present at the periphery (Figure 2.3D.). We generated strains expressing fluorescent-protein fusions of the polar cap marker (Bem1-mRuby2) and MAPK (Fus3-EGFP) in the presence of the phospho-mimetic and unphosphorylatable RGS mutants. We then imaged those strains in a microfluidic device in the presence of 300 nM pheromone for 12 hours, as above.

In both RGS mutants, the presence of MAPK at the cell periphery was much more pronounced than we observed in WT cells (Figure 2.3B. vs 2.4A.). This consistently high signal is evident in the decreased noise in the kymographs (Figure 2.3D., 2.4B.). We see that the unphosphorylatable ~~p~~RGS mutant (*sst2*^{S539A}) shows a distinct peak at the center with a local minimum peripheral to the peak (Figure 2.4B-C.). These local minima are also readily visible in the average distributions (Figure 2.4C.), where the unphosphorylatable ~~p~~RGS mutant (*sst2*^{S539A}) displays a very similar average MAPK distribution to WT (Figure 2.5C.) with a peak at the center, and local minima 1-2 µm from the center. The p*RGS (*sst2*^{S539D}) however, displayed an enrichment of MAPK at the polar cap (Figure 2.5C.), and decreases steadily toward the edge without the local minima next to the peak seen in the WT and ~~p~~RGS (Figure 2.4B-C.).

There are two potential explanations for these changes in MAPK distribution: 1) a change in the absolute distribution of MAPK at individual times; or 2) MAPK distribution is unchanged, but has a different spatial relationship with the polar cap. To assess these possibilities, we examined the distribution of MAPK (Fus3-GFP) spatially normalized to itself instead of Bem1 (Figure 2.5A.). This shows the shape of MAPK localization at any given time in the cell. We see very little difference in the distribution of MAPK in both phospho-mutants

when compared to WT RGS (Figure 2.5A.). Although the changes are statistically significant, they are not large enough to account for the changes in the MAPK localization relative to the polar cap seen in Figure 4. If MAPK has the same shape within the cell under these different conditions, then the offset of this shape relative to the polar cap is changing (possibility 2 above). To test this, we examined the distribution of the maximum and minimum MAPK intensity relative to maximal polar cap intensity (Figure 2.5B.). The localization of the maxima appears to recapitulate the average distributions in Figure 2.4C., with the phospho-mimetic p*RGS leading to much more frequent MAPK localization to the polar cap. Perhaps more surprising is the distribution of the minima. In WT cells, the most common place to have a minimum intensity of MAPK is immediately proximal to the center of the polar cap, peaking approximately 1 um away (Figure 2.5B.). In the unphosphorylatable ~~p~~RGS mutant, the minima are again proximal to the center of the polar cap, however they are closer than in WT, peaking at 0.3 to 0.5 µm from the center. In the phosphomimetic p*RGS cells the minima appear to be much more evenly distributed across the membrane. This suggests an RGS-dependent negative feedback to MAPK proximal to the polar cap that is disrupted by the phosphorylation of the RGS.

We then plotted the cumulative distribution of the distance of maxima and minima from the polar cap. This is effectively measuring the offset along the membrane between Bem1 and Fus3, which bind, respectively, active Cdc42 and active Gα. We find that 50% of MAPK maxima for WT and ~~p~~RGS fall within ~ 2.3 µm of the polar cap peak, while 50% of MAPK maxima in the p*RGS fall within ~1.5 µm of the polar cap peak (p-values calculated using pairwise Kolmogorov-Smirnov tests). We provide some example images of the localizations of

the maximum Bem1 and Fus3 in Figure 2.5D.. In examining where there is a large offset between the polar cap and MAPK, it most often appears in those situations where the MAPK intensity at the polar cap is low, and therefore other sites along the periphery may be maximal without a significant accumulation of MAPK. Thus, unphosphorylated RGS drives a greater distance between the polar cap and MAPK, and based on their binding partners, active Gα and active Cdc42.

When examining the minima (Figure 2.6C.) in the unphosphorylatable ~~p~~RGS we have drawn attention to the 25th percentile mark, as approximately 25% of minima in WT occur within 1 μm, corresponding to the WT peak of minima identified in Figure 6B. In the unphosphorylatable ~~p~~RGS mutant, 25% of minima occur within ~0.6 μm, while in the phospho-mimetic p*RGS, 25% of minima occur within 1.2 μm. The difference in the distributions of the minima are statistically significant between all three strains, and recapitulate our summary of Figure 5B. We conclude that the phosphorylation of the RGS likely disrupts a negative feedback event targeted proximal to the site of polarity.

2.4.4. RGS Phosphorylation Peaks Early in the Pheromone Response and Diminishes at Later Time Points

Previous characterization of the phosphorylation of Sst2 at serine 539 showed Fus3-dependent phosphorylation at one-hour of pheromone treatment [58]. Our results suggest that much of the RGS we are quantifying is unphosphorylated RGS, as the ~~p~~RGS mutant routinely looks more like WT than the p*RGS. This led us to hypothesize that Sst2 phosphorylation at S539 may be dynamic: peaking earlier in the response and decreasing at later times. To test the dynamics of phosphorylation, we developed a rabbit polyclonal antibody to detect Sst2 phosphorylated on

serine 539, LHPH**S**PLSEC, where the underlined serine is phosphorylated. Western blotting of Sst2-GFP versus untagged Sst2 shows a GFP-dependent size shift in the detected band, indicating that the antibody is specific for Sst2 (Figure B.3.). Western blotting is done in the presence of excess unphosphorylated peptide to ensure that it is specific for the phospho-epitope.

To determine the dynamics of RGS phosphorylation, we treated *SST2-GFP* with pheromone and took samples every hour for four hours. We find that phosphorylation of the RGS peaks between 1 and 2 hours consistent with the literature [58], but phosphorylation levels decrease to lower levels by four hours post pheromone treatment (Figure 2.6A-B.). A complication of examining a decrease in pheromone-driven signaling is the desensitizing role of the protease Bar1, which degrades pheromone [144]. However, we find this decrease is independent of Bar1 activity (Figure A.3.). Decreasing levels of phospho-RGS suggest that the role of the phosphorylated form of the RGS may be more important earlier in the pheromone response.

2.4.5. Phosphorylation Promotes Coordination of Cytokinesis with the Pheromone Response

Cells which have already left G1 must complete mitosis and cytokinesis prior to polarizing and forming a mating projection in response to pheromone. We found that some mother-daughter pairs in our unphosphorylatable ~~p~~RGS mutant (*sst2*^{S539A}) formed mating projections before they had finished cytokinesis (Figure 2.8A.). The frequency of the event was low and we never observed these defects in wild type cells or cells expressing the phosphomimetic mutant during microfluidics experiments. Previous studies have found genetic interactions between the RGS and two proteins involved in cytokinesis, Bnr1 and Kel1 [126, 127].

Both of these proteins play a role in mitosis, Bnr1 through the regulation of actin polymerization at the mitotic septin ring and Kel1 through promoting the mitotic exit network (MEN) [145-149]. Additionally, Kel1 serves as a negative regulator of Bnr1, and may impact cytokinesis through that role as well [128]. Therefore, we hypothesized the cytokinetic defect may be mediated through interactions with these proteins.

We examined *bnr1Δ* and *kel1Δ* cells responding to saturating pheromone and found that *kel1Δ* cells also occasionally fail to complete cytokinesis prior to responding to pheromone (Figure 2.8A., negative data for *bnr1Δ* not shown). These were both rare events and our microfluidic experiments do not contain large numbers of yeast, so we grew wild type, ~~p~~RGS, and *kel1Δ* yeast in culture, treated with saturating pheromone, and counted the frequency of cells with failed cytokinesis based on visual inspection for conjoined yeast responding to pheromone by DIC imaging. We found that both mutants lead to rates of failed cytokinesis of ~3-4% (Figure 2.7B., minimum of 1350 cells per strain). From this, we conclude that both Sst2 and Kel1 are both involved in a mechanism that ensures cytokinesis finishes prior to the pheromone response.

The rate of spontaneous cytokinetic defects under ideal growth conditions is relatively low. Thus, we took advantage of hydroxyurea (HU) to damage DNA and cause stalled cytokinesis [150], forcing cells to contend with the competing signals of receptor mediated polarity and an unresolved cytokinetic furrow. To test the role of phosphorylation of the RGS in promoting cytokinesis, we pretreated with 100 mM HU for two hours followed by treatment with pheromone (10 μM) while maintaining HU (Figure 2.7C.). We then examined cells after

four hours of pheromone treatment to assess polarized growth and cytokinesis. We found that WT cells frequently stalled cytokinesis with two round cells joined at the bud neck. We scored phenotypes as a normal response if the cells showed evidence of completing cytokinesis prior to undergoing polarized growth, if they arrested as a mother daughter pair with no evidence of polarized growth, or if they had completed cytokinesis and began mating projection formation (Figure 2.7D-E.). In cells with the unphosphorylatable ~~p~~RGS, we found more cells that had both failed cytokinesis and began polarized growth in one or both the mother and daughter cells. A particularly striking phenotype involves one cell remaining round, while the other shows hyper-polarized growth, which we refer to as asymmetric hyperpolarized growth (Figure 2.8F.). The asymmetric hyperpolarized growth was suppressed by the phospho-mimetic p*RGS mutant ($sst2^{S539D}$). Data sets with non-overlapping 95% confidence intervals are statistically significant for p = 0.05 (Figure 2.7F.). Both phospho-mutants have overlapping confidence intervals with the WT, which does not preclude a statistically significant difference. To compare these, we bootstrapped the confidence interval of the difference in means between each phospho-mutant strain and the wild-type strain. We then checked whether the 0 mean difference fell within the 95% confidence interval. If a difference of 0 falls outside of the 95% confidence interval, we reject the null hypothesis and determine that the difference is statistically significant with a cutoff of p = 0.05. The differences in hyperpolarized growth between WT and the phospho-mimetic p*RGS were not statistically significant, but the increase in hyperpolarized growth in the unphosphorylatable ~~p~~RGS mutant compared to WT was statistically significant.

When we examine *kel1Δ* cells under these conditions, we find that the asymmetric hyperpolarized growth is a dominant phenotype (Figure 2.8G.). Thus, unphosphorylatable ~~p~~RGS partially phenocopies the loss of Kel1 function. This suggests that phosphorylation of RGS promotes a Kel1 dependent mechanism that prevents the mating pathway from commandeering the polarity machinery prior to the completion of cytokinesis.

Kel1 has been identified as a negative regulator of the formin Bnr1 [128]. Yeast have two formins: Bni1 is associated with the polar cap and is activated by Cdc42 and the Gα/MAPK complex [151]. Bnr1 is associated with mitotic septin structures and has no known role in the pheromone response. Given the central role that formins play in both mitosis and the pheromone response, we hypothesized that the formins may facilitate the coordination of cytokinesis and the beginning of pheromone induced polarized growth. We performed the same experiment as above, inducing cytokinetic defects with hydroxyurea followed by pheromone treatment, and assessed the ability of cells lacking either Bni1 or Bnr1 to prevent pheromone induced polarization prior to the completion of cytokinesis. Deletion of Bni1 largely stopped polarization of cells prior to completion of cytokinesis, and completely abrogated the asymmetric hyper-elongated phenotype (Figure 2.8E-G.). Deletion of Bnr1 resulted in increased polarization prior to the completion of cytokinesis and increased levels of asymmetric hyper-polarized growth (Figure 2.8E-G.). The asymmetric hyper-elongated growth phenotype is clearly dependent upon Bni1 and inhibited by Bnr1. Thus, coordination of pheromone induced polarity with the completion of cytokinesis is promoted by Bnr1 function and antagonized by Bni1.

2.4.6. The RGS Forms a Complex with Kel1 That is Enhanced by the Unphosphorylatable S539A Mutant

The above cytokinesis experiments show that Kel1 is important for the completion of cytokinesis prior to pheromone-induced polarity. The unphosphorylatable RGS ($sst2^{S539A}$) shows a dominant negative effect on cytokinesis, but with far less penetrance than Kel1 deletion. While Kel1 has been found to interact genetically with Sst2 through yeast-two-hybrid, this has not been examined biochemically. To test whether the RGS forms a complex with Kel1, we generated cells expressing Kel1-GFP from the KEL1 genomic locus and a 3x Flag tagged RGS from the ADH1 promoter from a plasmid (pRSII 416). The expressed RGS was either WT RGS (Sst2-3XFlag), ~~p~~RGS ($sst2^{S539A}$-3XFlag), or p*RGS ($sst2^{S539D}$-3xFlag). Cells were treated with pheromone for 1 hour and lysed using a bead homogenizer. Kel1-GFP was immunoprecipitated using GFP-trap M270 magnetic resin. We performed SDS-PAGE and western blotting on the immunoprecipitated sample and probed for the RGS with anti-Flag antibody. We found that all forms of the RGS co-immunoprecipitated with Kel1 (Figure 8A), but that we consistently recovered less of the phospho-mimetic mutant (Figure 2.8B.).

Together, these data suggest the following hypothesis: Free Kel1 promotes proper cytokinesis, and unphosphorylated RGS binds to Kel1, inhibiting its function, while phosphorylation of the RGS relieves its inhibition of Kel1 (Figure 2.8C.). This hypothesis would suggest that higher levels of the RGS would be more detrimental to cytokinesis, while higher levels of Kel1 would be predicted to rescue the defects induced by the unphosporylatable ~~p~~RGS (Figure 2.8C.).

We tested the overexpression of WT and phospho-mutant RGS using the ADH1 promoter driven Sst2-3xFlag plasmids described above in the HU/pheromone experiment as in

Figure 7. Overexpression of WT RGS had minimal effect on the frequency of normal cytokinesis, while overexpression of either phosphomutant RGS lead to much lower normal response to HU followed by pheromone. The unphosphorylatable ~~p~~RGS mutant resulted in the strongest disruption of normal response, while the phospho-mimetic p*RGS mutant lead to a larger defect than anticipated based on its behavior in other experiments (Figure 2.7D.). It does still bind to Kel1 in the Co-IP experiments (Figure 2.7A-B.), and so the overexpression may be sufficient to still have the dominant negative effect, or this may be a limitation of the aspartic acid mutation. In either case, the disruption of cytokinesis is clearly dependent upon the dose of RGS mutant present in the cell.

We tested the ability of Kel1 overexpression to rescue the RGS mutant defects in the HU/pheromone experiment by creating an ADH1 promoter-driven Kel1-3xFLAG plasmid. We transformed this plasmid into WT, ~~p~~RGS, and p*RGS strains and performed the HU and pheromone experiment as above. Kel1 overexpression was able to improve the response in every background (Figure 2.7E.). Thus, Kel1 is genetically in the same pathway as the unphosphorylatable ~~p~~RGS for control of cytokinesis in the presence of pheromone.

2.5. Discussion

Here we set out to determine the role of feedback phosphorylation of the RGS, Sst2. We found that the phosphorylation is dynamic through the pheromone response, reaching a maximal level between 1 and 2 hours into the response (Figure 2.6.). We found that phosphorylation of the RGS alters the localization of the RGS relative to the polar cap during the pheromone response and leads to a broadened distribution of the Gα-interacting MAPK, Fus3 (Figure 2.3 & 2.4.). Strikingly, cells unable to phosphorylate the RGS sometimes began polarized growth in

response to pheromone without waiting for the completion of cytokinesis. By inducing cytokinetic defects with hydroxyurea, we were able to determine that phosphorylation of the RGS enhances the ability of the cell to stall cytokinesis without initiating pheromone induce polarity, thereby correctly integrating both an internal stress response and an external morphogenesis response (Figure 2.7.). This coordination appears to use the kelch repeat protein Kel1, and the formin Bnr1, while the formin Bni1 antagonizes completion of cytokinesis in the presence of pheromone. We found that the RGS forms a complex with Kel1 that is affected by Serine 539 mutants, and that cytokinetic defects are exacerbated by higher levels of RGS mutants, while higher levels of Kel1 can rescue RGS-induced cytokinetic defects.

2.5.1. Coordination of the End of Cytokinesis with the Beginning of Receptor Mediated Morphogenesis

In an unsynchronized population, cells will be evenly distributed through the 90-minute yeast cell cycle. Upon stimulation with pheromone, receptor signaling will immediately begin with subsequent MAPK activation, and downstream phosphorylation of the protein Far1 [152]. Far1 serves two purposes in the pheromone response: (1) to inhibit cyclin dependent kinase activity, leading to arrest in G1 [114], and (2) to couple the Cdc42 GEF, Cdc24, to free Gβ, thereby promoting polarization to sites of active receptor [39]. The duration of receptor signaling prior to the repurposing of the polarity machinery will vary depending on where in the cell cycle each cell is when pheromone signaling begins. Thus, some cells may be an hour or more into pheromone signaling prior to completing cytokinesis, while others may be able to immediately start mating projection formation or experience a delay of only a few minutes. A potentially significant difference between these two scenarios is the amount of RGS present in the cell

(Figure 2.2.), as SST2 transcription is upregulated by pheromone signaling [56], and so cells that must delay receptor driven polarity for a long time prior to cytokinesis may be more prone to RGS-induced errors and be more dependent upon MAPK phosphorylation of the RGS. Indeed, our overexpression experiments suggest this is the case, as higher levels of unphosphorylatable RGS leads to an increase in failed cytokinesis (Figure 2.8.).

An obvious question arises from these findings: Does the RGS play a role in cytokinesis in the absence of pheromone? There are multiple lines of evidence to suggest that RGS has no role in normal cytokinesis. First, in previous studies on cells lacking the RGS, we have not observed any cytokinetic defects [139]. Secondly, baseline Sst2 levels are an order of magnitude higher in haploids than in diploids [153]. If the RGS played a role in cytokinesis in the absence of pheromone, then haploid and diploid cells would need different mechanisms for regulating cytokinesis, an unlikely scenario.

Our data is consistent with unphosphorylated RGS inhibiting a subset of Kel1 function, as the unphosphorylatable ~~p~~RGS phenocopies the spontaneous failure to complete cytokinesis before mating projection formation that we see in cells lacking Kel1 and overexpression of this mutant enhances the penetrance of the phenotype (Figures 2.7. & 2.8.). We would expect this inhibition of Kel1 to involve stochiometric binding (directly or through an intermediary) and so in the absence of pheromone, where RGS levels are low (Figure 2.3C. and [56]) there would be very little impact of unphosphorylated RGS on Kel1 activity. Phosphorylation of the RGS, however, would prevent its inhibition of Kel1. We conclude that RGS is phosphorylated early in the response to allow normal Kel1 function during the completion of the cell cycle (Figure 2.8.).

Kel1 associates with the polar cap, regulates the formin Bnr1, is required for efficient mating, and takes part in the mitotic exit network (MEN) [128-130, 154]. Kel1 contributes to the MEN by anchoring the Ras regulator Lte1 to the daughter cell during mitosis [146, 155]. In addition to promoting mitotic exit, Kel1 and Lte1 have been found to suppress spurious polarization prior to the completion of mitosis, a role that may be separate from their role in MEN [155]. Failure of Lte1 suppression of polarized growth leads to asymmetric hyperpolarized growth very similar to what we see in HU (Figure 2.8.) [155]. Future studies will be needed to examine whether LTE1 is responsible for the delay in receptor-mediated polarization to allow completion of cytokinesis.

The cytokinetic target of Kel1 may be the formin, Bnr1, but Bnr1 appears to have little role in the pheromone pathway. Bni1 would seem a more likely candidate, and while there is no evidence that Kel1 can regulate Bni1, neither is there clear evidence that it cannot [128]. Our hydroxyurea experiments show that the asymmetric hyper-polarized growth requires Bni1 and is inhibited by Kel1, consistent with a role for Kel1 negatively regulating Bni1 during the pheromone response.

2.5.2. The Role of RGS Phosphorylation in the Pheromone Response

At later time points we observe less phosphorylated RGS (Figure 2.7.), suggesting a switch in the requirements for RGS as the pheromone response progresses. Our data suggest that the functional consequence of RGS phosphorylation is altered spatial regulation of the pathway (Figure 2.9.). Unphosphorylated RGS (e.g. WT at later time points or the ~~p~~RGS mutant) drives a larger distance between the MAPK Fus3 and the polar cap marker Bem1, proteins that interact with active large G-protein (Gpa1) and active small G-protein (Cdc42), respectively (Figure 2.5.). The simplest explanation of this observation is that the presence of RGS at the

polar cap locally suppresses Gα activation. This is bolstered by the concentration of minimum MAPK concentration immediately proximal to the center of the polar cap, a phenomenon that is disrupted by the phospho-mimetic mutation that decreases RGS association with the polar cap. This type of negative feedback to the center of active signaling could help drive wandering of the polar cap by promoting large G-protein signaling further from the current site of polarization [156]. Wandering of the polar cap is important for sensitive gradient tracking [157], and so the small difference in the ability to track the gradient very well that we see in the p*RGS mutant (Figure 2.1.) may be due to its decreased offset between the receptor driven large G-protein and the Cdc42 driven polarity machinery. Additionally, an offset between receptor signaling and the polar cap has recently been proposed to play a role in gradient tracking [158], and while we did not see an effect on gradient tracking here, under more difficult tracking conditions, the observed Gα offset may enhance chemotropic growth.

Our data is consistent with unphosphorylated RGS inhibiting Kel1 function later in the pheromone response. Recent work by Garcia and colleagues [131] has found that Kel1 suppresses spontaneous activation of the pheromone pathway and suppresses noise in the pheromone pathway, both roles that have been previously identified for the RGS, Sst2 [72, 125]. Given our finding that Kel1 and Sst2 form a complex, and it may be that Kel1 promotes Sst2 function more broadly.

2.6. Conclusion

Here we have established a role for the phosphorylation of the RGS, Sst2, in promoting the completion of cytokinesis prior to the pheromone pathway repurposing the mitotic Cdc42 machinery for production of the mating projection, or shmoo. The exacerbation of this defect

by the presence of a DNA-damaging agent emphasizes that the cell must integrate the competing signals of a check point instructing the cell to stop mitosis with a GPCR signaling pathway instructing the cell to polarize towards a mating partner. The use of a short-term phosphorylation event to temporarily alter RGS function and thereby allow the mitotic checkpoint to complete seems a likely motif to repeat in other systems.

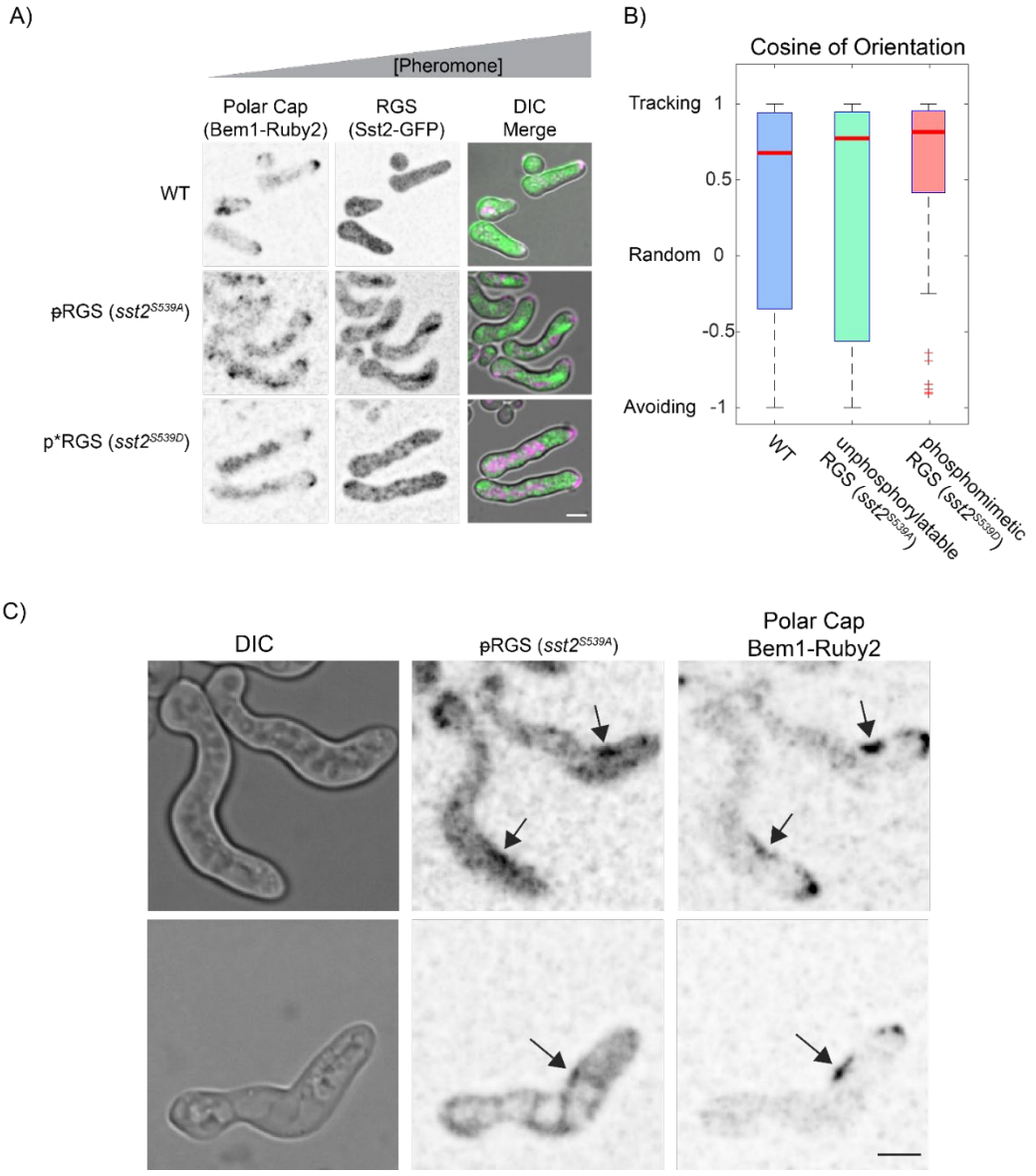

Figure 2.1. Phosphorylation state of the RGS does not stop gradient tracking.

A) Representative live-cell images of WT, unphosphorylatable (pRGS), and phosphomimetic (p*RGS) RGS expressing the polar cap marker (Bem1-mRuby2) and the RGS (Sst2-EGFP) tracking a 0-150nM gradient of pheromone, with pheromone increasing to the right. B) Quantification of gradient tracking cells measured by the cosine of orientation for WT (n =95), pRGS (sst2S539A, n =39), and p*RGS (sst2S539D, n =45) from three experiments. Scale bars represent 5 µm. The differences in gradient tracking were not significant by pairwise Two Sample Kolmogorov–Smirnov test for p< 0.05.

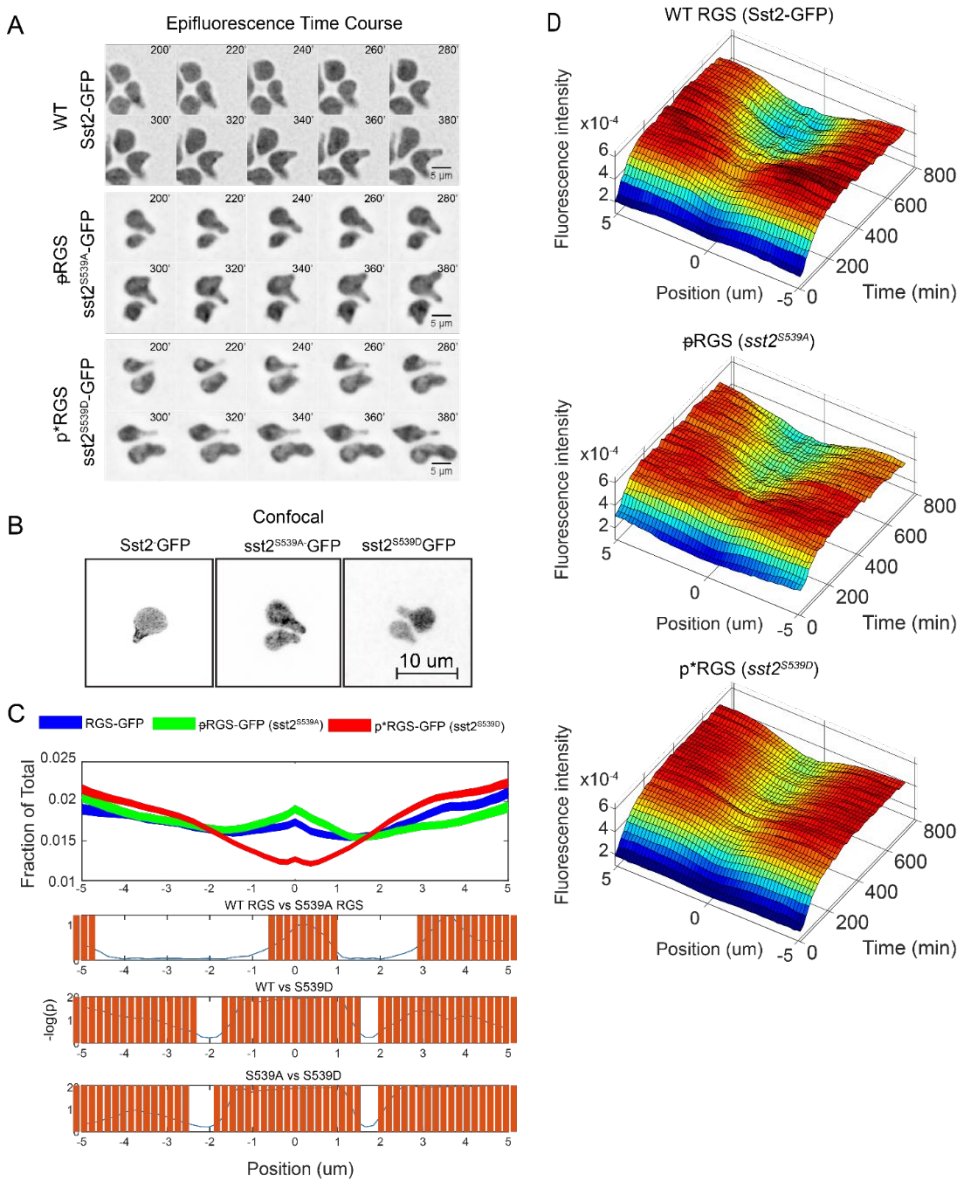

Figure 2.2. Localization of the RGS is dependent on phosphorylation state.

A) Epifluorescence time course images of the strains expressing the indicated RGS mutants (Sst2-GFP) imaged in a microfluidic device exposed to 300 nM pheromone for the indicated time. Blue squares indicate area shown enlarged below. Arrows indicated the local maxima of MAPK. B) Confocal images of WT, unphosphorylatable (pRGS), and phosphomimetic (p*RGS) RGS fused to EGFP in saturating pheromone (10 µM). C) Quantification of the average RGS spatial distribution normalized to the polar cap marker (Bem1-mRuby2) in saturating pheromone over a 12hr time-course in a microfluidic gradient chamber, imaged by epifluorescence microscopy. Lines are derived from averaging from 180 min. onward. Bottom graphs display statistical analysis using one-way ANOVA followed by Tukey's HSD, with -log(p-value) plotted in blue, and statistically significant ($p < 0.05$), differences in localization noted by light red bars. Data is derived from n = 89 cells (WT), n = 88 pRGS (unphosporylatable), and n = 139 p*RGS (phospho-mimetic) cells per strain, with 29 time points per cell. D) 3-D kymographs of the spatial distribution of the RGS over 12hrs for WT, pRGS, and p*RGS with 37 time points per cell from (A).

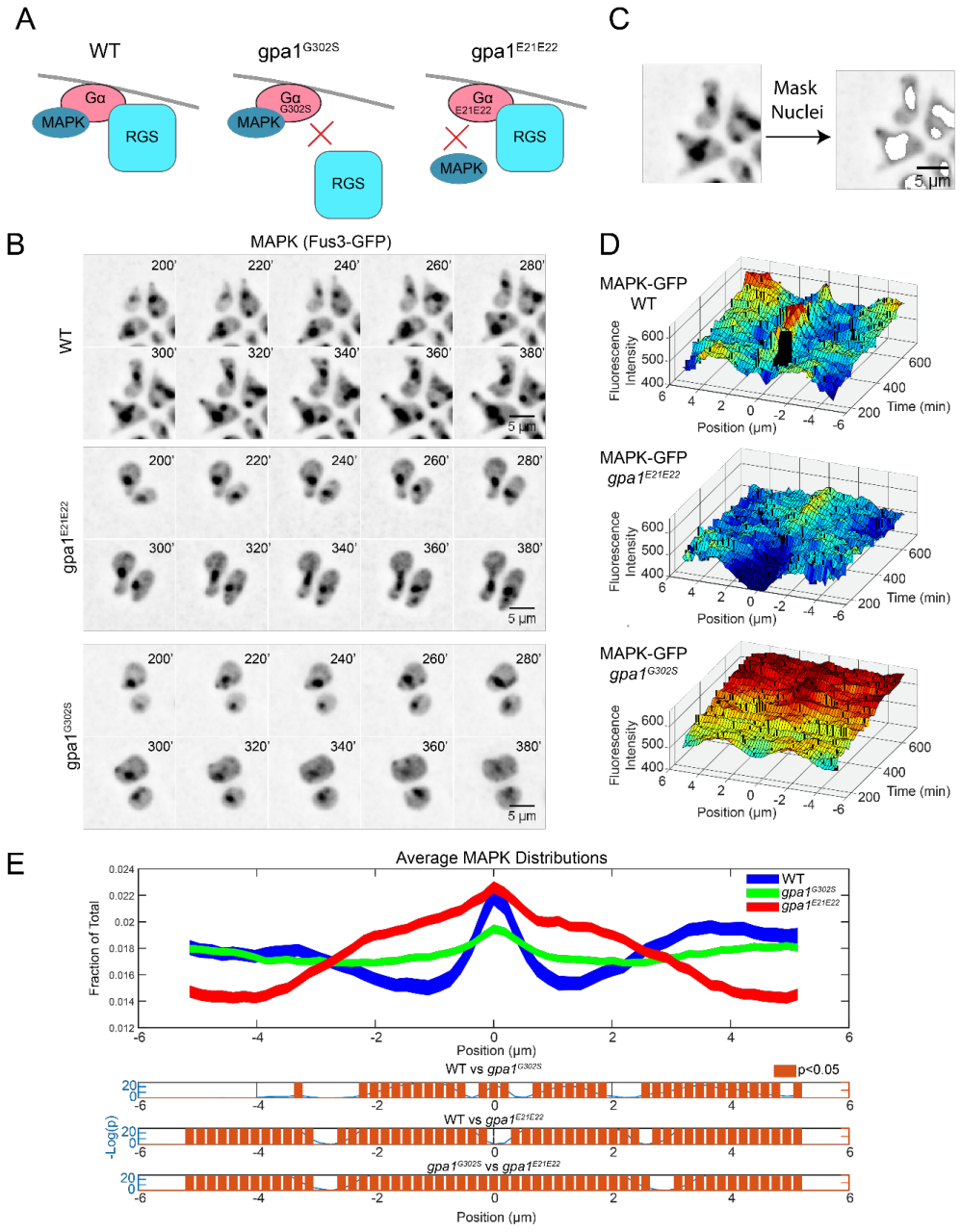

Figure 2.3. The localization of the MAPK Fus3 is influenced by binding active Gα.

A) Diagram of the effect of the hyperactive gpa1G302S mutant and the MAPK-uncoupling gpa1E21E22 mutants. B) Epifluorescence time course images of Fus3-GFP with the indicated Gα mutants. Cells were imaged in a microfluidic device for the indicated time and exposed to a flat 300nM pheromone concentration. C) In order to quantify peripheral MAPK, the nuclear signal was masked for each cell prior to quantitation (Shown in Figure A.2.).

Figure 2.3. Cont'd
D) Average kymographs of MAPK localization in the indicated cell line from (B). E) Quantification of the amount of MAPK on the periphery of the cell spatially normalized to the center of the polar cap as in Figure 2.2.. Shaded areas represent 95% confidence intervals. Data is derived from n = 51 (WT), n = 157 (gpa1G302S), and n = 86 (gpa1E21E22), with 29 time points per cell. Bottom graphs display statistical analysis using one-way ANOVA followed by Tukey's HSD, with -log(p-value) plotted in blue, and statistically significant ($p < 0.05$), differences in localization noted by light red bars.

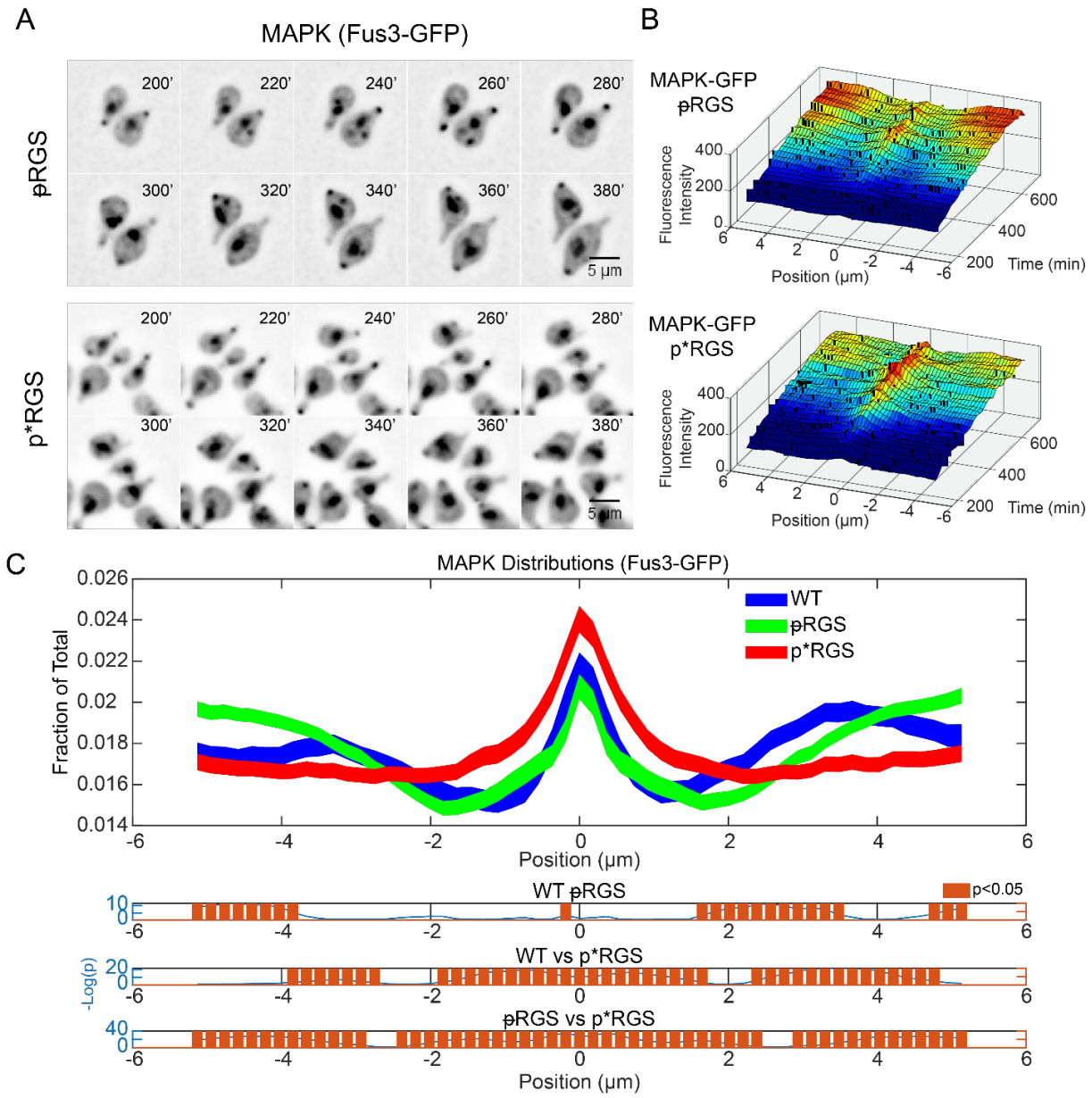

Figure 2.4. RGS Phosphorylation increase Gα/MAPK complex levels at the center of the polar cap.

A) Epifluorescence time course images of the MAPK Fus3-GFP with the indicated RGS phospho-mutants. Cells were imaged in a microfluidic device for the indicated time and exposed to a flat 300nM pheromone concentration. Arrows indicate MAPK associated with the site of polarized growth. B) Average kymographs of MAPK localization in the indicated cell line shown in (A). C) Average protein distribution profiles of MAPK (Fus3-GFP) in cells expressing the unphosphorylatable pRGS (sst2S539A) or the phosphomimetic p*RGS (sst2S539D) aligned to the center of the polar cap (Bem1) as described in Figure 2. The phosphomimetic p*RGS causes a broader distribution of MAPK at the center of the polar cap. Shaded areas represent 95% confidence intervals. Bottom graphs display statistical analysis using one-way ANOVA followed by Tukey's HSD, with -log(p-value) plotted in blue, and statistically significant ($p < 0.05$), differences in localization noted by light red bars. Data is derived from n = 89 (pRGS) and n = 73 (p*RGS) cells and 29 time points per cell.

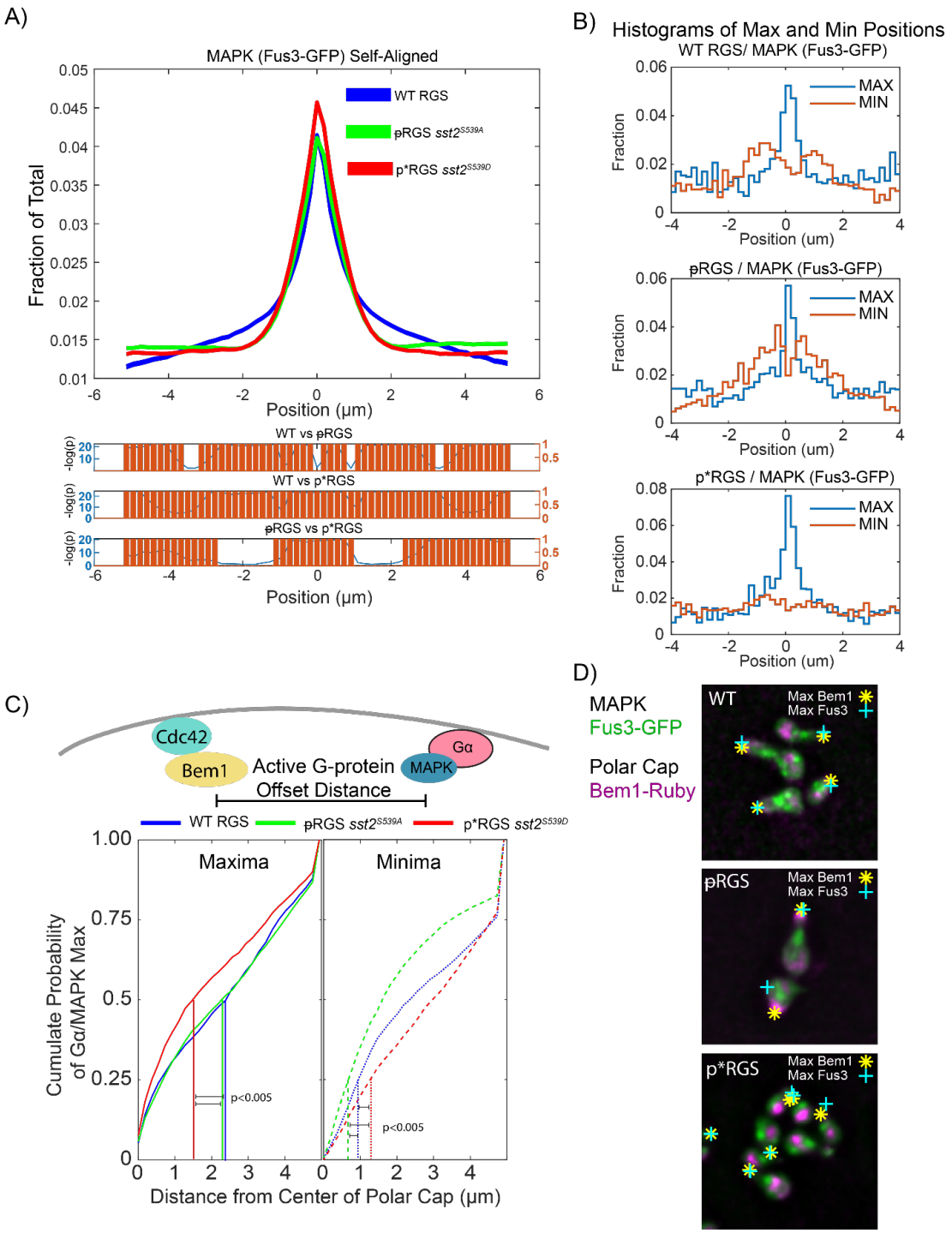

Figure 2.5. RGS induced changes in Gα/MAPK distribution.

A) Distribution of MAPK (Fus3-GFP) from Figure 2.4., spatially normalized to peak MAPK (Fus3) rather than to the polar cap (Bem1). Shaded areas represent 95% confidence intervals. Statistical analysis was performed as in Figure 2.2. and is shown in graphs below. B) Histograms of the location of maxima and minima of MAPK spatially registered to the polar cap in the indicated strain.

Figure 2.5. Cont'd
C) We compare the distance between the maxima of the Bem1 and MAPK, which bind active Cdc42and active Gα, respectively. Graphed is the cumulative sum of MAPK maxima (left) and minima (right) versus distance from the polar cap. Vertical lines show the distance where 50% of maxima have appeared and where 25% of minima have appeared. Statistical significance was evaluated by pairwise Two-Sample Kolomogorov-Smirnov tests. D) Examples of the offset between maximum Bem1 and maximum Fus3 intensity with the indicated RGS mutants.

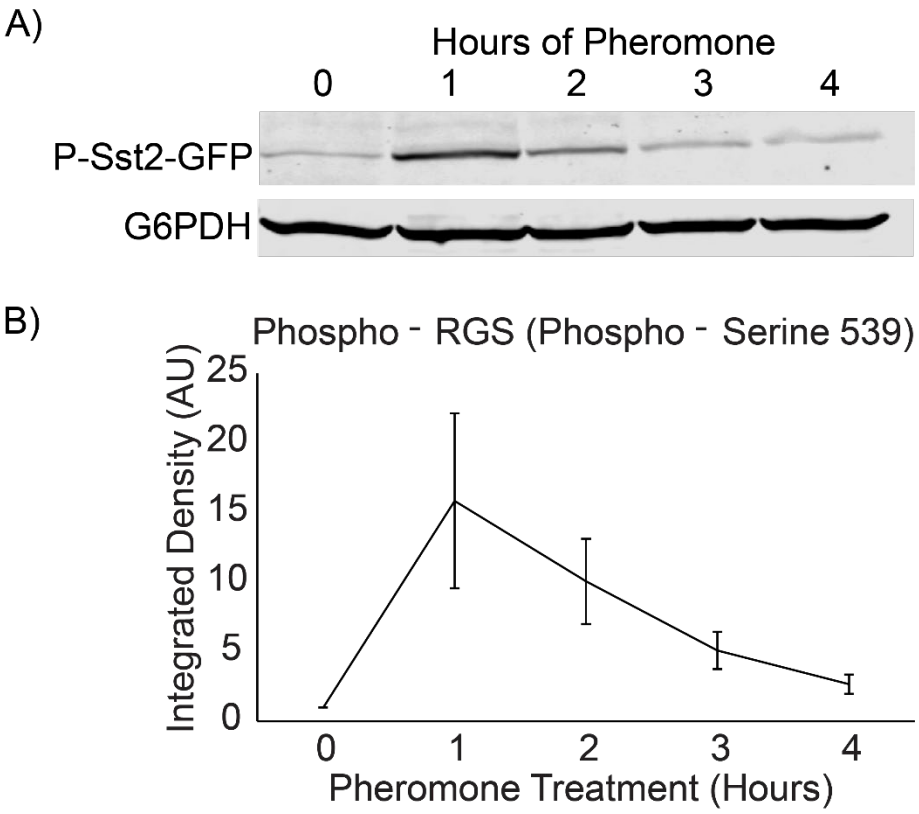

Figure 2.6. RGS phosphorylation peaks 1hr in the pheromone response.

A) Western blotting of phospho-RGS-GFP responding to saturating pheromone over four hours. G6PDH was probed as a loading control. B) Quantification of Western blotting shown in A, normalized to G6PDH levels. Error bars represent standard error of the mean, n=3.

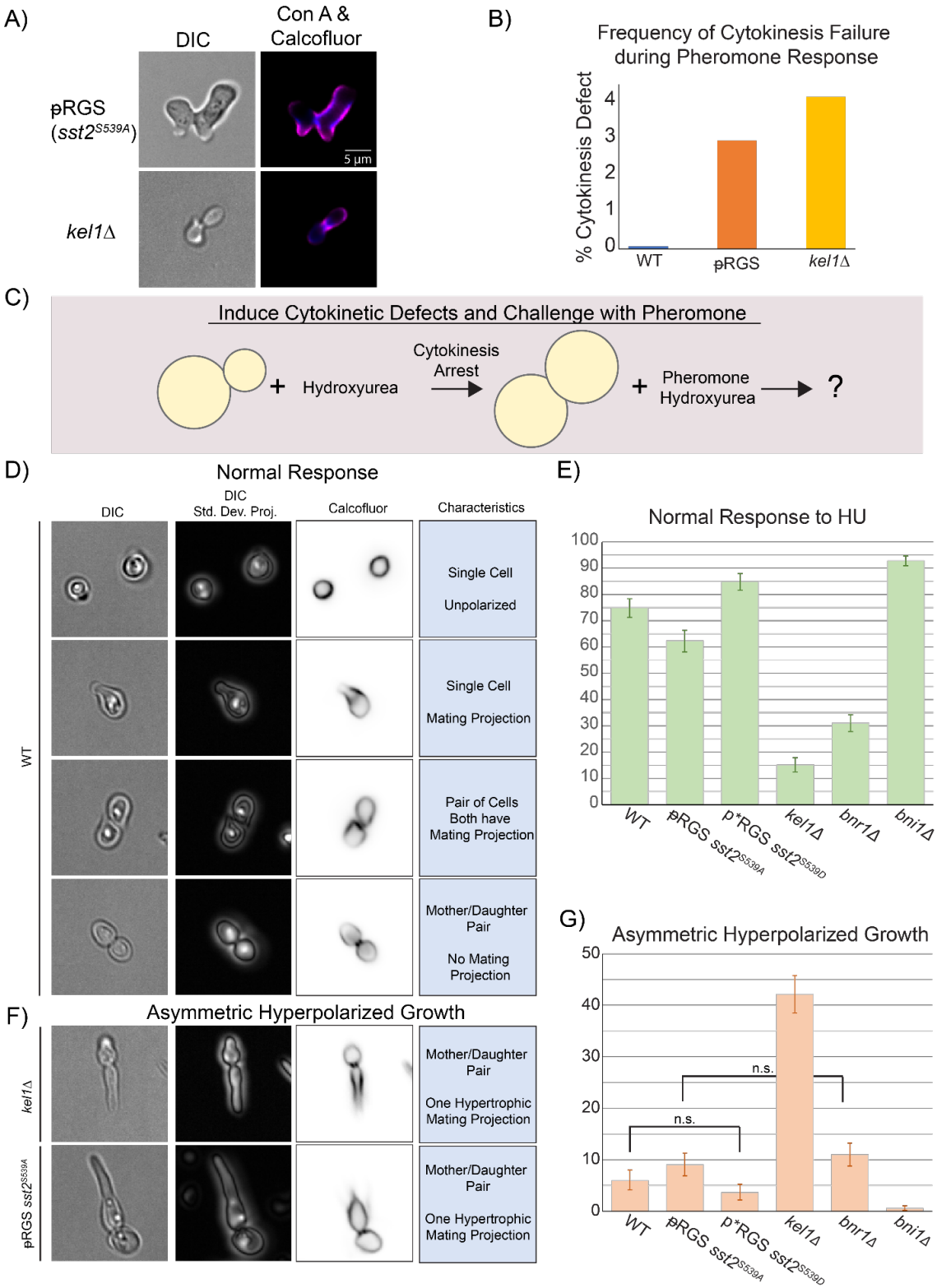

Figure 2.7. Phosphorylated Sst2 and the Kelch-repeat protein Kel1 promote completion of cytokinesis prior to pheromone induced polarization.

Figure 2.7. Cont'd

A) Images of pRGS mutant and kel1Δ which have failed to complete cytokinesis prior to pheromone induce polarized growth. Cell walls were stained with Calcofluor White and Concanavalin-A 647 to verify the open bud neck. B) Wild type and mutant pRGS and kel1Δ strains were exposed to pheromone in culture for 90 minutes, fixed, and then failed cytokinetic events were counted. n = 1412 (WT), 1350 (pRGS), and 1396 (kel1Δ) from two separate experiments. Total count is shown. C) In order to drive cytokinetic defects, we pretreated cells with 100mM hydroxyurea, followed by treatment with both hydroxyurea and pheromone to investigate the role of the indicated proteins in delay of pheromone induced polarity until completed mitosis. D) Images of normal phenotypes in response to HU + pheromone. Shown are a single focal plane of DIC, a standard deviation projection of a stack of DIC images to better show the state of the bud neck, and cell wall staining with Calcofluor White. We considered a normal response to hydroxyurea and pheromone to be one of the following: 1) Completion of cytokinesis but arrest as a circular cell, in the event that stress signaling is suppressing the pheromone response (a minority of cells). 2) A lone cell responding to pheromone. 3) Completion of cytokinesis (if the cells had resolved their DNA damage), followed by pheromone induced morphogenesis. These cells may be still associated but show signs of completed cytokinesis 4) arrest of cytokinesis yielding a mother daughter pair with no polarized growth. E) Plots of the frequency of normal response to hydroxyurea and pheromone in the indicated strains. Error bars represent bootstrapped 95% confidence intervals. For each strain, n > 640 cells across 3 experiments. All differences are statistically significant for $p < 0.05$, as indicated by non-overlapping 95% confidence intervals. F) Examples of the asymmetric hyperpolarized growth phenotype. G) Plots of the frequency of asymmetric hyperpolarized growth in response to hydroxyurea and pheromone. For samples with overlapping confidence intervals, statistical significance was tested by bootstrapping the 95% confidence interval of the difference in means. By this metric, we are 95% confident that WT and sst2S539A have a non-zero difference in means ($p < 0.05$). Comparisons that are not statistically significant are marked "n.s."

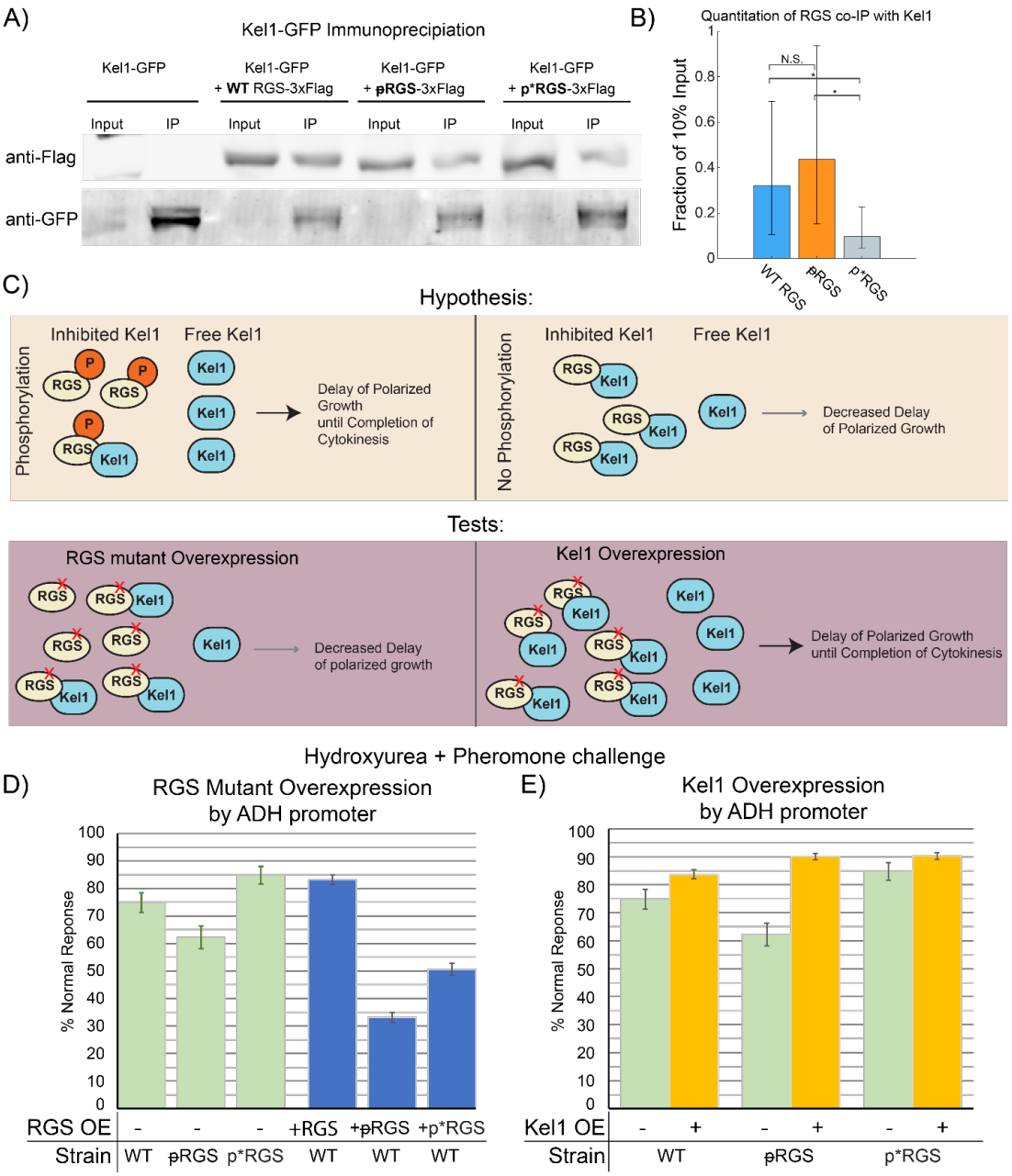

Figure 2.8. RGS and Kel1 form a complex and are in the same genetic pathway for regulation of cytokinesis.

A) Cells expressing Kel1-GFP and overexpressing RGS (pRSII 416 pADH Sst2-3xFlag) as either WT, pRGS, or p*RGS were treated with pheromone for 1 hour, lysed, and an immunoprecipitation was performed with a GFP antibody resin (GFP-trap). Westerns blots were probed for Flag-RGS and for Kel1-GFP. Input lanes contain lysate equivalent to 10% of protein used for the immunoprecipitation. B) Quantitation of the immunoprecipitation results from 6 separate experiments. Error bars represent 95% confidence intervals. Because these confidence intervals overlap, statistical significance was tested by bootstrapping the 95% confidence interval of the difference in means.

Figure 2.8. Cont'd
C) Our data thus far leads us to the hypothesis that unphosphorylated RGS binds Kel1, inhibiting it, and that phosphorylated RGS binds less well, allowing more Kel1 to function for cytokinesis. This can be tested by overexpressing the unphosphorylatable pRGS, which we would expect to decrease the delay in polarized growth and lead to increased cytokinetic defects. This hypothesis can also be tested by attempting to rescue cytokinetic defects in the pRGS mutant by overexpressing Kel1. D) We performed hydroxyurea and pheromone experiments as in Figure 7, with overexpression of WT and mutant RGS constructs from pRSII 416 pADH RGS-3xFlag, as above. Graphed is the percentage of cells that carried out a normal response as previously defined. The green bars are data from Figure 7 for comparison. Error bars represent bootstrapped 95% confidence intervals. Data consists of n = 1784 cells for WT RGS, n = 2398 for pRGS, and n = 1951 for p*RGS overexpression from 3 different experiments. E) We carried out the same experiments in (D), but with Kel1 overexpressed in WT or mutant RGS backgrounds from pRSII416 pADH Kel1-3xFlag. Green bars are data from Figure 7 for comparison. Error bars represent bootstrapped 95% confidence intervals. Data consists of n = 1936 cells for WT RGS, n = 2251 for pRGS, and n = 2574 for p*RGS from 3 different experiments.

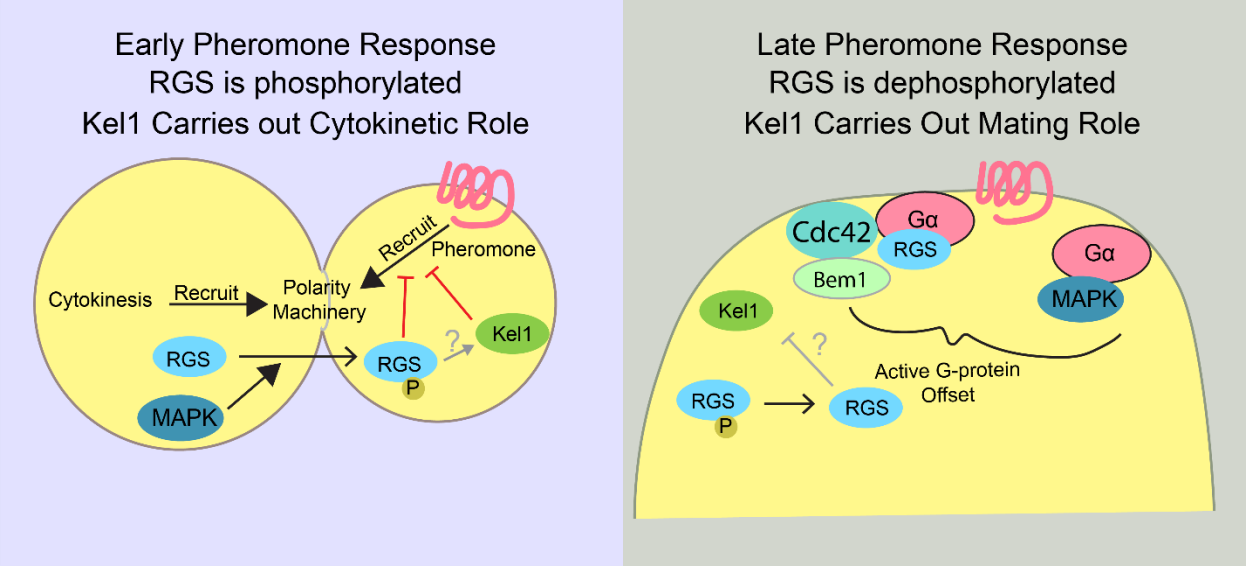

Figure 2.9. Proposed role of RGS phosphorylation.

In cells that have detected pheromone during mitosis and prior to cytokinesis, Kel1 inhibits the recruitment of the polarity machinery by active pheromone receptor. Formation of a complex between unphosphorylated RGS and Kel1 is inhibitory to this role, but phosphorylation of the RGS allows Kel1 to coordinate delay of polarity until completion of cytokinesis. During the pheromone response, while cells are generating a mating projection or tracking a gradient of pheromone, unphosphorylated RGS promotes a greater distance between active Cdc42 and active Gα, potentially enhancing polar cap wandering.

CHAPTER 3

EPSIN-MEDIATED ENDOCYTOSIS OF GA DIRECTS PHEROMONE-INDUCED SEPTIN DEPOSITION IN THE YEAST PHEROMONE RESPONSE

3.1. Abstract

Septins are cytoskeletal filaments that provide a plasma membrane diffusion barrier and scaffold for polarity proteins during the yeast cell cycle. Septins can also be found at the base of the shmoo during the yeast pheromone response and are thought to again prevent diffusion of polarity proteins from the leading edge of the cell. Additionally, other evidence points to septins as membrane stabilizers for turning during yeast gradient tracking. Previous research uncovered that cells lacking RGS activity on the Gα, Gpa1, were unable to form normal mating projections and exhibited abnormal septin distribution at the polar cap rather than peripheral to. We investigated the signaling pathway responsible for determining the spatial characteristics of septin deposition in the yeast pheromone response. We found that septin distribution is controlled by endocytosis via the epsin endocytic adaptor proteins through the Epsin-Gic1-Bem3 signaling axis. Additionally, we found that endocytosis of Gα via it's ubiquitin domain is the dominant spatial cue for septin deposition during the yeast pheromone response.

3.2. Introduction

Cells must detect and respond to chemical signal gradients in their environment to retain normal function. For instance, neurons require a gradient of secreted growth factors for axon guidance (Katz and Shatz, 1996). Similarly, the yeast, Saccharomyces cerevisiae, elongates toward a potential mate by detecting a gradient of mating pheromone and forming a mating projection or "shmoo"[107, 159]. This yeast mating response is driven by a G-protein coupled receptor (GPCR) signaling pathway. The pheromone receptor, Ste2, activates the large, heterotrimeric G-protein consisting of a Gα (Gpa1) and

Gβγ dimer (Ste4 and Ste18)[108]. Upon activation, the receptor exchanges GDP for GTP on the Gα subunit and promotes dissociation of the Gα and Gβγ subunits[160]. This is followed by Gβγ simultaneously initiating three downstream signals[160]: 1) Gβγ binds Far1, that recruits the Cdc42 guanine-nucleotide exchange factor (GEF), Cdc24, to Cdc42-GDP[38], 2) Gβγ binds Ste20, the founding member of the p21-activated protein kinase (PAK) family[161, 162], and promotes MAPK scaffolding at the plasma membrane, and 3) Gβγ binds Ste5, the MAPK scaffold that recruits all components of the MAPK signaling cascade and thus enhances signaling output[31-34, 44-51]. While much of Gβγ function is known, Gα's known contribution to pheromone-induced polarity is downregulation of Gβγ signaling through direct sequestration, downregulation of Gβγ independent of sequestration[27, 28], and enhancement of MAPK (Fus3) signaling[26]. Recent work suggests that Gα-activity influences pheromone-induced re-distribution of cytoskeletal filaments called septins[40].

Septins are dynamic cytoskeletal filaments that are known for their role as diffusion barriers during cytokinesis (i.e. septin-ring)[86, 103, 104]. During the yeast pheromone response, septins are constructed as filaments and are deposited at the base of the mating projection in yeast and are believed to provide structural support for projection formation[163, 164]. Septin deposition is heavily controlled by the interplay of several Cdc42 effectors, notably septin chaperones called GTPase interactive components (GICs), Cdc42, and Cdc42 GTPase activating proteins (Cdc42-GAPs)[165, 166] . Briefly, Gics are recruited to Cdc42-GTP followed by recruitment of Cdc42-GAPs, which hydrolyze Cdc42-GTP to Cdc42-GDP. While it is still unclear how septins are deposited on the plasma membrane, it is clear that it is through a Cdc42-dependent mechanism. Importantly, Cdc42-GAPs are known interactors of the Epsin endocytic adaptor family and are thought to be recruited to Cdc42 through epsin-mediated endocytosis[66].

Although we have evidence supporting the above description of septin deposition in yeast, the mechanism underlying the spatial distribution of septins during the pheromone response has not yet

been elucidated. The recent work by Kelley et al. in 2015 (mentioned above) found that septin distribution was significantly altered in cells lacking the regulator of G-protein signaling (RGS), which enhancemes Gα's intrinsic GTPase activity[40]. Specifically, in wild-type (WT) cells septins are distributed at the cell membrane and peripheral to the polar cap, marked by the polarity protein, bud emergence protein 1 (Bem1). However, in mutants lacking RGS activity, septins were distributed coincident with Bem,1 and therefore directly at the polar cap. This resulted in a loss of gradient tracking ability and a severe defect in mating projection morphogenesis.

These data led us to the question: How is the spatial distribution of septins controlled during the yeast pheromone response? Here, we report that septin distribution during the pheromone response is controlled by an Epsin-Cdc42GAP-Gic signaling axis. We also reveal that epsin-mediated endocytosis of Gα drives septin deposition, which is abberant in cells lacking RGS-Gα activity (hereafter Hyper Gα).

3.3. Methods and Materials

3.3.1. Yeast Strains

Strains used in this study are listed in Table A.1.. All strains were constructed in the MATa haploid Saccharomyces cerevisiae parent strain, BY4741. All plasmids used in this study are included in Table A.2.. Polar cap (Bem1) and septin (Cdc3) proteins were tagged with GFP[134] and mCherry at the native chromosomal locus through oligonucleotide-directed homologous recombination using primers listed in Table A.3..

Cells were grown in rich medium (YPD) or synthetic medium (SC) at 30°C unless otherwise indicated. PCR products were transformed into parent yeast strains using standard lithium acetate transformation[136]. Individual colonies were isolated by growth on standard selective media (SC leu-, SC ura-, SC his-, or YPD G418+). Transformants were verified using fluorescence microscopy, sequencing, and/or PCR using primers found in Table A.3..

3.3.2. Microluidic Experiments

Microfluidic devices were made by mixing SYLGARD 184 silicone polymer at 10(part A):1(part B) and poured directly onto a microfluidics device mold[137] that was fabricated by UMaine FIRST. Reagents A and B were mixed using a glass stirring rod (Dow) prior to mold application, then molds were placed in a vacuum chamber for at least 1hr to remove air bubbles. Once all air bubbles were removed, the mixture was placed in an oven at 80°C for 1hr to cure and cooled to room temperature.

From the cooled mold, devices were cut out using a razor and fluid ports were punctured using an 18g Leuer stub. Prepped devices and coverslips were cleaned by spraying with 100% methanol, 70% ethanol, then water, and dried using an air hose. Devices and coverslips were exposed to oxygen plasma for 50 seconds in a Harrick Plasma PDC32G Cleaner followed by fusion of the device to the coverslip. After initial fusing, the device was then placed in the oven at 80°C for at least 20 minutes to facilitate proper fusion of the mold to the coverslip. The device was then cooled to room temperature prior to use.

Cultures were grown in 0.45µm-filtered SC to an OD600 between 0.1-0.8 at 30°C. Live-cell microfluidics experiments were performed using an IX83 (Olympus, Waltham MA) microscope and a Prime 95B CMOS Camera (Photometrics) controlled by Cell Sens 1.17 (Olympus). Fluorescence and Differential Interference Contrast (DIC) images were acquired using an Olympus-APON-60X-TIRF objective. Z-stacks of GFP and mCherry images were acquired using an X-Cite 120 LEDBoost (Excelitas). Cells were imaged in a “Dial-a-wave” based microfluidic device that allowed for rapid switching of media while yeast remained in place (Bennet et al., 2011; Dixit et al., 2014b; Suzuki et al., 2021). Pheromone-containing media was verified using AlexaFluor 647 dye at 1:8000 dilution (Life Technologies) and imaged in a single plane. Cells were imaged at 20-minute intervals for 12 hours with 300nM pheromone present in the media. Imaging settings were determined based on experimental needs and were replicated for repeat experiments.

3.3.3. Image Analysis

Images were deconvolved using Huygens Software (Scientific Volume Imaging, Hilversum, Netherlands). For all fluorescent images, deconvolution was carried out with a theoretical point-spread function, 5 signal-to-noise ratio (GFP images) or 7 signal-to-noise ratio (mCherry images), maximum 500 iterations, and a quality change threshold of 0.01% using the classical algorithm. All other settings were set to default. Images were saved as 16-bit TIFF with linked-scale. Masks of fluorescent signal were created using a merged 8-bit RGB version of GFP and mCherry channels in FIJI and final segmentation was done prior to septin localization analysis in MATLAB. All septin localization analysis was conducted using whole_cell_cap_v4.m for cell tracking and combokeeper_v3.m for line scan analysis. Septin data was aligned to the polar cap profile using the aligned.mlx script and subsequently normalized to the fraction of total signal. Normalized data was used to construct bootstrapped 95% confidence intervals to the mean.

3.4. Results

3.4.1. Hyperactive Gα Drives Aberrant Septin Distribution

Recently, septin organization was linked RGS enhancement of Gα's intrinsic GTPase activity, (Kelley et al 2015). We reproduced the results from Kelley et al. to verify and establish our microfluidic imaging approach (Figure 3.1.). As expected, we found wild-type (WT) yeast deposit septins peripheral to the polar cap, whereas mutant yeast containing a Gpa1 (Gα) G302S mutation that inhibits Gpa1-RGS binding (hereafter Hyper Gα) yeast deposit septins at the center of the polar cap, whereas. We quantified this distribution using the computational method developed in Kelley et al. to analyze the distribution of septins (Cdc3-mCherry) relative to peak fluorescence of the polar cap (Bem1-GFP) (Figure 3.1C.).

3.4.2. Gic1, Not Gic2, Contributes to Pheromone Induced Septin Organization

Yeast express two GTPase interacting component (Gic) proteins, Gic1 and Gic2, which are homologous septin chaperones and are functional homologues to the human Borg proteins[167, 168]. Gics recruit septins to the bud neck during yeast cell division to promote assembly of the septin-ring. Specifically, Cdc42-GTP recruits Gics with septin octamers to Cdc42-GTP at the bud neck, where hydrolysis of Cdc42-GTP to Cdc42-GDP promotes release of Gic1 from septin filaments[169] However, differential Gic contribution to septin deposition during the pheromone response is unknown. Therefore, we aimed to determine if Gic1 and Gic2 differentially contribute to septin deposition during the yeast pheromone response.

We generated Hyper Gα mutant yeast lacking either Gic1 or Gic2 and subsequently imaged the polar cap (Bem1-GFP) and septins (Cdc3-mCherry) using the same parameters described in Figure 3.1. (Figure 3.2.). We found cells lacking Gic1 had distributed septins peripheral to the polar cap (Figure 3.2A.), while yeast lacking Gic2 distributed septins broadly across the cell membrane with more frequent and smaller “hotspots” (Figure 3.2B.). We then quantified septin distribution relative to the center of the polar cap, again using the same quantiation method used in Figure 3.1. (Figure 3.2C.) and found that hyperactive Gα mutants lacking Gic1, but not Gic2 rescued aberrant septin deposition. Our quantitation also reflected the broad distribution of septins found in mutants lacking Gic2 (Figure 3.2C.). These results suggest that while both Gics are responsible for septin recruitment to the membrane during the pheromone response, Gic1 is the primary contributor to the spatial component of pheromone-induced septin deposition.

3.4.3 The Cdc42-GAP, Bem3, Controls Deposition of Pheromone Induced Septin Structures

The master regulator of polarity is Cdc42, a small Rho family GTPase whose nucleotide coupling determines its action(s). For septin deposition, Cdc42-GTP requires Cdc42 GTPase activating proteins

(Cdc42GAPs) to hydrolyze GTP to GDP to promote dissociation of Gic1 from septin filaments[169]. Yeast express three Cdc42GAPs: Rga1, Rga2, and Bem3. Rga1 and Rga2 are nearly identical in structure and are considered functionally redundant proteins. However, Rga2 and not Rga1 localizes to the polar cap during the pheromone response[40]. Additionally, Bem3 also localizes to the polar cap during the pheromone response and is the only Cdc42GAP that contains a pleckstrin homology domain, which is used to anchor proteins to the cell membrane by binding phosphoinostitides[170]. Therefore, we hypothesized that Rga2 and Bem3 were likely more involved in pheromone-induced septin organization compared to Rga1. Upon visual inspection, we found heterogeneity and a partial rescue of septin distribution in cells lacking Rga1 or Rga2 (Figure 3A and 3B respectively). Surprisingly, we found that Hyper Gα mutants lacking Bem3 undoubtedly rescued the septin distribution defect (Figure 3.3C.). Quantitatively, we confirmed our qualitative analysis and found that cells lacking Rga1 or Rga2 partially rescued aberrant septin deposition and cells lacking Bem3 completely rescued the septin defect (Figure 3.3D.). These results suggest that Bem3 is the primary contributor to pheromone induced Cdc42GAP activity and subsequent septin deposition.

3.4.4. Epsin Mediated Endocytosis, With Either Ent1 or Ent2, Directs Pheromone Induced Septin Deposition

Epsins are endocytic adaptor proteins that bind and recruit ubiquitinated cargo to clathrin-coated endocytic pits. Yeast express two endocytic Epsin homologues, Ent1 and Ent2, that are functionally redundant. Previous research established differential genetic interactions between the epsins Ent1 and Ent2, and Cdc42GAPs using a yeast two-hybrid screen[66]. Therefore, we hypothesized that epsin-mediated endocytosis contributes to the spatial distribution of pheromone-induced septin deposits. To test this, we again conducted live-cell imaging in microfluidic chambers (Figure 3.4.). As expected, we found that Hyper Gα cells lacking either Ent1 or Ent2 redistributed septins peripheral to

the polar cap (Figure 3.4A. and 3.4B. respectively). Again, we validated our qualitative assessment using the same quantitative approach described previously and found that both epsin mutants rescued the Hyper Gα septin defect (Figure 3.4C.). Importantly, while septin distributions in cells lacking either epsin were quantitatively akin to wildtype, there is a significant increase in the fraction of septin at the periphery of the polar cap and decrease the center of the polar cap in Hyper Gα mutants lacking Ent1 compared to both mutants lacking Ent2 and WT cells (Figure 3.4C.). These results suggest that epsin-mediated endocytosis directs pheromone-induced septin deposition.

3.4.5. Endocytosis of Gα, But Not of the Receptor, Provides Spatial Cue for Septin Deposition

Our results suggesting that sites of epsin-mediated endocytosis are landmarks for the distribution of septins during the yeast pheromone response led us to ask: What specific endocytic cargo is responsible for septin distribution? Epsins recognize ubiquitinated cargo at the plasma membrane and facilitate their subsequent endocytosis by stabilizing the membrane curvature of clathrin coated pits[171]. During the pheromone response, there are few mating specific proteins at the leading edge of the mating projection, less are marked for endocytosis via ubiquitination. These data point to endocytic rate as a potential driver of septin deposition, where an increased rate of endocytosis would promote septin deposition too early at the polar cap – likely explaining the phenomenon we see in our hyperactive Galpha mutants.

The pheromone receptor, Ste2, is both phosphorylated and ubiquitinated at its C-terminus prior to its endocytosis and degradation. Previous research found that C-terminal truncation reduced the rate of receptor endocytosis[69]. In the presence of Hyper Gα, less receptor will be coupled to inactive G-protein and should result in a higher fraction of ubiquitinated receptor and ultimately lead to increased endocytic rate (Figure 3.5A.). We hypothesized that truncation of the receptor C-terminus to dampen endocytic rate would rescue the Hyper Gα septin phenotype. We found that cells lacking the receptor C-

terminus from codon 326 (Ste2 CΔ)[69] partially rescued our Hyper Gα septin defect (Figure 3.5B.), though there was heterogeneity in the degree of rescue across the population. To validate our qualitative assessment, we again quantified septin distribution relative to the polar cap (Figure 3.5D.). Indeed, we found Hyper Gα mutants lacking the C-terminus of the receptor partially rescued septin defects. Additionally, we found a distinct peak (similar in shape to WT but exaggerated) at the center of the polar cap (Figure 3.5D.). Our results suggest another endocytic cargo may be the primary driver of pheromone-induced septin deposition.

The yeast Gα is unique compared to human Gαs. It contains a ubiquitination domain (UD) that, when ubiquitinated, promotes endocytosis and subsequent trafficking of the Gα[70, 172]. Since Gα expression is pheromone-induced, its hyperactivity has driven aberrant septin distribution, and is also the cause of increased uncoupled receptor at the plasma membrane, we hypothesized that endocytosis of Gα (via the UD) directs septin deposition. Thanks to a generous contribution of the Dohlman Lab at UNC Chapel Hill, we constructed an integrating plasmid to replace the wildtype Gpa1 locus with a Hyper Gα lacking the UD (Hyper Gα-UDΔ) in cells tagged with Bem1-GFP (polar cap) and Cdc3-mCherry (septins) and analyzed septin distribution via live-cell imaging (consistent with methods previously described). As predicted, Hyper Gα mutants lacking the UD completely rescued septin defects found in a Hyper Gα (Figure 3.5C.). We again quantified our septin distribution profiles to validate our qualitative results (Figure 3.5D.). Indeed we found Hyper Gα-UDΔ septin distribution mimicked WT septin distribution. Interestingly, Hyper Gα-UDΔ cells were unable to maintain pheromone-induced morphologies for the full 12hr time course in the presence of 300nM pheromone and after approximately 8 hours of pheromone exposure, reverted to a mitotic cell state (data not shown).

Due to the Hyper Gα-UDΔ cells' inability to maintain pheromone-induced polarized growth in our standard 300nM pheromone treatment, we hypothesized that Hyper Gα-UDΔ cells are less

responsive to pheromone and may require increased saturation of pheromone receptor. Indeed, we found that increasing the pheromone dose from 300nM to 1μM led to sustained pheromone response for the 12hr time course. Importantly, the increased pheromone concentration did not affect the average distribution of septins in relation to the polar cap (Figure 5D). These data reveal that endocytosis of Gα during the pheromone response is the primary driver of septin deposition, and that the rate of endocytosis may play a role in the distribution of pheromone-induced septin distribution.

3.5. Discussion

Here, we describe a novel mechanism for pheromone-induced septin distribution during the yeast pheromone response. Specifically, we reveal two major components for this process. First, that endocytosis of Gα drives septin distribution. Second, that epsin-mediated endocytosis is responsible for pheromone-induced septin deposition and is genetically coupled to, what we call, the Epsin-Bem3-Gic1 septin signaling axis (Figure 3.6.). Normal mating projection morphology requires septin structures at the base of the projection to stabilize membrane curvature and promote cell elongation[40, 105, 163, 173, 174]. Additionally, gradient tracking relies on septins to direct mating projection growth toward the gradient of pheromone. In the absence of RGS, the distribution of septins is disrupted, gradient tracking is disabled[40], and cells must rely on endocytic mechanisms for downregulation of active Gα. Rapid accumulation of active Gα suggests an increased endocytic rate of Gα, followed by early and aberrant septin deposition (Figure 3.1.). Thus, the spatio-temporal coordination of RGS-mediated and endocytic-mediated control of Gα is essential to pheromone-induced septin organization.

3.5.1 The Role of Gα in Pheromone-Induced Septin Organization and Gradient Tracking

Few studies have elucidated Gα's role in the pheromone response, beyond regulation of Gβγ[27, 28] and enhancement of MAPK signaling[26]. The yeast Gα contains a ubiquitination domain (UD), which is unique and does not exist to our knowledge in human Gαs. Previous research revealed the UD is

required for endocytic transport of Gα[172]. Additionally in yeast lacking the UD, exposure to saturating pheromone concentrations promotes uncharacteristically broad mating projections, which is normally be found in cells tracking a gradient of pheromone[172]. In contrast, Hyper Gα yeast usually do not form mating projections, promote a 'bean-shape' morphology, deposit septins at the center of the polar cap, and ameliorate gradient tracking capabilities[40]. While we have not determined if Hyper Gα has an increased endocytic rate compared to their WT counterparts, we have determined that the absence of the UD in a Hyper Gα mutant completely rescues the mutant's septin defect, ability to form a mating projection, and abolishes the Hyper Gα bean-shape morphology. Thus, we predict these cells are also capable of tracking a gradient of pheromone.

3.5.2. Endocytic Rate Controls Septin Distribution

Endocytosis of Gα controls several aspects of signaling. In humans, endocytosis is canonically controlled by the β-arrestin family of endocytic adaptors, which recognize endocytically competent cargo (i.e. receptor), promote their endocytosis, and drive changes in signal location[175]. Yeast do not express β-arrestins. Instead, Gα contains a UD which engages the epsin endocytic machinery and is required for its internalization[172]. Our data provides the first evidence connecting Gα internalization and control of the septin cytoskeleton, and that slowing internalization of Gα in a Hyper Gα mutant promotes normal septin distribution. Therefore, we hypothesize that endocytic machinery is recruited more frequently in Hyper Gα and that this is driven by the epsin endocytic machinery (Figure 3.4.).

3.6. Conclusion

Here we have established a novel role for Gα as a driver of septin deposition during the yeast pheromone response. We find the absence of RGS activity promotes increased Gα signaling at the polar cap and likely results in a compensatory increase in endocytosis due to pheromone-induced ubiquitination of the Gα. This compensatory increase in endocytosis drives abberant septin deposition

through recruitment of the Epsin-Bem3-Gic1 signaling axis to the polar cap (Figure 3.6.), rather than peripheral sites of Cdc42-GTP where we would normally find post-translationally modified membrane-bound proteins. We conclude that pheromone-mediated septin structures are ultimately controlled by the amount of active Gα and their distribution is controlled by the spatial organization of epsin-mediated endocytosis.

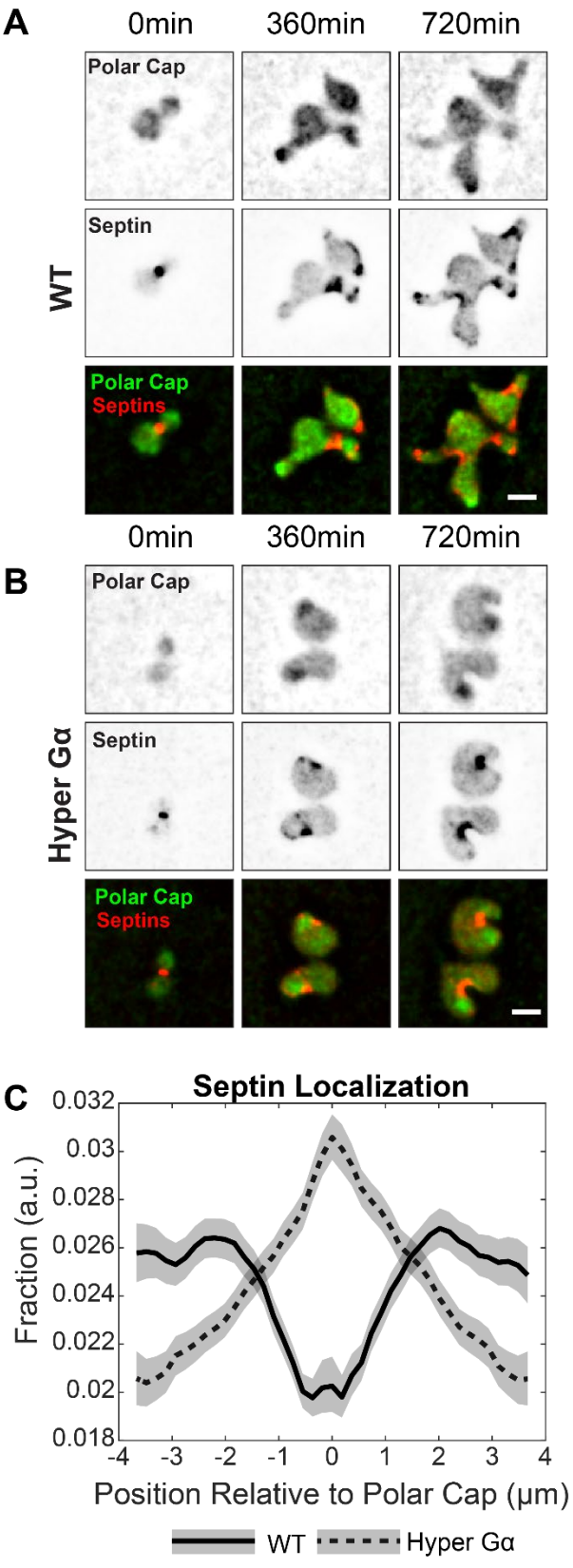

Figure 3.1. Pheromone-induced septin accumulation occurs at the center of the polar cap in Hyper Gα mutants.

(A) Representative images of wild-type (WT) yeast expressing endogenous Bem1-GFP (Polar Cap) and Cdc3-mCherry (Septin) exposed to saturating pheromone at 0min (left-panels), 360min (middle-panels), and 720min (right-panels). Split-channel (top and middle rows) and merged images (bottom row). Scale bar represents 5μm. (B) Representative images of Hyper Gα (Gpa1G302S) yeast expressing endogenous Bem1-GFP (Polar Cap) and Cdc3-mCherry (Septin) exposed to saturating pheromone at 0min (left-panels), 360min (middle-panels), and 720min (right-panels). Scale bar represents 5μm. (C) Time-averaged quantification of the fraction (y-axis) of septin distribution relative to the polar cap (x-axis). Lines are smoothed representations of time-averaged data (37 time points; 20min interval for 12hrs) and shaded regions surrounding lines are 95% confidence intervals. Lines are representative of two combined experiments (WT n = 51 cells and Hyper Gα n = 73 cells).

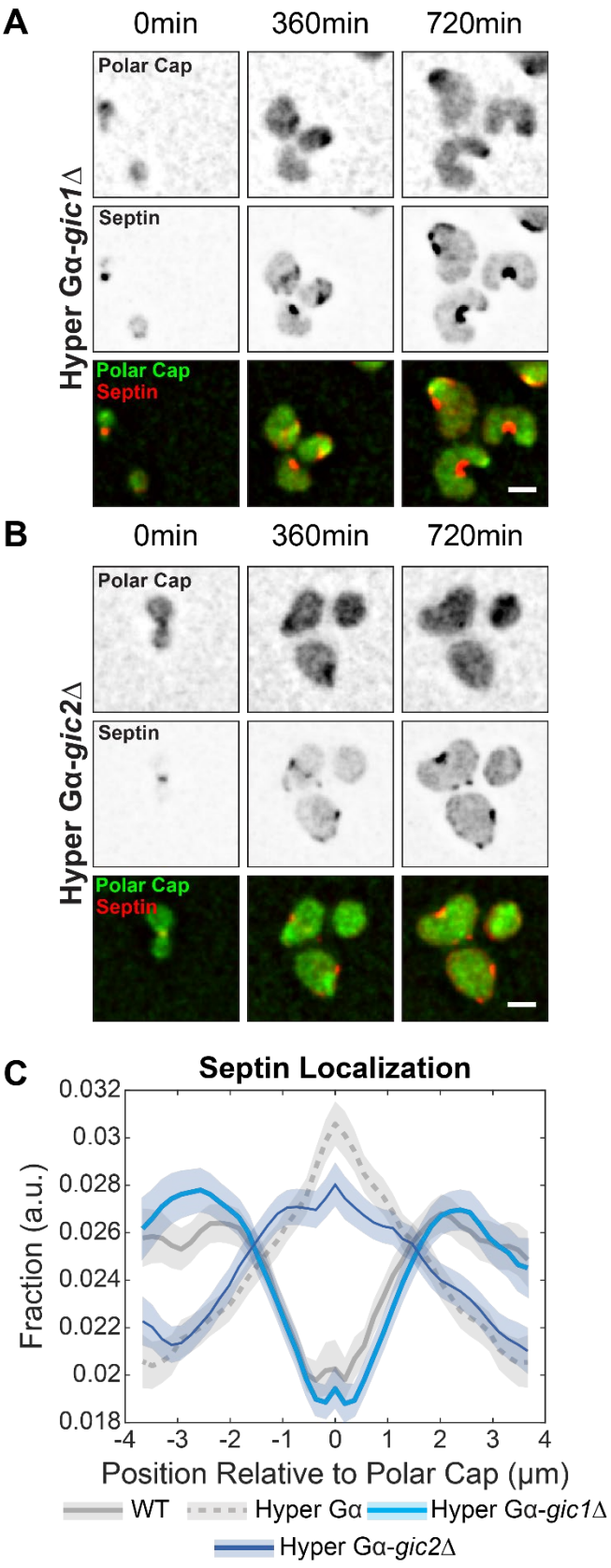

Figure 3.2. Gic septin chaperones differentially contribute to pheromone-induced septin deposition.

(A) Representative images of Hyper Gα mutants lacking Gic1 (Hyper Gα-gic1Δ) yeast expressing endogenous Bem1-GFP (Polar Cap) and Cdc3-mCherry (Septin) exposed to saturating pheromone at 0min (left-panels), 360min (middle-panels), and 720min (right-panels). Split-channel (top and middle rows) and merged images (bottom row). Scale bar represents 5μm. (B) Representative images of Hyper Gα mutants lacking Gic2 (Hyper Gα-gic2Δ) yeast expressing endogenous Bem1-GFP (Polar Cap) and Cdc3-mCherry (Septin) exposed to saturating pheromone at 0min (left-panels), 360min (middle-panels), and 720min (right-panels). Scale bar represents 5μm. (C) Time-averaged quantification of the fraction (y-axis) of septin distribution relative to the polar cap (x-axis). Lines are smoothed representations of time-averaged data (37 time points; 20min interval for 12hrs) and shaded regions surrounding lines are 95% confidence intervals. Lines are representative of two combined experiments (Hyper Gα-gic1Δ n = 63 cells and Hyper Gα-gic2Δ n = 68 cells).

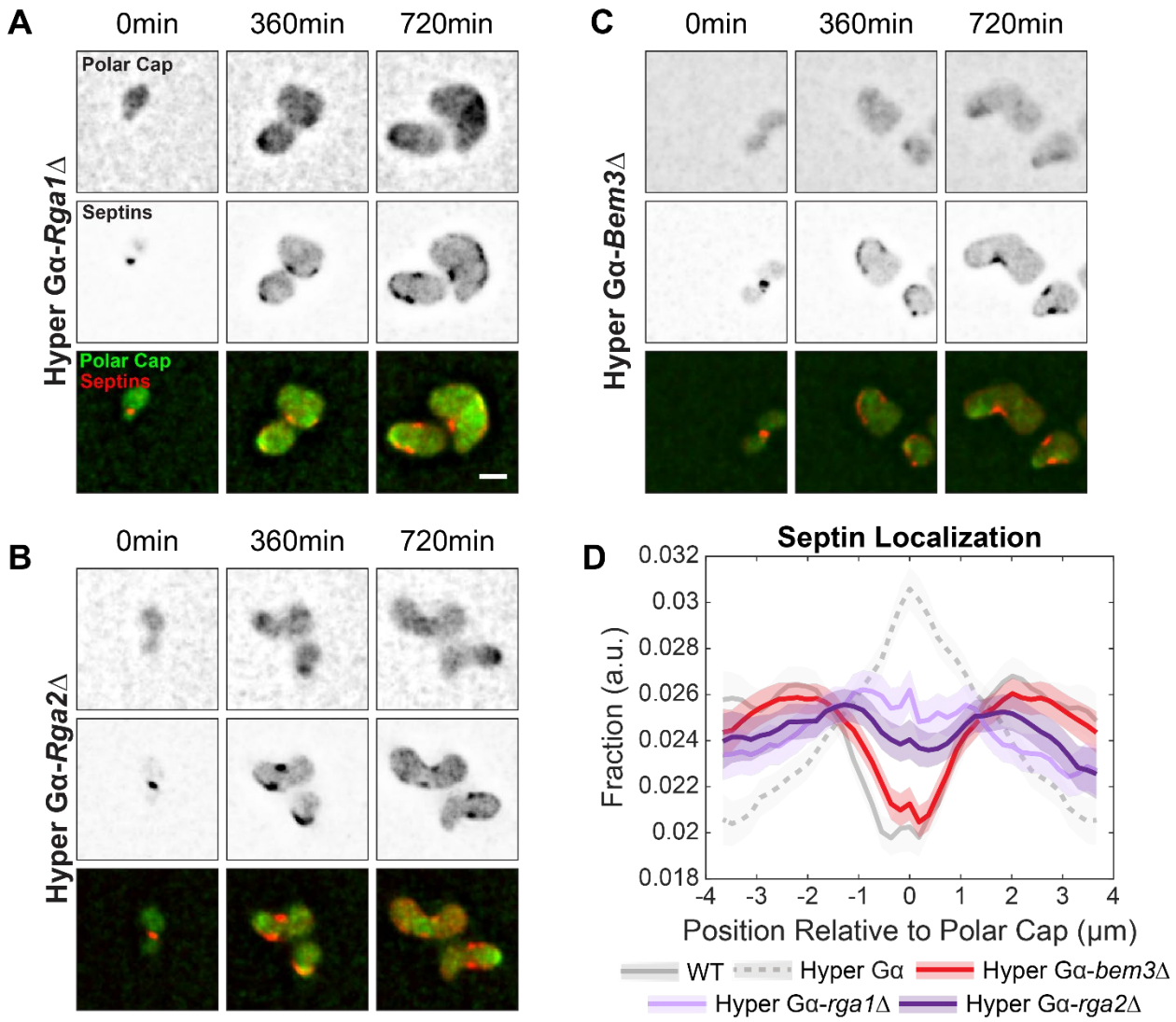

Figure 3.3. The Cdc42GAP, Bem3, drives pheromone-induced septin deposition.

(A) Representative images of Hyper Gα mutants lacking Rga1 (Hyper Gα-rga1Δ) yeast expressing endogenous Bem1-GFP (Polar Cap) and Cdc3-mCherry (Septin) exposed to saturating pheromone at 0min (left-panels), 360min (middle-panels), and 720min (right-panels). Split-channel (top and middle rows) and merged images (bottom row). Scale bar represents 5μm. (B) Representative images of Hyper Gα mutants lacking Rga2 (Hyper Gα-rga2Δ) yeast expressing endogenous Bem1-GFP (Polar Cap) and Cdc3-mCherry (Septin) exposed to saturating pheromone at 0min (left-panels), 360min (middle-panels), and 720min (right-panels). Scale bar represents 5μm. (C) Representative images of Hyper Gα mutants lacking Bem3 (Hyper Gα-bem3Δ) yeast expressing endogenous Bem1-GFP (Polar Cap) and Cdc3-mCherry (Septin) exposed to saturating pheromone at 0min (left-panels), 360min (middle-panels), and 720min (right-panels). Scale bar represents 5μm. (D) Time-averaged quantification of the fraction (y-axis) of septin distribution relative to the polar cap (x-axis). Lines are smoothed representations of time-averaged data (37 time points; 20min interval for 12hrs) and shaded regions surrounding lines are 95% confidence intervals. Lines are representative of two combined experiments (Hyper Gα-rga1Δ n = 79 cells, Hyper Gα-rga2Δ n = 80 cells, and Hyper Gα-bem3Δ n = 87 cells).

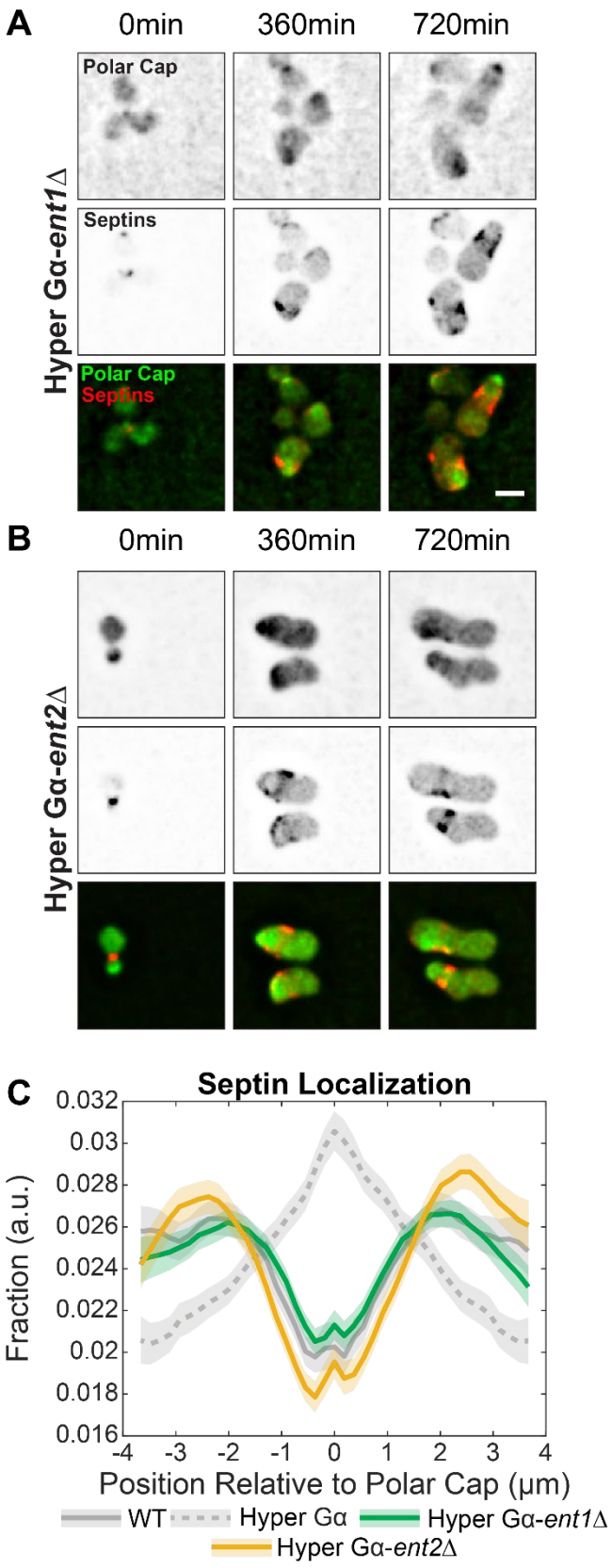

Figure 3.4. Ent1 and Ent2 are functionally redundant in pheromone-induced septin deposition.

(A) Representative images of Hyper Gα mutants lacking Ent1 (Hyper Gα-ent1Δ) yeast expressing endogenous Bem1-GFP (Polar Cap) and Cdc3-mCherry (Septin) exposed to saturating pheromone at 0min (left-panels), 360min (middle-panels), and 720min (right-panels). Split-channel (top and middle rows) and merged images (bottom row). Scale bar represents 5μm. (B) Representative images of Hyper Gα mutants lacking Ent2 (Hyper Gα-ent2Δ) yeast expressing endogenous Bem1-GFP (Polar Cap) and Cdc3-mCherry (Septin) exposed to saturating pheromone at 0min (left-panels), 360min (middle-panels), and 720min (right-panels). Scale bar represents 5μm. (C) Time-averaged quantification of the fraction (y-axis) of septin distribution relative to the polar cap (x-axis). Lines are smoothed representations of time-averaged data (37 time points; 20min interval for 12hrs) and shaded regions surrounding lines are 95% confidence intervals. Lines are representative of two combined experiments (Hyper Gα-ent1Δ n = 92 cells and Hyper Gα-ent2Δ n = 55 cells).

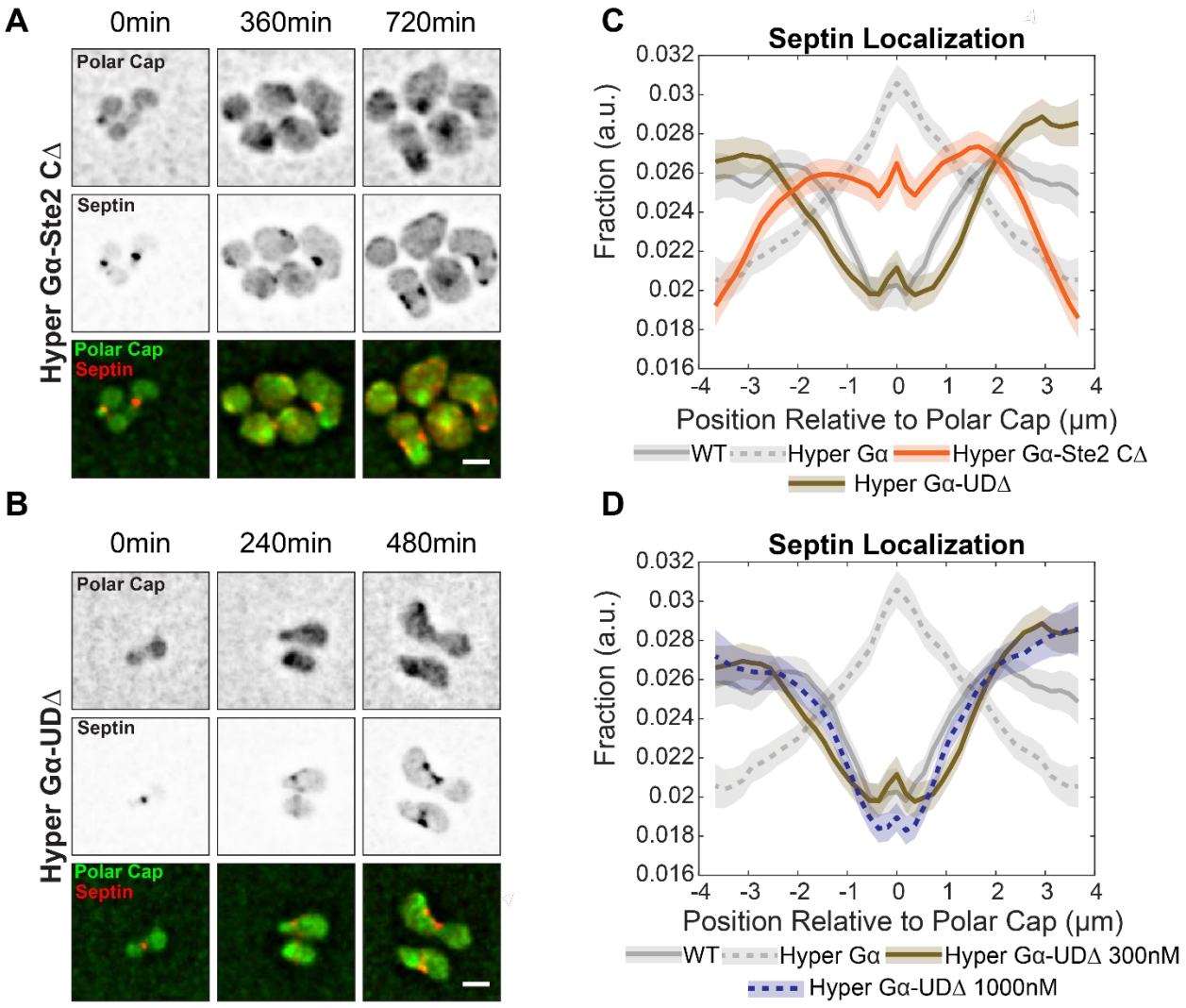

Figure 3.5. Pheromone-induced septin deposition is driven by the Gα ubiquitination domain.

(A) Representative images of Hyper Gα mutants lacking the Ste2 C-terminus beyond codon 326 (Hyper Gα-Ste2 CΔ) yeast expressing endogenous Bem1-GFP (Polar Cap) and Cdc3-mCherry (Septin) exposed to saturating pheromone at 0min (left-panels), 360min (middle-panels), and 720min (right-panels). Split-channel (top and middle rows) and merged images (bottom row). Scale bar represents 5μm. (B) Representative images of Hyper Gα mutants lacking the ubiquitination domain (Hyper Gα-UDΔ) yeast expressing endogenous Bem1-GFP (Polar Cap) and Cdc3-mCherry (Septin) exposed to saturating pheromone at 0min (left-panels), 360min (middle-panels), and 720min (right-panels). Scale bar represents 5μm. (C) Time-averaged quantification of the fraction (y-axis) of septin distribution relative to the polar cap (x-axis). Lines are smoothed representations of time-averaged data (37 time points; 20min interval for 12hrs) and shaded regions surrounding lines are 95% confidence intervals. Lines are representative of two combined experiments (Hyper Gα-Ste2 CΔ n = 58 cells and Hyper Gα-UDΔ n = 93 cells).

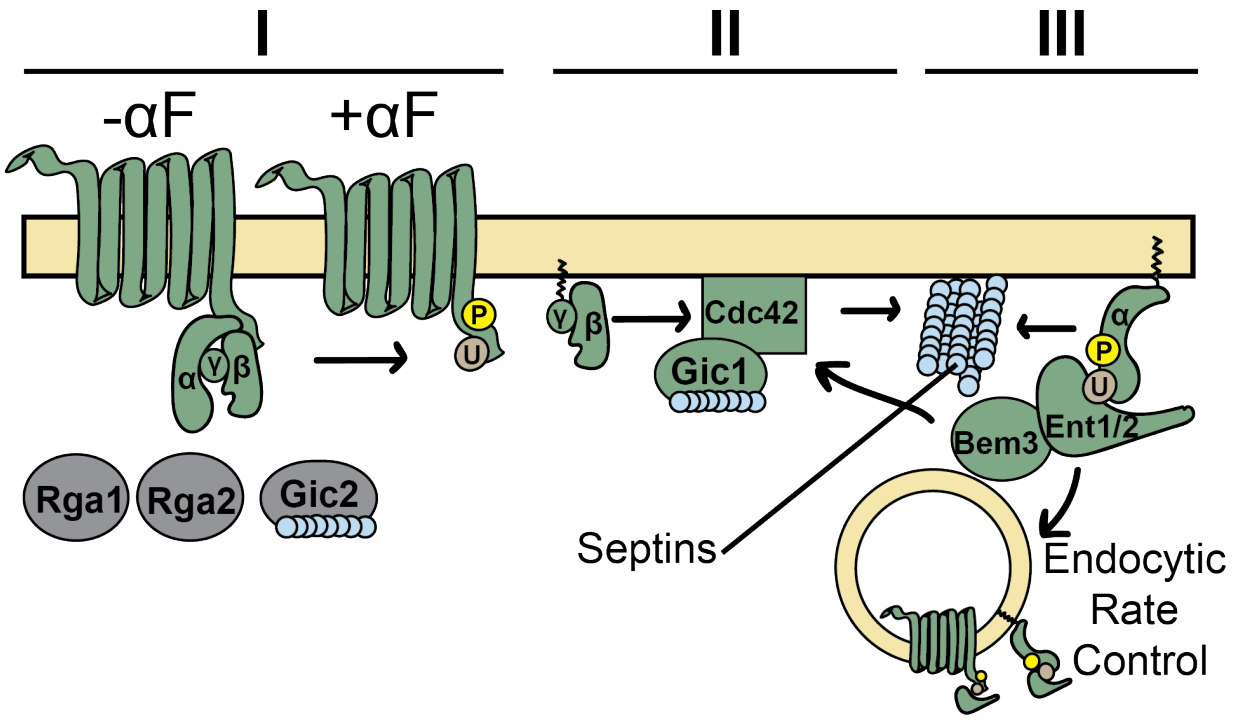

Figure 3.6. Schematic of the Gα-Epsin-Gic1-Bem3 Signaling Axis.

Schematic representation of the Gα-Epsin-Gic1-Bem3 signaling axis for pheromone-induced septin deposition. The signaling cascade can be described via three major components: I) Addition of pheromone activates the receptor and initiates G-protein coupled signaling mechanisms. II) Gα releases the Gβγ-complex that indirectly activates Cdc42, which recruits the septin-bound chaperone Gic1 to Cdc42. III) Active Gα recruits Bem3-bound Ent1/Ent2 to sites of active Cdc42. Bem3 accelerates hydrolysis of Cdc42-GTP to Cdc42-GDP which alters Cdc42's affinity from Gic1 to the bond septin filament. Gic1 is released and septins are deposited at the plasma membrane.

CHAPTER 4

THOUGHTS AND PERSPECTIVES

4. Thoughts and Perspectives

In this dissertation I have described two novel stories of Gα contributing to the yeast pheromone response signaling pathway. In the first story, I showed you how phosphorylation of the RGS is involved in the transition between cytokinesis and pheromone-induced polarization and how the phosphorylation state of RGS also controls the distribution of Fus3-MAPK in the cell. In the second story, I described how endocytosis of Gα dictates the spatial dynamics of septin deposition in the pheromone response (Figure 4.1.). You may be asking, how are both of these stories connected and what questions and future directions do these results generate for further investigation?

4.1. Gα-MAPK Signaling is Influenced By The RGS

In Chapter 2, I showed that both the localization of RGS and the distribution of Gα -MAPK is influenced by the state of RGS phosphorylation (Figure 2.2. and Figure 2.6. respectively). I also mentioned that phosphorylation of the RGS is dependent on active Fus3-MAPK[58]. But why is this important? This would appear to be a negative regulatory mechanism for a negative regulatory mechanism, let me explain. Gα binds active MAPK and enhances downstream signaling and RGS downregulates signaling by turning off Gα. However, RGS in proximity to the Fus3-MAPK is phosphorylated and delocalizes from the polar cap (Figure 2.2.). This phosphorylated RGS would then re-localize once dephosphorylated by a protein phosphatases. While this mechanism is likely specific to yeast, it is unlikely that a similar signaling motif is not found in mammalian cells. Ngyuen and Hadwiger found that Gα4 in *Dictostelium* interacts directly with the MAPK, ERK2 to regulate developmental morphogenesis[176], further supporting a potential RGS-MAPK feedforward loop for MAPK signaling in other systems.

4.2. The Ubiquitin Domain of Yeast Pheromone Gα May Promote Endosomal Signaling

G-protein signaling is complex. Spatial dynamics and intracellular compartmental dynamics of signaling are major contributors to this complexity[177]. Canonically, a receptor signals through its cognate G-protein from signals at the plasma membrane, the signal is transmitted through the cell by effector proteins, and the signal is terminated by RGS activity on Gα or endocytic desensitization of the receptor. However, we have learned that G-proteins and GPCRs can signal in several internal membrane-bound compartments of the cell as well[178]. Not only is this possible, but it is commonly found in mammalian cells that endocytosis of a GPCR promotes sustained signaling patterns at the endosome[178]. One example of this is the opioid receptor, which is known to signal across several cellular compartments including the endosome[179], though this is in part accomplished by β-arrestins, which yeast do not express.

Here in Chapter 3, I show that epsins are more than endocytic adaptors, but also critical signaling components and regulators of Gα signaling (Figure 3.4. and Figure 3.6. respectively). I also mentioned that Gα also complexes with MAPK to enhance signaling. Therefore, it is reasonable to think that Gα endocytosis could drive spatial signaling of MAPK to endosomes (Figure 4.1.).

Although there is a plethora of endosomal signaling evidence in mammalian cells, there is little known about subcellular signaling of GPCRs in yeast. One study reported that Gα promotes phosphoinostitide 3-kinase (PI3K) signaling at the endosome by binding the vesicular sorting protein Vps34[180]. This interaction promotes vacuolar targeting of the endosome. Rangarajan *et al*. also note that VPS34 binds directly to Gαi in mammalian cells[180, 181], which supports conservation of the model from yeast to humans. This evidence supports endosomal signaling during the yeast pheromone response. Together with our evidence implicating Gα in epsin-mediated septin deposition (Figure 3.6.) these data support alternate roles of Gα signaling at the endosome.

4.3. Final Thoughts

The work presented in this dissertation clearly demonstrates novel findings for Gα signaling in the pheromone response. Additionally, I have provided insight to potential implications with mammalian systems. As I conclude I want to put forth some future directions for this work and future questions that will need to be answered.

While we have identified a Gα-specific mechanism for septin distribution in the pheromone response, there remain some unanswered questions. First, are there other membrane-bound cargo contributing to septin deposition and/or distribution? And, what signal(s) are occurring at the endosome upon epsin-mediated endocytosis (e.g. MAPK)?

The RGS in yeast is dynamically phosphorylated to facilitate a smooth transition from mitosis to the pheromone response (Figure 2.9.). But there are more phosphorylation sites on the RGS, what do those phosphorylation sites modulate? I showed data indicating that unphosphorylatable RGS promotes hyperpolarization (Figure 2.8.) and phosphomimetic RGS delocalizes RGS from the polar cap (Figure 2.2.). Additionally, Kel1 is a known negative regulator of the formin Bnr1 but is not known to regulate the pheromone-specific formin Bni1. Could Kel1 be recruited to sites of active Gα to negatively regulate Bni1 during the pheromone response by unphosphorylated RGS? Answering these questions would both provide a better understanding of the influence Gα signaling has in the pheromone response but would also provide critical insight for mechanisms underlying chemotropic and chemotactic growth in mammalian cells.

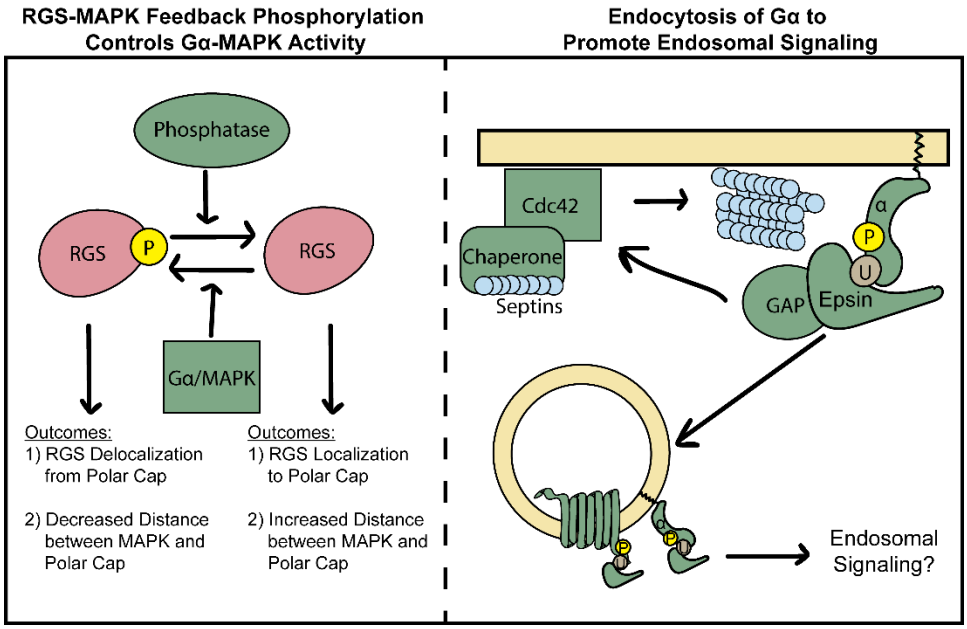

Figure 4.1. New roles for Gα signaling during the yeast pheromone response.

At left, RGS activity is negatively influenced by Gα-MAPK phosphorylation and its dephosphorylation promotes negative regulation of Gα-MAPK, that the promotes MAPK phosphorylation of RGS. Thus promoting a positive feedback loop to enhance MAPK signaling during the pheromone response. At right, epsin-mediated endocytosis of Gα drives septin deposition, but may also drive endosomal signaling.

REFERENCES

1. Sriram, K. & Insel, P.A. G Protein-Coupled Receptors as Targets for Approved Drugs: How Many Targets and How Many Drugs? *Mol Pharmacol* **93**, 251-258 (2018).

2. Kamato, D. *et al.* Structure, Function, Pharmacology, and Therapeutic Potential of the G Protein, Gα/q,11. *Front Cardiovasc Med* **2**, 14 (2015).

3. Dixon, R.A. *et al.* Cloning of the gene and cDNA for mammalian beta-adrenergic receptor and homology with rhodopsin. *Nature* **321**, 75-79 (1986).

4. Rasmussen, S.G. *et al.* Crystal structure of the human beta2 adrenergic G-protein-coupled receptor. *Nature* **450**, 383-387 (2007).

5. Rasmussen, S.G. *et al.* Crystal structure of the β2 adrenergic receptor-Gs protein complex. *Nature* **477**, 549-555 (2011).

6. Cho, R.J. *et al.* A genome-wide transcriptional analysis of the mitotic cell cycle. *Mol Cell* **2**, 65-73 (1998).

7. Botstein, D. & Fink, G.R. Yeast: an experimental organism for 21st Century biology. *Genetics* **189**, 695-704 (2011).

8. Botstein, D. & Fink, G.R. Yeast: an experimental organism for modern biology. *Science* **240**, 1439-1443 (1988).

9. Goffeau, A. *et al.* Life with 6000 Genes. *Science* **274**, 546-567 (1996).

10. Liu, W. *et al.* From Saccharomyces cerevisiae to human: The important gene co-expression modules. *Biomed Rep* **7**, 153-158 (2017).

11. Giaever, G. *et al.* Functional profiling of the Saccharomyces cerevisiae genome. *Nature* **418**, 387-391 (2002).

12. Winzeler, E.A. *et al.* Functional Characterization of the S. cerevisiae Genome by Gene Deletion and Parallel Analysis. *Science* **285**, 901-906 (1999).

13. Jones, G.M. *et al.* A systematic library for comprehensive overexpression screens in Saccharomyces cerevisiae. *Nat Methods* **5**, 239-241 (2008).

14. Huh, W.-K. *et al.* Global analysis of protein localization in budding yeast. *Nature* **425**, 686-691 (2003).

15. Ghaemmaghami, S. *et al.* Global analysis of protein expression in yeast. *Nature* **425**, 737-741 (2003).

16. Lashkari, D.A. *et al.* Yeast microarrays for genome wide parallel genetic and gene expression analysis. *Proc Natl Acad Sci U S A* **94**, 13057-13062 (1997).

17. DeRisi, J.L., Iyer, V.R. & Brown, P.O. Exploring the Metabolic and Genetic Control of Gene Expression on a Genomic Scale. *Science* **278**, 680-686 (1997).

18. Zhu, H. *et al.* Global Analysis of Protein Activities Using Proteome Chips. *Science* **293**, 2101-2105 (2001).

19. Villas-Bôas, S.G., Moxley, J.F., Akesson, M., Stephanopoulos, G. & Nielsen, J. High-throughput metabolic state analysis: the missing link in integrated functional genomics of yeasts. *Biochem J* **388**, 669-677 (2005).

20. Jewett, M.C., Hofmann, G. & Nielsen, J. Fungal metabolite analysis in genomics and phenomics. *Curr Opin Biotechnol* **17**, 191-197 (2006).

21. Dohlman, H.G., Thorner, J., Caron, M.G. & Lefkowitz, R.J. Model systems for the study of seven-transmembrane-segment receptors. *Annu Rev Biochem* **60**, 653-688 (1991).

22. Versele, M., Lemaire, K. & Thevelein, J.M. Sex and sugar in yeast: two distinct GPCR systems. *EMBO Rep* **2**, 574-579 (2001).

23. Velazhahan, V. *et al.* Structure of the class D GPCR Ste2 dimer coupled to two G proteins. *Nature* **589**, 148-153 (2021).

24. Bardwell, L. A walk-through of the yeast mating pheromone response pathway. *Peptides* **26**, 339-350 (2005).

25. Hartwell, L.H. Mutants of Saccharomyces cerevisiae unresponsive to cell division control by polypeptide mating hormone. *J Cell Biol* **85**, 811-822 (1980).

26. Metodiev, M.V., Matheos, D., Rose, M.D. & Stone, D.E. Regulation of MAPK function by direct interaction with the mating-specific Gα in yeast. *Science* **296**, 1483-1486 (2002).

27. Stratton, H.F., Zhou, J., Reed, S.I. & Stone, D.E. The mating-specific G (alpha) protein of Saccharomyces cerevisiae downregulates the mating signal by a mechanism that is dependent on pheromone and independent of G (beta)(gamma) sequestration. *Molecular and Cellular Biology* **16**, 6325-6337 (1996).

28. Zhou, J., Arora, M. & Stone, D.E. The yeast pheromone-responsive Gα protein stimulates recovery from chronic pheromone treatment by two mechanisms that are activated at distinct levels of stimulus. *Cell biochemistry and biophysics* **30**, 193-212 (1999).

29. Masuho, I. *et al.* A global map of G protein signaling regulation by RGS proteins. *Cell* **183**, 503-521. e519 (2020).

30. Sethakorn, N., Yau, D.M. & Dulin, N.O. Non-canonical functions of RGS proteins. *Cellular signalling* **22**, 1274-1281 (2010).

31. Dowell, S.J., Bishop, A.L., Dyos, S.L., Brown, A.J. & Whiteway, M.S. Mapping of a yeast G protein βγ signaling interaction. *Genetics* **150**, 1407-1417 (1998).

32. Feng, Y., Song, L.Y., Kincaid, E., Mahanty, S.K. & Elion, E.A. Functional binding between Gβ and the LIM domain of Ste5 is required to activate the MEKK Ste11. *Current biology* **8**, 267-282 (1998).

33. Inouye, C., Dhillon, N. & Thorner, J. Ste5 RING-H2 domain: role in Ste4-promoted oligomerization for yeast pheromone signaling. *Science* **278**, 103-106 (1997).

34. Whiteway, M.S. *et al.* Association of the yeast pheromone response G protein βγ subunits with the MAP kinase scaffold Ste5p. *Science* **269**, 1572-1575 (1995).

35. Garrenton, L.S., Young, S.L. & Thorner, J. Function of the MAPK scaffold protein, Ste5, requires a cryptic PH domain. *Genes Dev* **20**, 1946-1958 (2006).

36. Lamson, R.E., Winters, M.J. & Pryciak, P.M. Cdc42 regulation of kinase activity and signaling by the yeast p21-activated kinase Ste20. *Mol Cell Biol* **22**, 2939-2951 (2002).

37. Winters, M.J. & Pryciak, P.M. Interaction with the SH3 domain protein Bem1 regulates signaling by the Saccharomyces cerevisiae p21-activated kinase Ste20. *Mol Cell Biol* **25**, 2177-2190 (2005).

38. Butty, A.-C., Pryciak, P.M., Huang, L.S., Herskowitz, I. & Peter, M. The role of Far1p in linking the heterotrimeric G protein to polarity establishment proteins during yeast mating. *Science* **282**, 1511-1516 (1998).

39. Nern, A. & Arkowitz, R.A. A Cdc24p-Far1p-Gbetagamma protein complex required for yeast orientation during mating. *The Journal of cell biology* **144**, 1187-1202 (1999).

40. Kelley, J.B. *et al.* RGS proteins and septins cooperate to promote chemotropism by regulating polar cap mobility. *Current Biology* **25**, 275-285 (2015).

41. Pryciak, P.M. & Huntress, F.A. Membrane recruitment of the kinase cascade scaffold protein Ste5 by the Gbetagamma complex underlies activation of the yeast pheromone response pathway. *Genes Dev* **12**, 2684-2697 (1998).

42. Wu, C., Leberer, E., Thomas, D.Y. & Whiteway, M. Functional characterization of the interaction of Ste50p with Ste11p MAPKKK in Saccharomyces cerevisiae. *Mol Biol Cell* **10**, 2425-2440 (1999).

43. Ramezani-Rad, M. The role of adaptor protein Ste50-dependent regulation of the MAPKKK Ste11 in multiple signalling pathways of yeast. *Curr Genet* **43**, 161-170 (2003).

44. Burack, W.R. & Shaw, A.S. Signal transduction: hanging on a scaffold. *Current opinion in cell biology* **12**, 211-216 (2000).

45. Elion, E.A. The ste5p scaffold. *Journal of Cell Science* **114**, 3967-3978 (2001).

46. Ferrell Jr, J.E. & Cimprich, K.A. Enforced proximity in the function of a famous scaffold. *Molecular cell* **11**, 289-291 (2003).

47. Harris, K. *et al.* Role of scaffolds in MAP kinase pathway specificity revealed by custom design of pathway-dedicated signaling proteins. *Current Biology* **11**, 1815-1824 (2001).

48. Park, S.-H., Zarrinpar, A. & Lim, W.A. Rewiring MAP kinase pathways using alternative scaffold assembly mechanisms. *Science* **299**, 1061-1064 (2003).

49. Ptashne, M. & Gann, A. Imposing specificity on kinases. *Science* **299**, 1025-1027 (2003).

50. Sette, C., Inouye, C., Stroschein, S., Iaquinta, P. & Thorner, J. Mutational analysis suggests that activation of the yeast pheromone response MAPK pathway involves conformational changes in the Ste5 scaffold protein. *Mol. Biol. Cell* **11**, 4033-4049 (2000).

51. Wang, Y. & Elion, E.A. Nuclear export and plasma membrane recruitment of the Ste5 scaffold are coordinated with oligomerization and association with signal transduction components. *Molecular biology of the cell* **14**, 2543-2558 (2003).

52. Cook, J.G., Bardwell, L., Kron, S.J. & Thorner, J. Two novel targets of the MAP kinase Kss1 are negative regulators of invasive growth in the yeast Saccharomyces cerevisiae. *Genes Dev* **10**, 2831-2848 (1996).

53. Tedford, K., Kim, S., Sa, D., Stevens, K. & Tyers, M. Regulation of the mating pheromone and invasive growth responses in yeast by two MAP kinase substrates. *Curr Biol* **7**, 228-238 (1997).

54. Roberts, C.J. *et al.* Signaling and circuitry of multiple MAPK pathways revealed by a matrix of global gene expression profiles. *Science* **287**, 873-880 (2000).

55. White, J.M. & Rose, M.D. Yeast mating: getting close to membrane merger. *Curr Biol* **11**, R16-20 (2001).

56. Dohlman, H.G., Song, J., Ma, D., Courchesne, W.E. & Thorner, J. Sst2, a negative regulator of pheromone signaling in the yeast Saccharomyces cerevisiae: expression, localization, and genetic interaction and physical association with Gpa1 (the G-protein alpha subunit). *Mol Cell Biol* **16**, 5194-5209 (1996).

57. Apanovitch, D.M., Slep, K.C., Sigler, P.B. & Dohlman, H.G. Sst2 is a GTPase-activating protein for Gpa1: purification and characterization of a cognate RGS-Galpha protein pair in yeast. *Biochemistry* **37**, 4815-4822 (1998).

58. Garrison, T. *et al.* Feedback phosphorylation of an RGS protein by MAP kinase in yeast. *The Journal of biological chemistry* **274**, 36387-36391 (1999).

59. Siekhaus, D.E. & Drubin, D.G. Spontaneous receptor-independent heterotrimeric G-protein signalling in an RGS mutant. *Nature Cell Biology* **5**, 231-235 (2003).

60. Parnell, S. *et al.* Phosphorylation of the RGS protein Sst2 by the MAP kinase Fus3 and use of Sst2 as a model to analyze determinants of substrate sequence specificity. *Biochemistry* **44**, 8159-8166 (2005).

61. Schandel, K.A. & Jenness, D.D. Direct evidence for ligand-induced internalization of the yeast alpha-factor pheromone receptor. *Molecular and Cellular Biology* **14**, 7245-7255 (1994).

62. Emmerstorfer-Augustin, A., Augustin, C.M., Shams, S. & Thorner, J. Tracking yeast pheromone receptor Ste2 endocytosis using fluorogen-activating protein tagging. *Mol Biol Cell* **29**, 2720-2736 (2018).

63. Alvaro, C.G. *et al.* Specific α-arrestins negatively regulate Saccharomyces cerevisiae pheromone response by down-modulating the G-protein-coupled receptor Ste2. *Mol Cell Biol* **34**, 2660-2681 (2014).

64. Dores, M.R., Schnell, J.D., Maldonado-Baez, L., Wendland, B. & Hicke, L. The function of yeast epsin and Ede1 ubiquitin-binding domains during receptor internalization. *Traffic* **11**, 151-160 (2010).

65. Messa, M. *et al.* Epsin deficiency impairs endocytosis by stalling the actin-dependent invagination of endocytic clathrin-coated pits. *eLife* **3**, e03311 (2014).

66. Aguilar, R.C. *et al.* Epsin N-terminal homology domains perform an essential function regulating Cdc42 through binding Cdc42 GTPase-activating proteins. *Proceedings of the National Academy of Sciences* **103**, 4116-4121 (2006).

67. Hicke, L. & Riezman, H. Ubiquitination of a yeast plasma membrane receptor signals its ligand-stimulated endocytosis. *Cell* **84**, 277-287 (1996).

68. Chen, Q. & Konopka, J.B. Regulation of the G-protein-coupled alpha-factor pheromone receptor by phosphorylation. *Molecular and Cellular Biology* **16**, 247-257 (1996).

69. Konopka, J.B., Jenness, D.D. & Hartwell, L.H. The C-terminus of the S. cerevisiae α-pheromone receptor mediates an adaptive response to pheromone. *Cell* **54**, 609-620 (1988).

70. Wang, Y., Marotti, L.A., Jr., Lee, M.J. & Dohlman, H.G. Differential regulation of G protein alpha subunit trafficking by mono- and polyubiquitination. *The Journal of biological chemistry* **280**, 284-291 (2005).

71. Sprague, G.F., Jr. & Herskowitz, I. Control of yeast cell type by the mating type locus. I. Identification and control of expression of the a-specific gene BAR1. *J Mol Biol* **153**, 305-321 (1981).

72. Chan, R.K. & Otte, C.A. Physiological characterization of Saccharomyces cerevisiae mutants supersensitive to G1 arrest by a factor and alpha factor pheromones. *Molecular and cellular biology* **2**, 21-29 (1982).

73. Sabbagh, W., Jr., Flatauer, L.J., Bardwell, A.J. & Bardwell, L. Specificity of MAP kinase signaling in yeast differentiation involves transient versus sustained MAPK activation. *Mol Cell* **8**, 683-691 (2001).

74. Doi, K. *et al.* MSG5, a novel protein phosphatase promotes adaptation to pheromone response in S. cerevisiae. *Embo j* **13**, 61-70 (1994).

75. Zhan, X.L., Deschenes, R.J. & Guan, K.L. Differential regulation of FUS3 MAP kinase by tyrosine-specific phosphatases PTP2/PTP3 and dual-specificity phosphatase MSG5 in Saccharomyces cerevisiae. *Genes Dev* **11**, 1690-1702 (1997).

76. Esch, R.K. & Errede, B. Pheromone induction promotes Ste11 degradation through a MAPK feedback and ubiquitin-dependent mechanism. *Proc Natl Acad Sci U S A* **99**, 9160-9165 (2002).

77. Wang, Y. & Dohlman, H.G. Pheromone-dependent ubiquitination of the mitogen-activated protein kinase kinase Ste7. *J Biol Chem* **277**, 15766-15772 (2002).

78. Wang, Y. *et al.* Regulation of Ste7 ubiquitination by Ste11 phosphorylation and the Skp1-Cullin-F-box complex. *J Biol Chem* **278**, 22284-22289 (2003).

79. Gartner, A. *et al.* Pheromone-dependent G1 cell cycle arrest requires Far1 phosphorylation, but may not involve inhibition of Cdc28-Cln2 kinase, in vivo. *Mol Cell Biol* **18**, 3681-3691 (1998).

80. Bender, A. & Pringle, J.R. Multicopy suppression of the cdc24 budding defect in yeast by CDC42 and three newly identified genes including the ras-related gene RSR1. *Proc Natl Acad Sci U S A* **86**, 9976-9980 (1989).

81. Chant, J., Corrado, K., Pringle, J.R. & Herskowitz, I. Yeast BUD5, encoding a putative GDP-GTP exchange factor, is necessary for bud site selection and interacts with bud formation gene BEM1. *Cell* **65**, 1213-1224 (1991).

82. Chant, J. & Herskowitz, I. Genetic control of bud site selection in yeast by a set of gene products that constitute a morphogenetic pathway. *Cell* **65**, 1203-1212 (1991).

83. Bender, A. Genetic evidence for the roles of the bud-site-selection genes BUD5 and BUD2 in control of the Rsr1p (Bud1p) GTPase in yeast. *Proc Natl Acad Sci U S A* **90**, 9926-9929 (1993).

84. Park, H.O., Chant, J. & Herskowitz, I. BUD2 encodes a GTPase-activating protein for Bud1/Rsr1 necessary for proper bud-site selection in yeast. *Nature* **365**, 269-274 (1993).

85. Miller, K.E., Kang, P.J. & Park, H.O. Regulation of Cdc42 for polarized growth in budding yeast. *Microb Cell* **7**, 175-189 (2020).

86. Glomb, O. & Gronemeyer, T. Septin Organization and Functions in Budding Yeast. *Front Cell Dev Biol* **4**, 123 (2016).

87. Meitinger, F. & Palani, S. Actomyosin ring driven cytokinesis in budding yeast. *Seminars in Cell & Developmental Biology* **53**, 19-27 (2016).

88. Schwob, E., Böhm, T., Mendenhall, M.D. & Nasmyth, K. The B-type cyclin kinase inhibitor p40SIC1 controls the G1 to S transition in S. cerevisiae. *Cell* **79**, 233-244 (1994).

89. Amon, A., Irniger, S. & Nasmyth, K. Closing the cell cycle circle in yeast: G2 cyclin proteolysis initiated at mitosis persists until the activation of G1 cyclins in the next cycle. *Cell* **77**, 1037-1050 (1994).

90. McKinney, J.D. & Cross, F.R. FAR1 and the G1 phase specificity of cell cycle arrest by mating factor in Saccharomyces cerevisiae. *Mol Cell Biol* **15**, 2509-2516 (1995).

91. McKinney, J.D., Chang, F., Heintz, N. & Cross, F.R. Negative regulation of FAR1 at the Start of the yeast cell cycle. *Genes Dev* **7**, 833-843 (1993).

92. Oehlen, L.J., McKinney, J.D. & Cross, F.R. Ste12 and Mcm1 regulate cell cycle-dependent transcription of FAR1. *Mol Cell Biol* **16**, 2830-2837 (1996).

93. Bi, E. *et al.* Involvement of an actomyosin contractile ring in Saccharomyces cerevisiae cytokinesis. *J Cell Biol* **142**, 1301-1312 (1998).

94. Rodriguez, J.R. & Paterson, B.M. Yeast myosin heavy chain mutant: maintenance of the cell type specific budding pattern and the normal deposition of chitin and cell wall components requires an intact myosin heavy chain gene. *Cell Motil Cytoskeleton* **17**, 301-308 (1990).

95. Watts, F.Z., Shiels, G. & Orr, E. The yeast MYO1 gene encoding a myosin-like protein required for cell division. *Embo j* **6**, 3499-3505 (1987).

96. Hartwell, L.H. Genetic control of the cell division cycle in yeast: IV. Genes controlling bud emergence and cytokinesis. *Experimental cell research* **69**, 265-276 (1971).

97. Sanders, S.L. & Field, C.M. Cell division. Septins in common? *Curr Biol* **4**, 907-910 (1994).

98. Pringle, J.R. (2008).

99. Longtine, M.S. *et al.* The septins: roles in cytokinesis and other processes. *Current opinion in cell biology* **8**, 106-119 (1996).

100. Field, C.M. & Kellogg, D. Septins: cytoskeletal polymers or signalling GTPases? *Trends in cell biology* **9**, 387-394 (1999).

101. Zhang, J. *et al.* Phosphatidylinositol polyphosphate binding to the mammalian septin H5 is modulated by GTP. *Current Biology* **9**, 1458-1467 (1999).

102. Bertin, A. *et al.* Phosphatidylinositol-4, 5-bisphosphate promotes budding yeast septin filament assembly and organization. *Journal of molecular biology* **404**, 711-731 (2010).

103. Oh, Y. & Bi, E. Septin structure and function in yeast and beyond. *Trends in Cell Biology* **21**, 141-148 (2011).

104. Weems, A. & McMurray, M. The step-wise pathway of septin hetero-octamer assembly in budding yeast. *eLife* **6**, e23689 (2017).

105. Douglas, L.M., Alvarez, F.J., McCreary, C. & Konopka, J.B. Septin Function in Yeast Model Systems and Pathogenic Fungi. *Eukaryotic Cell* **4**, 1503-1512 (2005).

106. Alvaro, C.G. & Thorner, J. Heterotrimeric G Protein-coupled Receptor Signaling in Yeast Mating Pheromone Response. *J Biol Chem* **291**, 7788-7795 (2016).

107. Arkowitz, R.A. Chemical gradients and chemotropism in yeast. *Cold Spring Harbor perspectives in biology* **1**, a001958 (2009).

108. Wang, Y. & Dohlman, H.G. Pheromone signaling mechanisms in yeast: a prototypical sex machine. *Science* **306**, 1508-1509 (2004).

109. Peter, M., Gartner, A., Horecka, J., Ammerer, G. & Herskowitz, I. FAR1 links the signal transduction pathway to the cell cycle machinery in yeast. *Cell* **73**, 747-760 (1993).

110. Chiou, J.G., Balasubramanian, M.K. & Lew, D.J. Cell Polarity in Yeast. *Annu Rev Cell Dev Biol* **33**, 77-101 (2017).

111. Park, H.O. & Bi, E. Central roles of small GTPases in the development of cell polarity in yeast and beyond. *Microbiol Mol Biol Rev* **71**, 48-96 (2007).

112. Metodiev, M.V., Matheos, D., Rose, M.D. & Stone, D.E. Regulation of MAPK function by direct interaction with the mating-specific Galpha in yeast. *Science* **296**, 1483-1486 (2002).

113. Hao, N. *et al.* Regulation of cell signaling dynamics by the protein kinase-scaffold Ste5. *Molecular cell* **30**, 649-656 (2008).

114. Pope, P.A., Bhaduri, S. & Pryciak, P.M. Regulation of cyclin-substrate docking by a G1 arrest signaling pathway and the Cdk inhibitor Far1. *Current biology : CB* **24**, 1390-1396 (2014).

115. Elion, E.A., Satterberg, B. & Kranz, J.E. FUS3 phosphorylates multiple components of the mating signal transduction cascade: evidence for STE12 and FAR1. *Mol Biol Cell* **4**, 495-510 (1993).

116. Matheos, D., Metodiev, M., Muller, E., Stone, D. & Rose, M.D. Pheromone-induced polarization is dependent on the Fus3p MAPK acting through the formin Bni1p. *The Journal of cell biology* **165**, 99-109 (2004).

117. Chasse, S. *et al.* Genome-scale analysis reveals Sst2 as the principal regulator of mating pheromone signaling in the yeast Saccharomyces cerevisiae. *Eukaryotic cell* **5**, 330-346 (2006).

118. Segall, J.E. Polarization of yeast cells in spatial gradients of alpha mating factor. *Proc Natl Acad Sci U S A* **90**, 8332-8336 (1993).

119. Dohlman, H., Apaniesk, D., Chen, Y., Song, J. & Nusskern, D. Inhibition of G-protein signaling by dominant gain-of-function mutations in Sst2p, a pheromone desensitization factor in Saccharomyces cerevisiae. *Molecular and cellular biology* **15**, 3635-3643 (1995).

120. Bar-Shavit, R. *et al.* G Protein-Coupled Receptors in Cancer. *Int J Mol Sci* **17** (2016).

121. Hauser, A.S., Attwood, M.M., Rask-Andersen, M., Schioth, H.B. & Gloriam, D.E. Trends in GPCR drug discovery: new agents, targets and indications. *Nat Rev Drug Discov* **16**, 829-842 (2017).

122. Lappano, R. & Maggiolini, M. GPCRs and cancer. *Acta Pharmacol Sin* **33**, 351-362 (2012).

123. DiBello, P.R. *et al.* Selective uncoupling of RGS action by a single point mutation in the G protein alpha-subunit. *The Journal of biological chemistry* **273**, 5780-5784 (1998).

124. Ballon, D.R. *et al.* DEP-domain-mediated regulation of GPCR signaling responses. *Cell* **126**, 1079-1093 (2006).

125. Dixit, G., Kelley, J.B., Houser, J.R., Elston, T.C. & Dohlman, H.G. Cellular noise suppression by the regulator of G protein signaling Sst2. *Molecular cell* **55**, 85-96 (2014).

126. Burchett, S. *et al.* Regulation of stress response signaling by the N-terminal dishevelled/EGL-10/pleckstrin domain of Sst2, a regulator of G protein signaling in Saccharomyces cerevisiae. *The Journal of biological chemistry* **277**, 22156-22167 (2002).

127. Yu, H. *et al.* High-Quality Binary Protein Interaction Map of the Yeast Interactome Network. **322**, 104-110 (2008).

128. Gould, C.J. *et al.* Saccharomyces cerevisiae Kelch proteins and Bud14 protein form a stable 520-kDa formin regulatory complex that controls actin cable assembly and cell morphogenesis. *The Journal of biological chemistry* **289**, 18290-18301 (2014).

129. Smith, J.A. & Rose, M.D. Kel1p Mediates Yeast Cell Fusion Through a Fus2p- and Cdc42p-Dependent Mechanism. *Genetics* **202**, 1421-1435 (2016).

130. Hofken, T. & Schiebel, E. A role for cell polarity proteins in mitotic exit. *The EMBO journal* **21**, 4851-4862 (2002).

131. Garcia, I. *et al.* Kel1 is a phosphorylation-regulated noise suppressor of the pheromone signaling pathway. *Cell reports* **37**, 110186 (2021).

132. Chee, M.K. & Haase, S.B. New and Redesigned pRS Plasmid Shuttle Vectors for Genetic Manipulation of Saccharomycescerevisiae. *G3 (Bethesda)* **2**, 515-526 (2012).

133. Lee, S., Lim, W.A. & Thorn, K.S. Improved Blue, Green, and Red Fluorescent Protein Tagging Vectors for S. cerevisiae. *PLoS ONE* **8**, e67902 (2013).

134. Huh, W.K. *et al.* Global analysis of protein localization in budding yeast. *Nature* **425**, 686-691 (2003).

135. Storici, F. & Resnick, M.A. The delitto perfetto approach to in vivo site-directed mutagenesis and chromosome rearrangements with synthetic oligonucleotides in yeast. *Methods Enzymol* **409**, 329-345 (2006).

136. Burke, D., Dawson, D. & Stearns, T. *Methods in Yeast Genetics: A Cold Spring Harbor Laboratory Course Manual*, Edn. 200 Edition. (2000).

137. Suzuki, S.K., Kelley, J.B., Elston, T.C. & Dohlman, H.G. Gradient Tracking by Yeast GPCRs in a Microfluidics Chamber, in *G Protein-Coupled Receptor Screening Assays* 275-287 (2021).

138. Schindelin, J. *et al.* Fiji: an open-source platform for biological-image analysis. *Nature methods* **9**, 676-682 (2012).

139. Kelley, J.B. *et al.* RGS proteins and septins cooperate to promote chemotropism by regulating polar cap mobility. *Current biology : CB* **25**, 275-285 (2015).

140. Shellhammer, J.P. *et al.* Quantitative analysis of the yeast pheromone pathway. *Yeast* **36**, 495-518 (2019).

141. Hunn, J.C., Hutchinson, K.M., Kelley, J.B. & Reines, D. An Algorithm to Quantify Inducible Protein Condensates In Eukaryotic Cells. *bioRxiv*, 2021.2008.2026.457826 (2021).

142. Errede, B., Vered, L., Ford, E., Pena, M.I. & Elston, T.C. Pheromone-induced morphogenesis and gradient tracking are dependent on the MAPK Fus3 binding to Galpha. *Mol Biol Cell* **26**, 3343-3358 (2015).

143. Wang, Y. & Dohlman, H.G. Pheromone signaling mechanisms in yeast: a prototypical sex machine. *Science* **306**, 1508-1509 (2004).

144. Ciejek, E. & Thorner, J. Recovery of S. cerevisiae a cells from G1 arrest by alpha factor pheromone requires endopeptidase action. *Cell* **18**, 623-635 (1979).

145. Seshan, A., Bardin, A.J. & Amon, A. Control of Lte1 localization by cell polarity determinants and Cdc14. *Current biology : CB* **12**, 2098-2110 (2002).

146. Hotz, M. & Barral, Y. The Mitotic Exit Network: new turns on old pathways. *Trends Cell Biol* **24**, 145-152 (2014).

147. Buttery, S.M., Yoshida, S. & Pellman, D. Yeast formins Bni1 and Bnr1 utilize different modes of cortical interaction during the assembly of actin cables. *Mol Biol Cell* **18**, 1826-1838 (2007).

148. Gao, L., Liu, W. & Bretscher, A. The yeast formin Bnr1p has two localization regions that show spatially and temporally distinct association with septin structures. *Mol Biol Cell* **21**, 1253-1262 (2010).

149. Pruyne, D., Gao, L., Bi, E. & Bretscher, A. Stable and dynamic axes of polarity use distinct formin isoforms in budding yeast. *Mol Biol Cell* **15**, 4971-4989 (2004).

150. Amaral, N. *et al.* The Aurora-B-dependent NoCut checkpoint prevents damage of anaphase bridges after DNA replication stress. *Nat Cell Biol* **18**, 516-526 (2016).

151. Breitsprecher, D. & Goode, B.L. Formins at a glance. *J Cell Sci* **126**, 1-7 (2013).

152. Arkowitz, R.A. Chemical gradients and chemotropism in yeast. *Cold Spring Harbor perspectives in biology* **1**, a001958 (2009).

153. de Godoy, L.M. *et al.* Comprehensive mass-spectrometry-based proteome quantification of haploid versus diploid yeast. *Nature* **455**, 1251-1254 (2008).

154. Philips, J. & Herskowitz, I. Identification of Kel1p, a kelch domain-containing protein involved in cell fusion and morphology in Saccharomyces cerevisiae. *The Journal of cell biology* **143**, 375-389 (1998).

155. Geymonat, M., Spanos, A., Jensen, S. & Sedgwick, S.G. Phosphorylation of Lte1 by Cdk prevents polarized growth during mitotic arrest in S. cerevisiae. *The Journal of cell biology* **191**, 1097-1112 (2010).

156. Howell, A. *et al.* Negative feedback enhances robustness in the yeast polarity establishment circuit. *Cell* **149**, 322-333 (2012).

157. Dyer, J.M. *et al.* Tracking shallow chemical gradients by actin-driven wandering of the polarization site. *Current biology : CB* **23**, 32-41 (2013).

158. Ghose, D., Jacobs, K., Ramirez, S., Elston, T. & Lew, D. Chemotactic movement of a polarity site enables yeast cells to find their mates. *Proc Natl Acad Sci U S A* **118** (2021).

159. Segall, J.E. Polarization of yeast cells in spatial gradients of alpha mating factor. *Proceedings of the National Academy of Sciences* **90**, 8332-8336 (1993).

160. Dohlman, H.G. & Thorner, J. Regulation of G protein–initiated signal transduction in yeast: paradigms and principles. *Annual review of biochemistry* **70**, 703-754 (2001).

161. Mösch, H.-U., Roberts, R.L. & Fink, G.R. Ras2 signals via the Cdc42/Ste20/mitogen-activated protein kinase module to induce filamentous growth in Saccharomyces cerevisiae. *Proceedings of the National Academy of Sciences* **93**, 5352-5356 (1996).

162. Wu, C., Whiteway, M., Thomas, D.Y. & Leberer, E. Molecular Characterization of Ste20p, a Potential Mitogen-activated Protein or Extracellular Signal-regulated Kinase Kinase (MEK) Kinase Kinase from Saccharomyces cerevisiae (∗). *Journal of Biological Chemistry* **270**, 15984-15992 (1995).

163. Giot, L. & Konopka, J.B. Functional analysis of the interaction between Afr1p and the Cdc12p septin, two proteins involved in pheromone-induced morphogenesis. *Molecular biology of the cell* **8**, 987-998 (1997).

164. Longtine, M.S., Fares, H. & Pringle, J.R. Role of the yeast Gin4p protein kinase in septin assembly and the relationship between septin assembly and septin function. *The Journal of cell biology* **143**, 719-736 (1998).

165. Smith, G.R., Givan, S.A., Cullen, P. & Sprague, G.F., Jr. GTPase-activating proteins for Cdc42. *Eukaryot Cell* **1**, 469-480 (2002).

166. Gladfelter, A.S., Bose, I., Zyla, T.R., Bardes, E.S. & Lew, D.J. Septin ring assembly involves cycles of GTP loading and hydrolysis by Cdc42p. *J Cell Biol* **156**, 315-326 (2002).

167. Joberty, G. *et al.* Borg proteins control septin organization and are negatively regulated by Cdc42. *Nature cell biology* **3**, 861-866 (2001).

168. Sheffield, P.J. *et al.* Borg/septin interactions and the assembly of mammalian septin heterodimers, trimers, and filaments. *Journal of Biological Chemistry* **278**, 3483-3488 (2003).

169. Sadian, Y. *et al.* The role of Cdc42 and Gic1 in the regulation of septin filament formation and dissociation. *Elife* **2**, e01085 (2013).

170. Wang, D.-S., Shaw, R., Winkelmann, J.C. & Shaw, G. Binding of PH domains of β-adrenergic-receptor kinase and β-spectrin to WD40/β-transducin repeat containing regions of the β-subunit of trimeric G-proteins. *Biochemical and biophysical research communications* **203**, 29-35 (1994).

171. Aguilar, R.C., Watson, H.A. & Wendland, B. The Yeast Epsin Ent1 Is Recruited to Membranes through Multiple Independent Interactions *. *Journal of Biological Chemistry* **278**, 10737-10743 (2003).

172. Dixit, G., Baker, R., Sacks, C.M., Torres, M.P. & Dohlman, H.G. Guanine Nucleotide-binding Protein (Gα) Endocytosis by a Cascade of Ubiquitin Binding Domain Proteins Is Required for Sustained Morphogenesis and Proper Mating in Yeast *. *Journal of Biological Chemistry* **289**, 15052-15063 (2014).

173. DeMattei, C.R., Davis, C.P. & Konopka, J.B. Point Mutations Identify a Conserved Region of the Saccharomyces cerevisiae AFR1 Gene That Is Essential for Both the Pheromone Signaling and Morphogenesis Functions. *Genetics* **155**, 43-55 (2000).

174. Konopka, J.B., DeMattei, C. & Davis, C. AFR1 promotes polarized apical morphogenesis in Saccharomyces cerevisiae. *Molecular and Cellular Biology* **15**, 723-730 (1995).

175. Ranjan, R., Dwivedi, H., Baidya, M., Kumar, M. & Shukla, A.K. Novel Structural Insights into GPCR–β-Arrestin Interaction and Signaling. *Trends in Cell Biology* **27**, 851-862 (2017).

176. Nguyen, H.N. & Hadwiger, J.A. The Galpha4 G protein subunit interacts with the MAP kinase ERK2 using a D-motif that regulates developmental morphogenesis in Dictyostelium. *Dev Biol* **335**, 385-395 (2009).

177. Hanyaloglu, A.C. & von Zastrow, M. Regulation of GPCRs by endocytic membrane trafficking and its potential implications. *Annu Rev Pharmacol Toxicol* **48**, 537-568 (2008).

178. Eichel, K. & von Zastrow, M. Subcellular Organization of GPCR Signaling. *Trends Pharmacol Sci* **39**, 200-208 (2018).

179. Stoeber, M. *et al.* A Genetically Encoded Biosensor Reveals Location Bias of Opioid Drug Action. *Neuron* **98**, 963-976.e965 (2018).

180. Rangarajan, N. *et al.* Systematic analysis of F-box proteins reveals a new branch of the yeast mating pathway. *Journal of Biological Chemistry* **294**, 14717-14731 (2019).

181. Boularan, C., Kamenyeva, O., Cho, H. & Kehrl, J.H. Resistance to inhibitors of cholinesterase (Ric)-8A and Gαi contribute to cytokinesis abscission by controlling vacuolar protein-sorting (Vps)34 activity. *PLoS One* **9**, e86680 (2014).

APPENDICIES

APPENDIX A: Supplemental Tables

Table A.1. List of Strains.

Strain	Parent	Description
BY4741	N/A	*Mata leu2Δ met15Δ his3Δ ura3Δ*
SST2-GFP	BY4741	*SST2-GFP::HIS3*
SST2-GFP BEM1-RUBY2	BY4741	*SST2-GFP::HIS3 BEM1-RUBY2::KanMX4*
$SST2^{S539A}$	BY4741	$sst2^{S539A}$
$SST2^{S539D}$	BY4741	$sst2^{S539D}$
$SST2^{S539A}$-GFP BEM1-RUBY2	BY4741	$sst2^{S539A}$*-GFP::URA3 BEM1-RUBY2::KanMX4*
$SST2^{S539D}$-GFP BEM1-RUBY2	BY4741	$sst2^{S539D}$*-GFP::URA3 BEM1-RUBY2::LEU2*
KEL1Δ	BY4741	*kel1Δ::KanMX4*
KEL1-GFP	BY4741	*KEL1-GFP::HIS3*
KEL1-GFP BEM1-RUBY2	BY4741	*KEL1-GFP::HIS3 BEM1-RUBY2:KanMX4*
$GPA1^{G302S}$	BY4741	$Gpa1^{G302S}$*::URA3*
$GPA1^{G302S}$ SST2-GFP BEM1-RUBY2	BY4741	$Gpa1^{G302S}$*::URA3 SST2-GFP::HIS3 BEM1-RUBY2::LEU2*
BEM1-GFP CDC3MCHERRY	BY4741	*BEM1-GFP:HIS3 CDC3MCHERRY:LEU2*
$GPA1^{G302S}$ BEM1-GFP CDC3MCHERRY	BY4741	$Gpa1^{G302S}$*::URA3 BEM1-GFP:HIS3 CDC3MCHERRY:LEU2*
RGA1Δ BEM1-GFP CDC3MCHERRY	BY4741	*Rga1Δ::KanMX4 BEM1-GFP:HIS3 CDC3MCHERRY:LEU2*
RGA2Δ BEM1-GFP CDC3MCHERRY	BY4741	*Rga2Δ::KanMX4 BEM1-GFP:HIS3 CDC3MCHERRY:LEU2*
Bem3Δ BEM1-GFP CDC3MCHERRY	BY4741	*Bem3Δ::KanMX4 BEM1-GFP:HIS3 CDC3MCHERRY:LEU2*

Table A.1. Cont'd

ENT1Δ BEM1-GFP CDC3MCHERRY	BY4741	*Ent1Δ::KanMX4 BEM1-GFP:HIS3 CDC3MCHERRY:LEU2*
ENT1Δ BEM1-GFP CDC3MCHERRY	BY4741	*Ent2Δ::KanMX4 BEM1-GFP:HIS3 CDC3MCHERRY:LEU2*
RGA1Δ GPA1^{G302S} BEM1-GFP CDC3MCHERRY	BY4741	*Rga1Δ::KanMX4 Gpa1^{G302S}::URA3 BEM1-GFP:HIS3 CDC3MCHERRY:LEU2*
RGA2Δ GPA1^{G302S} BEM1-GFP CDC3MCHERRY	BY4741	*Rga2Δ::KanMX4 Gpa1^{G302S}::URA3 BEM1-GFP:HIS3 CDC3MCHERRY:LEU2*
BEM3Δ GPA1^{G302S} BEM1-GFP CDC3MCHERRY	BY4741	*BEM3Δ::KanMX4 Gpa1^{G302S}::URA3 BEM1-GFP:HIS3 CDC3MCHERRY:LEU2*
ENT1Δ GPA1^{G302S} BEM1-GFP CDC3MCHERRY	BY4741	*Ent1Δ::KanMX4 Gpa1^{G302S}::URA3 BEM1-GFP:HIS3 CDC3MCHERRY:LEU2*
ENT2Δ GPA1^{G302S} BEM1-GFP CDC3MCHERRY	BY4741	*Ent2Δ::KanMX4 Gpa1^{G302S}::URA3 BEM1-GFP:HIS3 CDC3MCHERRY:LEU2*
Ste2^{T326} GPA1^{G302S} BEM1-GFP CDC3MCHERRY	BY4741	*Ste2^{T326}::KanMX4 Gpa1^{G302S}::URA3 BEM1-GFP:HIS3 CDC3MCHERRY:LEU2*
SST2Δ	BY4741	*Sst2Δ::KanMX4*

Table A.2. List of Plasmids.

PLASMID	VECTOR	DESCRIPTION
PRSII405-BEM1-RUBY2	pRSII405	Integrating BEM1-RUBY::LEU2 Vector
PRSII406-GPA1^{G302S}	pRSII406	Integrating gpa1^{G302S}::URA3 Vector
PRSII406-SST2-GFP	pRSII406	Integrating SST2-GFP::URA3 Vector
PRSII406-SST2^{S539A}-GFP	pRSII406	Integrating sst2^{S539A}-GFP::URA3 Vector
PRSII416-PADH-SST2-3XFLAG	pRSII406	ADH1 promoter driven overexpression of Sst2-3xFlag
PRSII416-PADH-SST2-S539A-3XFLAG	pRSII416	ADH1 promoter driven overexpression of Sst2(S539A)-3xFlag
PRSII416-PADH-SST2-S539D-3XFLAG	pRSII416	ADH1 promoter driven overexpression of Sst2(S539D)-3xFlag
PRSII416-PADH-KEL1-3XFLAG	pRSII416	ADH1 promoter driven overexpression of Kel1-3xFlag

Table A.3. List of Primers.

OLIGONUCLEOTIDE NAME	SEQUENCE	GENE	DESCRIPTION
AHM-22	GATGCGGTTTTTTACAGGGC	FUS3	Forward primer for amplifying FUS3
AHM-23	ATGGATCACCCCTTGTGGTTCT	FUS3	Reverse primer for amplifying FUS3
AHM-26	TCTACAGAACGAAGAGGCCAATGATGTCATC	GPA1	Forward primer for mutagenesis for GPA1 EE
AHM-27	AAAGGATCACTTTCGTCTC	GPA1	Reverse primer for mutagenesis for GPA1 EE, Primer from NEB
AHM-32	AAAGACTACAAGCATTACAGAAAC	GPA1	FP for mutagenesis for GPA1G302S
AHM-33	ATACGGCCCTTCAAAATG	GPA1	RP for mutagenesis of GPA1G302S
JKM-16	CATAATCCAAGCCAAACTGAAAATTTCCGTTCA CGATATTGGTGACGGTGCTGGTTTA	BEM1	Forward primer pFA6a labeling for BEM1
JKM-17	CAAGTAAAGAAGAAAAATGCTTCGTCTTCTA ACACTAGATTCGATGAATTCGAGCTCG	BEM1	Reverse primer pFA6a labeling for BEM1
JKM-18	GTCTGCGAATTCGGTGACGGTGCTGGTTTAAT	yomRUBY2	EcoRI Ruby2 primer for cloning into pRSII405 with Bem1
JKM-19	CGTAGCTCTAGATTACTTATACAATTCATCCA	yomRUBY2	XbaI Ruby2 reverse primer for cloning into pRSII405 with Bem1
JKM-20	CTGAACGGTACCGACAACTTATGTGGGAGAGA	BEM1	KpnI-Bem1 primer for cloning into pRSII405
JKM-21	CGTACCGAATTCAATATCGTGAACGGAAATTT	BEM1	
RTM-5	CAAAGATGCTAGCGCTTTAATAGAAATCCAAG AAAAGTGCGGTGACGGTGCTGGTTTA	SST2	Forward primer pFA6a yo-tagging for Sst2
RTM-6	GTGCAATTGTACCTGAAGATGAGTAAGAC TCTCAATGAAATCGATGAATTCGAGCTCG	SST2	Reverse primer pFA6a yo-tagging for Sst2
SVM-17	GAACTTTACAACTTGTACCCTTCATCACCT	KEL1	Deletion cassette (250 bp out)
SVM-18	GCACCGCCCAAATACTGCAATCGGACTATTCTGCG	KEL1	Deletion cassette (250 bp out)`
SVM-21	ACTGGACGTACGATGGTGTT	KEL1	Deletion verification cassette (500 bp)

Table A.3. Cont'd

SVM-22	CGAACAGCTTCAACGTACCT	KEL1	Deletion verification cassette (500 bp)
WSM-13	ATCATGTTGCACCCTCATTC	SST2	Forward primer SST2 c-terminal tag verification
WSM-14	GAATGAATTTGCGTTCAATC	SST2	Reverse primer SST2 C-terminal tag verification
WSM-21	TCCATCATAACTTGCGTCAGAATATTTCTGA CATCATGTTGCACCCTCATGAGCTCGTTTTCGACACTGG	SST2	pcore s539 insert
WSM-22	GATGCAGGTGATGGATCGTATAGATTAGTAGGAAAGTG TTCCGATAATGGTCCTTACCATTAAGTTGATC	SST2	pcore s539 insert
WSM-23	TGCGTCAGAATATTTCTGACATCATGTTGCACCC TCATGCTCCATTATCGGAACACTTTCCTACTAATCTATACGATCCA	SST2	S539A
WSM-24	TGGATCGTATAGATTAGTAGGAAAGTGTTCCGATAA TGGAGCATGAGGGTGCAACATGATGTCAGAAATATTCTGACGCA	SST2	S539A
WSM-28	ATGCATGGATCCGTGCTTATAACTTTAAGAAAAACCAGCGTC	SST2	With Kpn1 cut-site for creation of integrating vector
WSM-29	ATGCATGGTACCGCCGGTAGAGGTGTGGTCAATAA	SST2	With BamHI cut-site for creation of integrating vector
WSM-37	GCACCCTCATGCTCCATTATCGG	SST2	Creation of S539A
WSM-38	AACATGATGTCAGAAATATTCTGACG	SST2	Creation of S539A
WSM-44	ACACTGAGATTATAGTCCAG	SST2	Verify Sst2 Integration Vector, Binds upstream of sst2
WSM-45	TACTATACCTGAGAAAGCAA	SST2	Verify Sst2 Integration Vector, Binds Downstream of GFP on vector sequence
WSM-46	TGCGTCAGAATATTTCTGACATCATGTTGCA CCCTCATGATCCATTATCGGAACACTTTCCTACTAATC	SST2	Creation of Sst2 S539D from pCORE KO
WSM-46	TGGATCGTATAGATTAGTAGGAAAGTGTTCC GATAATGGATCATGAGGGTGCAACATGATGTCAGAA	SST2	Creation of Sst2 S539D from pCORE KO
WSM-52	GTACTCAGAGCCACAAGAAA	BNR1	amplify bnr1 del insert
WSM-53	CCCGATGAACTCATTGAGAA	BNR1	verify bnr1 deleted

Table A.3. Cont'd

WSM-54	CTAGCGTTCAATTGCCTTCT	BNR1	verify bnr1 deleted
WSM-55	CTGACGGCTGTGTGTTAATT	BNI1	amplify bni1 del insert
WSM-56	AGCGAACGCGAAATACAAGT	BNI1	amplify bni1 del insert
WSM-57	CCAAATCCTTGCTCAACTCT	BNI1	verify bni1 deleted
WSM-66	GAAAGACCTCAAGAAACTCATTTGGAACGAAAT ATTTAGTGGTGACGGTGCTGGTTTA	FUS3	pFA6a tagging
WSM-67	TACATTGTTCTTCGGGTTGATATTTTAATGATA ATGATGGCGATGAATTCGAGCTCG	FUS3	pFA6a tagging
JKM-56	tcgaggtcgacggtatcgatAAGGTGAGACGCGCATAAC	ADH1	ADH1 promoter amplification forward primer for pRSII416 PADH-Sst2-3xFlag
JKM-66	tatccaccatTGTATATGAGATAGTTGATTGTATGCTTG	ADH1	AHD1 promoter amplification reverse primer for pRSII416 PADH-Sst2-3xFlag
JKM-67	ctcatatacaATGGTGGATAAAAATAGGAC	SST2	Sst2 gene forward for pRSII416 PADH-Sst2-3xFlag
JKM-68	ctttgtagtcGCACTTTTCTTGGATTTC	SST2	Sst2 gene reverse for pRSII416 PADH-Sst2-3xFlag
JKM-69	agaaaagtgcGACTACAAAGACCATGAC	3xFlag	3xFlag forward for pRSII416 PADH-Sst2-3xFlag
JKM-61	gcggccgctctagaactagtCTACTTGTCATCGTCATC	3xFlag	3xFlag reverse for pRSII416 PADH-Sst2-3xFlag
JKM-54	GACTACAAAGACCATGACGGTGATTATAAAGATC ATGACATCGACTACAAGGATGACGATGACAAGTAG	3xFlag	3xFlag sequence for annealing, forward
JKM-55	CTACTTGTCATCGTCATCCTTGTAGTCGATGTCAT GATCTTTATAATCACCGTCATGGTCTTTGTAGTC	3xFlag	3xFlag sequence for annealing, reverse
CJM-64	ggcgaattgggtaccgggccAAGGTGAGACGCGCATAAC	ADH1	ADH1 promoter amplification forward primer for pRSII416 PADH-Kel1-3xFlag
CJM-65	atccagccatTGTATATGAGATAGTTGATTGTATGCTTG	ADH1	ADH1 promoter amplification reverse primer for pRSII416 PADH-Kel1-3xFlag
CJM-66	ctcatatacaATGGCTGGATTCAGCTTC	KEL1	Kel1 amplification forward primer pRSII416 PADH-Kel1-3xFlag

Table A.3. Cont'd

CJM-67	ctttgtagtcTAGTAGATCGCTGTCAGC	KEL1	Kel1 amplification reverse primer pRSII416 PADH-Kel1-3xFlag
CJM-68	cgatctactaGACTACAAAGACCATGAC	3xFLAG	3xFlag forward for pRSII416 PADH-Kel1-3xFlag
CJM-69	agggaacaaaagctggagctCTACTTGTCATCGTCATC	3xFLAG	3xFlag reverse for pRSII416 PADH-Kel1-3xFlag
AHM-44	5' GCGGCCGTTTTATAAAGAACAA 3'	BEM3	Replicate deletion of Bem3
AHM-45	5' AGAAGTGGTGGAAGATGGTGAT 3'	BEM3	Replicate deletion of Bem3
AHM-46	5' TTACAGCTTTGCCACATATCGG 3'	BEM3	Verification of Bem3 del
AHM-47	5' AACAAAACTTTCAATCGCACGG 3'	BEM3	Verification of Bem3 del
AHM-50	5' GATGAGAAGGTGTAAAGTGCCC 3'	RGA1	Replicate deletion of Rga1
AHM-51	5' GCCCGTAAAAGGTTCTTGTCTA 3'	RGA1	Replicate deletion of Rga1
AHM-52	5' AGTGTACCCTTTGAACCCTCTT 3'	RGA1	Verify Replication of Rga1 del
AHM-53	5' ATCTCTGTCGCTCAAAAGTTGG 3'	RGA1	Verify Replication of Rga1 del
AHM-54	5' AATCGTTGCATCGCTTCAGTAA 3'	RGA2	Replicate deletion of Rga2
AHM-55	5' CCGCACAAAAGTACGACAAATG 3'	RGA2	Replicate deletion of Rga2
AHM-56	5' CTCTGTAGAAGCTTTTCCGGAC 3'	RGA2	Verify Replication of Rga2 del
AHM-57	5' CTTTACAGAAGTCGCGTCAACT 3'	RGA2	Verify Replication of Rga2 del
CJM-3	5' CAATGTGGGCCACGGCTGCTAA 3'	STE2	Verify Ste2 C-terminal del
CJM-4	5' ACAGCGTACCTTTAGACACGTGGG 3'	STE2	Verify Ste2 C-terminal del
CJM-5	5' CATCCACAGATAGGTTTTATCCAGGCACGCT GTCTAGCGTTTAGCTTGCCTCGTCCCCGC 3'	STE2	Amplify pFA6-KanMX with Ste2 T-326 homology
CJM-6	5' AGGTCACGAAATTACTTTTTCAAAGCCGTAA ATTTTGACGTTTAAACTGGATGGCGGCGT 3'	STE2	Amplify pFA6-KanMX with Ste2 T-326 homology
SLM-3	5' TAGGCTTCTTACCGGCAGAG 3'	ENT1	Amplify Ent1 del

Table A.3. Cont'd

SLM-4	5' AGGACATGAGTACAGAGCACA 3'	ENT1	Amplify Ent1 del
SLM-5	5' AGATAGATGGCCGAACGTGG 3'	ENT2	Amplify Ent2 del
SLM-6	5' GACTCCAAAGGTGAATCTGGC3'	ENT2	Amplify Ent2 del
SLM-7	5' GGGAGAAGGAGTACCTTCTG 3'	ENT1	Verify Ent1 del
SLM-8	5' CCAGAATTATCTTTCGGGCC 3'	ENT1	Verify Ent1 del
SLM-9	5' ATGGCTCAAATTCCACGGTCC 3'	ENT2	Verify Ent2 del
SLM-10	5' CGAAGATGGCCGAATGATTGG 3'	ENT2	Verify Ent2 del

APPENDIX B: Supplemental Figures

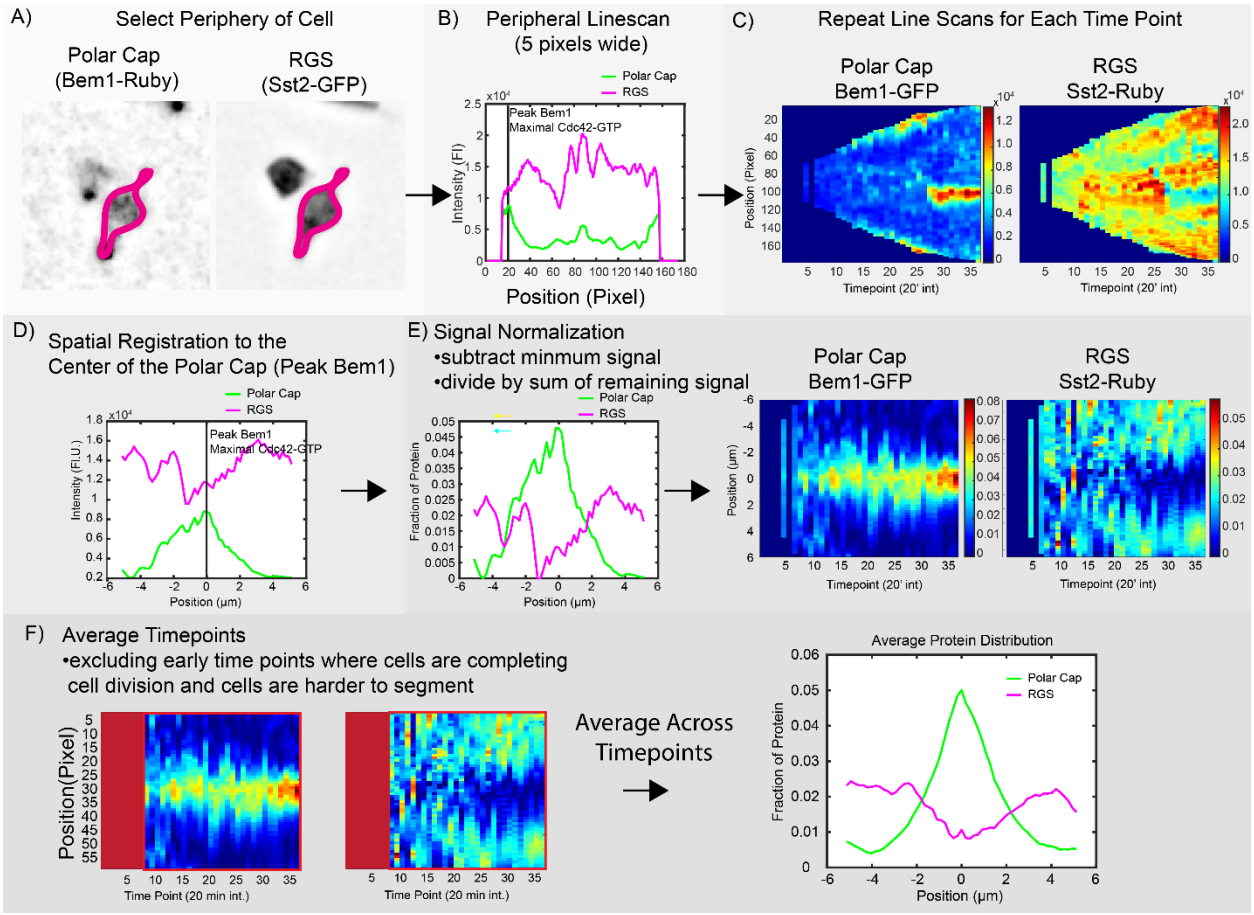

Figure B.1. Method for determining protein distribution on the cell periphery.

A) The periphery of the cell is defined for a specific time point. B) The intensity of fluorescence signal from each channel is measured with a line width of 5 pixels. C) The periphery for each channel at every time point is measured, here shown as kymograph. D) The linescans are adjusted such that the peak intensity of the polar cap marker Bem1 is set to the center, and the other channel is moved to maintain its original spatial relationship with Bem1. E) The intensity profiles are normalized by subtracting the minimum value and then dividing by the total intensity in the line such that the new line sums to 1. F) for the average distributions, all lines after time point 9 are averaged. Time points before this often still include cells that need to complete cytokinesis and are less easily segmented.

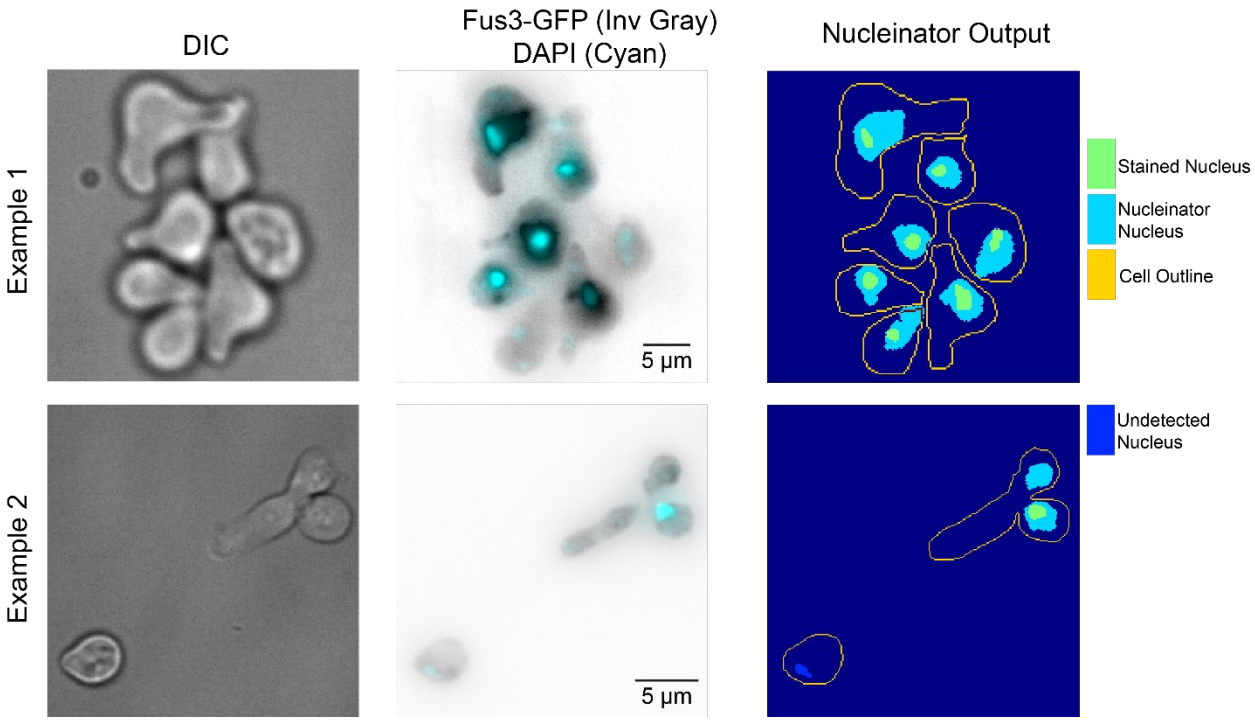

Figure B.2. Validation of nucleinator method for removing MAPK fluorescence.

The nucleateinor algorithm calculates the mean and standard deviation of Fus3-GFP in each cell and selects pixels which are above 1 standard deviation above the mean and are part of a contiguous object that is larger than 25 pixels. Here, we test the ability of the algorithm to detect nuclear pixels by treating cells expressing Fus3-GFP with pheromone followed by fixation and nuclear staining with Hoechst dye. Shown are examples of DIC images, inverted grayscale images of Fus3-GFP, and Hoechst stain in cyan. At the right are the cell outlines with the Nucleinator detected nuclei, and the actual nuclei (either successfully detected, above, or missed, below). Missed nuclei generally appear to be dim in both the Fus3-GFP image and in the Hoechst stain. Over 77 cells, 87.66% of Hoechst defined pixels were identified based on Nucleinator analysis of Fus3-GFP signal.

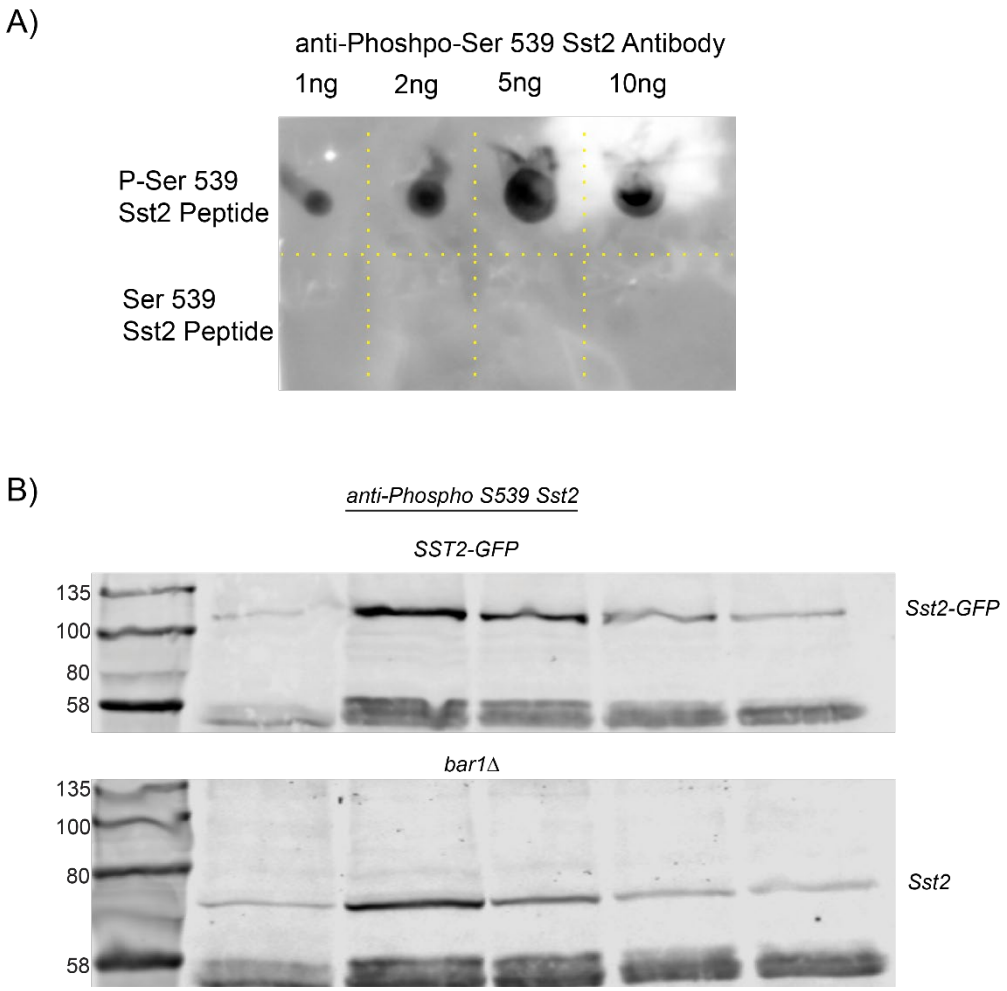

Figure B.3. Characterization of the phosphor-Sst2 antibody.

A) Dot blot with the indicated quantities of peptide. The antibody is specific for phospho-peptide under the conditions used. All blotting is carried out with excess unphosphorylated peptide to stop nonspecific binding. B) out anti-phospho-Sst2 antibody detects a higher molecular weight band when detecting Sst2-GFP than when detecting native Sst2. Additionally, the time dependent decrease in phosphor-Sst2 is not dependent upon Bar1-mediated degradation of pheromone.

BIOGRAPHY OF THE AUTHOR

Cory Johnson was born in Rockport, Maine on December 15, 1989. He was raised in Camden, Maine and graduated from Camden Hills Regional High School in 2008. He attended the University of Maine and graduated in 2018 with a bachelor's degree in Biology. The summer of 2018 he entered the Graduate School of Biomedical Science and Engineering's Biomedical Science graduate program at The University of Maine. After receiving his degree, Cory will be joining the Haller Lab at Mount Desert Island Biological Laboratories as a postdoctoral researcher. He will be studying renal vascularization in human pluripotent stem cell derived organoids. Cory is a candidate for the Doctor of Philosophy degree in Biomedical Science from the University of Maine in August 2022.